Dissertation
submitted to the
Combined Faculty of Natural Sciences and Mathematics of the Ruperto Carola University Heidelberg, Germany for the degree of
Doctor of Natural Sciences

Presented by: M. Sc. Naima Florence Antonie Ruhland

Born in: Wiesbaden

Oral examination 25th of September 2020

Mesoderm internalisation in *Chironomus riparius* as an example of ingression

Referees: Jun.-Prof. Dr. Steffen Lemke

Prof. Dr. Joachim Wittbrodt

Abstract

Cell movements are an important part of animal multicellularity. They can be found in processes of development and body maintenance, as well in wound healing or cancer formation. A group of cells can either move collectively, showing similar cellular behaviour in all cells, or individually and differ in cellular behaviour. Here, I use the model of early fly gastrulation to investigate how cells differ in their cellular behaviour in the context of single cells movements. Mesoderm internalisation in the insect order of flies (Diptera) shows great differences on a cellular level, while the genetics controlling the process are conserved. This sets the stage to study how single, stochastic cell movement differs from collective cell movement. I focused my work primarily on understanding the cellular behaviour of single cell movement. In the midge *Chironomus riparius* (*C. riparius*) mesoderm internalisation has been proposed to be facilitated via single cell ingression. My data, focused on the changes on the apical side of presumptive mesodermal cells, validates again that ingression is a salt and pepper like process. Apical constriction is interrupted by bursts of expansion, that differ in their frequency and length between individual cells. The differences in these bursts cause heterogeneous constriction behaviour between cells. I found strong indications that non-uniform junction mobility is the key component for the stochastic process of apical area reduction. The heterogeneous behaviours of junctions can be found intra- and inter-cellular level, going hand in hand with low cell-cell connectivity, first in the pre-gastrulation stage and then continuously during process of mesoderm internalisation. In addition to apical constriction, neighbour exchange is happening in the mesoderm as well as translocation of cells in response to other gastrulating movements happening simultaneously. It was previously shown that the GPCR signalling ligand Folded gastrulation (Fog), has an effect on the mode of mesoderm internalisation. Going into cellular detail I could show that the major effect of *fog* over expression on the presumptive mesoderm is not a harmonisation of apical constriction between cells. I have evidence that Fog causes a homogenisation of junction behaviour and induces a stronger cell-cell connectivity. This might enhance stiffening of the tissue, causing the cells to internalise collectively rather than individually.

Zusammenfassung

Zellbewegungen sind ein wichtiger Bestandteil der Mehrzelligkeit von Tieren. Sie finden sich in Entwicklungs- und Erhaltungsprozessen sowie in der Wundheilung oder Krebsentstehung. Eine Gruppe von Zellen kann sich entweder gemeinsam bewegen, wobei allen Zellen ein ähnliches zelluläres Verhalten zeigen, oder Zellen bewegen sich einzeln und im zellulären Verhalten unterschiedlich. Hier verwende ich das Modell der frühen Fliegengastrulation, um zu untersuchen, wie sich Zellen in ihrem zellulären Verhalten im Kontext von Einzelzellbewegungen unterscheiden. Die Mesoderminternalisierung in der Insektenordnung der Fliegen (Diptera) zeigt große Unterschiede auf zellulärer Ebene, während die den Prozess steuernde Genetik konserviert ist. Dies schafft die Voraussetzungen, um zu untersuchen, wie sich die stochastische Bewegung einzelner Zellen von der kollektiven Bewegung vieler Zellen unterscheidet. Ich konzentrierte meine Arbeit hauptsächlich auf das Verständnis des zellulären Verhaltens der Bewegung einzelner Zellen. Es wird angenommen, dass die Mesoderminternalisierung in der Mücke *Chironomus riparius* (*C. riparius*) durch das Einwandern einzelner Zellen erreicht wird. Meine Daten, die sich auf die Veränderungen der apikalen Seite von mesodermalen Zellen konzentrieren, bestätigen erneut, dass das Eindringen ein salz- und pfefferähnlicher Prozess ist. Die apikale Verengung wird durch Expansionsschübe unterbrochen, die sich in ihrer Häufigkeit und Länge zwischen einzelnen Zellen unterscheiden. Die Unterschiede in diesen Expansionsschübe verursachen ein heterogenes Verengungsverhalten zwischen Zellen. Ich fand starke Hinweise darauf, dass eine ungleichmäßige Mobilität der Zell-Zell-Verbindungen die Schlüsselkomponente für den stochastischen Prozess der Reduzierung der apikalen Fläche ist. Das heterogene Verhalten von Zellseiten kann auf intra- und interzellulärer Ebene festgestellt werden, was mit einer geringen Zell-Zell-Konnektivität einhergeht, zuerst in der Vorgastrulationsphase und dann kontinuierlich während des Prozesses der Mesoderminternalisierung. Zusätzlich zur apikalen Verengung findet ein Nachbaraustausch im Mesoderm sowie eine Translokation von Zellen als Reaktion auf andere gleichzeitig stattfindende Gastrulationsbewegungen statt. Es wurde zuvor gezeigt, dass der GPCR-Signalligand Folded Gastrulation (Fog) einen Einfluss auf die Art der Mesoderminternalisierung hat. Im zellulären Detail konnte ich zeigen, dass der Haupteffekt von Fog nicht darin besteht eine Harmonisierung der apikalen Verengung zwischen Zellen ist hervorzurufen. Ich habe Hinweise darauf, dass Fog

eine Homogenisierung des Zellseiten verursacht und eine stärkere Zell-Zell-Konnektivität induziert. Dies könnte die Versteifung des Gewebes verbessern und dazu führen, dass die Zellen kollektiv und nicht einzeln einwandern.

Abbreviations

A	Adenin
AJ	Adherens Junctions
AP	Anterior-Posterior
C	Celcius
cDNA	complementary DNA
cm	centimeter
Cri	*Chironomus riparius*
C. riparius	*Chironomus riparius*
cta	concertina
DAPI	4,6-diamidino-2-phenylindole
D. melanogaster	Drosophila melanogaster
DNA	deoxyribonucleic acid
dNTP	deoxynucleoside triphosphate
dsRNA	double stranded RNA
DV	Dorsoventral
E-cad	E-cadherin
E. coli	*Escherichia coli*
EDTA	ethylendiamine tetraacetic acid
eGFP	enhanced green fluorescent protein
EtOH	Ethanol
F-actin	Filamentous actin
Fog	Folded Gastrulation
GBE	Germband extension
GPCR	Guanine protein coupled receptor
GTP	guanosine triphosphate
H_20	Water
IAA	Isoamylalcohol
LB	lysogeny broth
MeOH	Methanol
min	minutes

Mist	Mesoderm Invagination Signal Transducer
ml	milliliter
mRNA	messenger RNA
mV	milliVolt
mya	million years ago
MyoII	Myosin II
NaOAC	Natriumacetat
NEE	neighbour exchange event
ng	nano gram
nM	nano Molar
NTP	Nukleosidtriphosphate
OD	optical density
PBS	Phosphate Buffered Saline
PBT	Phosphate Buffered Saline + Tween
PC	pointcloud
PCR	polymerase chain reaction
PMI	Posterior midgut invagination
RGB code	Red Blue Green code
Rok	RhoKinase
Rho1/RhoA	Ras homolog family member A
RhoGEF2	Rho-guanine exchange factor 2
RNA	Ribonucleic acid
rpm	rounds per minute
SDS	Sodium dodecyl sulfate
sec	seconds
SOC	Super Optimal Broth
sqh	Spaghetti squash
TAE	Tris-acetate-EDTA
Tris	Tris-(hydroxymethyl-) amino methane
UV	ultra violet
VE water	Deionized water

wt	wild type
µl	microliter
µm	micrometer

Content

1. Introduction

Epithelial tissues display astonishing plasticity during development, which ultimately gives rise to the phenotypic diversity visible in animals today. Studies of gastrulation, the first shape-giving (morphogenetic) event in animal embryos, have shed light on the cellular and molecular mechanisms of epithelial plasticity and shape changes. Gastrulation is the process in which cells organise to form specific tissues. Three germ layers are formed: the future mesoderm internalises and gives rise to muscles and haemocytes, the future ectoderm extends and gives rise to the epidermis and the nervous system and the future endoderm gives rise to the digestion tract [Wolpert, 1999].

The driving forces of tissue changes are the cells within the epithelium. To change the tissue composition, cells can either change their behaviour and move collectively, e.g. invagination, involution, epiboly or delamination, or individually, e.g. ingression. Comparing similar gastrulation movements in animals reveals that animals make use of both approaches of cellular movement to change their initial shape [Leptin, 2005].

A good system to study how migratory cell behaviour differ in the context of morphogenesis is the process of mesoderm internalisation in flies. The order of flies represents great developmental diversity, while at the same time many aspects of development been preserved and can still be compared between different flies. Dipteran flies shared a last common ancestor about 250 million years ago [Wiegmann et al., 2011] (Figure 1). The more basally a species is located in the phylogenetic tree, the more it is believed to resemble the ancestral species.

One aspect in which fly deploy different modes of cell movement is mesoderm internalisation. Different fly species make use of different modes of internalisation of mesodermal cells. In more basal flies, presumptive mesoderm is internalised via stochastic single cell movement [Goldsev et al., 2007, Urbansky et al., 2016], while in higher flies the cells are internalised as a coherent tissue [Leptin, 1991] in an organised manner. Over the past decades, mesoderm internalisation has been studied extensively in the model organism *Drosophila melanogaster* (*D. melanogaster*). In terms of genetics as well as morphological aspects of mesoderm invagination in *D. melanogaster* represents one of the best understood processes in

developmental biology. Therefore, it serves as a good reference for studying how changes in cellular behaviour cause morphogenetic movements.

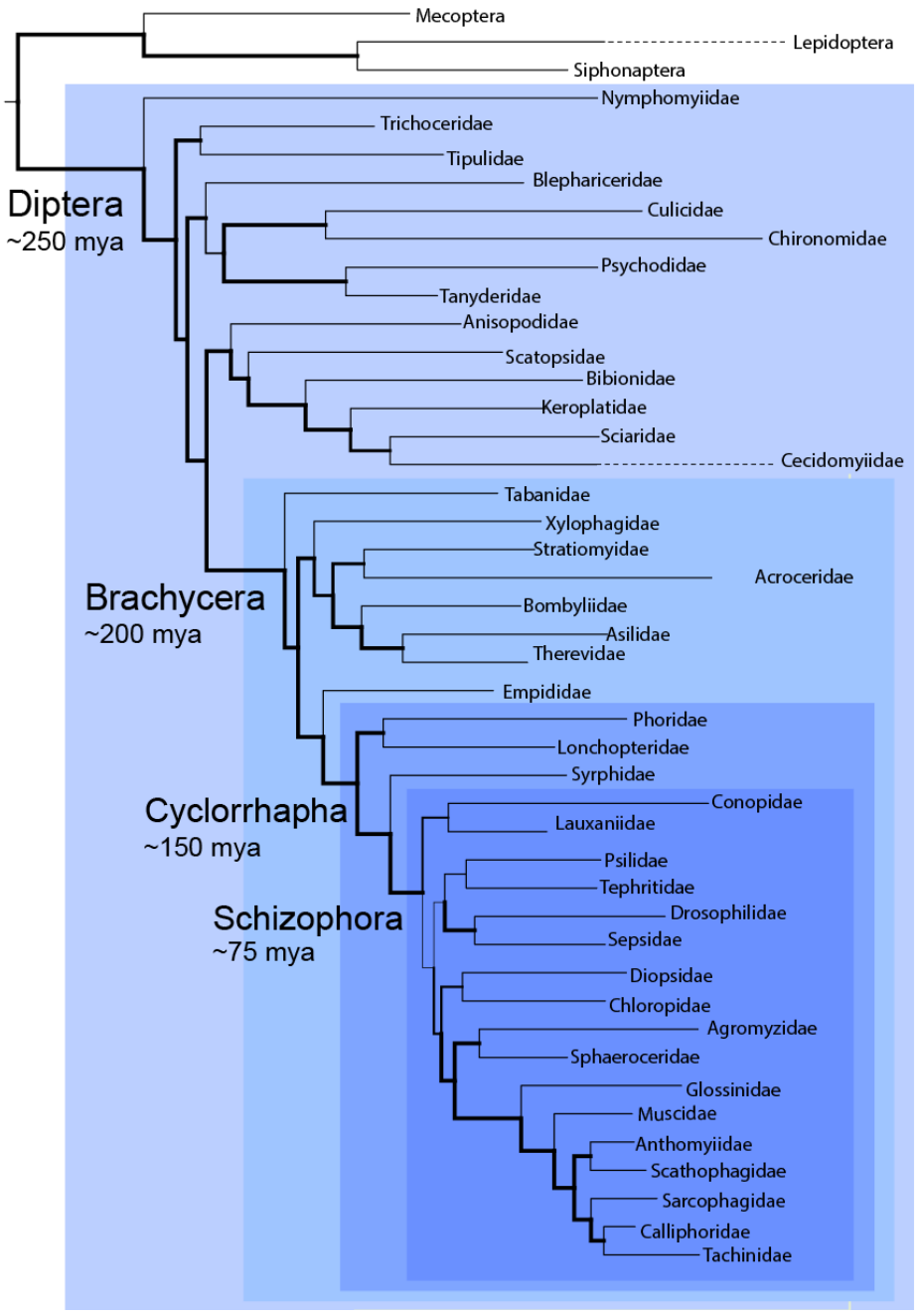

Figure1 Phylogenetic tree of dipteran flies
Adapted from [Wiegmann et al, 2011]

1.1. Early gastrulation in flies

Studying the fruit fly *D. melanogaster* much could be learned about the early development of the fly embryo. The basis for gastrulation is set up during the process of cellularisation. In *D. melanogaster*, after egg deposition, nuclei divide without cytokinesis, for 14 cell cycles. This results in a syncytium stage of the embryo, where about 6000 nuclei reside in the egg without being surrounded individually by cell membrane. After the 8th cycle, the nuclei, previously residing deep within the yolk, move to the periphery towards the egg shell. Here, another 4 to 5 rounds of mitosis happen [Mazumdar and Mazumdar, 2002]. Early during this process while most nuclei are still preparing for more divisions in the yolk, the first cells at the most posterior part of the egg start to form. The so-called pole cells will be set aside apart from the forming cell sheet. These cells constitute the germline and are specified by maternal factors deposited into the egg [Lehmann and Nüsslein-Vollhart, 1986]. They remain genetically as well as behaviourally distinct from the rest of the somatic cells and get internalised later in development [Callaini et al., 1995]. Once the somatic cells have undergone the 14th, last cell cycle, the process of cellularisation begins. Along a framework of microtubules, an actomyosin network grows from the apical side of the forming cell inside the embryo, thereby building the frame for the membrane to divide the cytoplasm into cells [Frescas et al., 2006]. At the end of cellularisation, the embryo consists of about 6000 cells that share similar morphology but differ in their genetic composition. Morphologically, all somatic cells form one coherent epithelium. On a cell biological level, the embryo now consists of a one layered coherent tissue formed around the yolk characterised by three main characteristics of an epithelium: (1) an established apical-basal polarity, (2) Adhenrens Juntions (AJ) connecting cells and (3) an interconnected contractile actomyosin cytoskeleton [Tepass et al., 2001]. The apical polarity is set up via Crumbs/Stardust/Discs Lost Complex and basolateral via the Lethal Giant Larvae/Discs Large/Scribble Complex [Tepass et al., 2001]. This differentiation is essential because it forms the foundation of the epithelial morphology important for morphogenesis and mesoderm internalisation.

The actomyosin network and AJs work together to form tight cell-cell connection. AJs are located circumferential in a subapical position at the membranes of the

individual cells. The main component of AJs are E-cadherins (E-cad). Two cells have the extracellular domain of their E-cad molecules connected via formation of homodimers. The inner part of the molecule is connected to an F-actin ring via a catenin chain [Tepass et al., 2001, Lecuit and Yap, 2015]. In addition to the F-actin ring, an actomyosin network spans over the apical side of the cell and together with junctional actin is important for cellular movement, such as apical constriction or junction rearrangement during the process of gastrulation. Apart from these two pools of active actin, actin is also found everywhere on the membranes as a scaffold for the cells [Mazumdar and Mazumdar, 2002]. Once cellularisation is complete, gastrulation begins.

During this process, cells become morphologically different from each other, depending on their position and subsequently function in the developing embryo. Four main populations of cells are present in the gastrulating embryo: Cells forming the future (1) mesoderm, (2) endoderm, (3) ectoderm and (4) extraembryonic tissue [Campos-Ortega, and Hartenstein,1985]. Depending on their fate, cells display specific cell behaviour. On the ventral side of the embryo, cells make up the presumptive mesoderm. Here, about 1000 cells constrict apically by contraction of the actomyosin network, form a furrow along the anterior- posterior (AP) axis and are invaginated to the inside of the embryo [Leptin, 1991]. Endodermal cells start to undergo apical constriction as well and invaginate at both the anterior and the posterior end of the embryo. They form the anterior and posterior midgut, respectively, which in later stages grow and connect to form the gastric system [Campos-Ortega, and Hartenstein,1985]. The lateral cells will give rise to the ectoderm. These cells are characterised by their potential to intercalate [Irvine and Wieschaus, 1994]. This causes the tissue to extend towards the posterior pole of the embryo. This movement is referred to as convergent extension, and together with posterior midgut invagination and, later on mitosis [da Silva and Vincent, 2007], cause the embryo to elongate along the AP axis, a process called germband extension (GBE) [Campos-Ortega, and Hartenstein,1985]. The extraembryonic tissue consists of the most dorsal cells of the embryo that stretch massively to cover specific parts of the embryo and are set aside from embryonic development of the fly [Wolper and Tickle, 2011] (Figure 2).

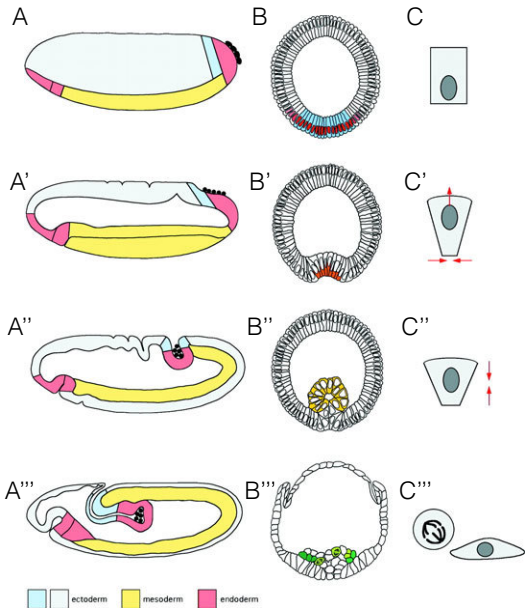

Figure2 Embryonic movements in *D. melanogaster* during gastrulation
Schematic depiction of gastrulation of embryo proper (**A-A'''**), a cross section through the embryo at a central position (**B-B'''**), and cell shape changes in the mesodermal cells (**C-C'''**). Pictures in each row represent the same timepoint. [Leptin,1991]

1.2. Mesoderm internalisation as example of collective cell behaviour

Mesoderm in *D. melanogaster* gets internalised as a coherent sheet of cells that folds inwards. The genetic and cellular regulation is well studied and follows a very defined and organised program. In an initial phase of about 2 min, cells constrict stochastically in the mesoderm anlage. After constriction, the apical side expands again, so that no net gain of apical area reduction can be observed [Martin et al., 2009]. Eventually, cells coordinate their constriction and massively constrict their apical surface area. Apical constriction is facilitated in a pulsed fashion, causing ratchet-like constriction phases [Martin et al., 2009]. Two pools of Myosin II (MyoII) are important for this movement. First, the medioapical MyoII pool constricts, causing a constriction of the apical surface. This new shape is then stabilised by junctional MyoII pool [Martin et al., 2009]. Constriction and stabilisation iterate and with each step, the apical area of the cell gets reduced. At the same time, the lateral side of mesodermal cells elongates [Gelbart et al., 2012]. These shape changes cause a

change from the original blastodermal columnar shape to a wedge-like cell shape. In addition to those cell shape changes, the nuclei of the mesodermal cells drop to the basal side of the cells [Leptin and Grunewald, 1990, Kam et al., 1991] and a shift of AJs from a subapical to an apical position can be observed [Weng and Wieschaus, 2016].

Since all cells undergo these changes at the same time and remain tightly connected via the AJs they induce a bending of the tissue. This bending is the formation of the ventral furrow. Then the mesodermal cells shorten their lateral side again [Leptin, 2005, Gelbart et al., 2012, Rauzi et al., 2013], but the precise mechanism of deep furrow invagination remains under investigation. Once all cells are internalised, they detach from each other and spread over the inner side of the ectoderm [McMahon et al., 2010]. It should be stated, that a small subpopulation of mesodermal cells does not share the same cellular changes as the majority of mesodermal cells. The cells, positioned at the periphery of the mesodermal domain, are called lateral mesodermal cells. Instead of constricting their apical side and elongating the lateral side, they expand their apical surface [Bhide, 2019]. The genetic and cellular basis for this distinct behaviour remains a question of ongoing interest.

1.3. Genetic network underlaying apical constriction

The process of apical constriction is well studied in *D. melanogaster* and the genetic underlaying the process are well known. The transcription factors that provide mesoderm cell identity are called *twist* and *snail* [Leptin, 1991]. They are regulated via the maternally provided protein Dorsal and are already expressed during preblastoderm stages [Leptin, 1991]. They activate the G-protein coupled receptor (GPCR) pathway. Twist induces expression of the secreted protein Folded gastrulation (Fog), which binds to the 7 transmembrane domain receptor Mesoderm Invagination Signal Transducer (Mist). Upon ligand binding, Mist releases the G-Protein subunit alpha, called Concertina (Cta). Release of Cta starts a phosphorylation cascade, with Cta activating the Guanin nucleotide exchange factor RhoGEF2, which in turn activities the small GTPase Rho1/RhoA, which in turns activates the RhoKinase Rok. Rok phosphorylates the small regulatory subunit of

MyoII [Manning and Rogers, 2014]. (Figure 3). This phosphorylation leads to an activation of the MyoII molecule and causes a constriction of the actomyosin meshwork in the cell. Localisation of this constriction to the medioapical side of the cell is achieved via the membrane anchored protein T48 [Kölsch et al., 2007]. T48 is also regulated by Twist and binds RhoGEF2 to the apical side of the cell. At the same time, constriction is actively inhibited at the periphery by the local expression of the GTPase-activating protein, Cumberland, which regulates the activity of RhoA [Mason et al., 2016]. Additionally, a physical advection has been proposed to play a role in the localisation to the apical side as well [Munjal et al., 2015]. During mesoderm internalisation, mitosis is inhibited by the expression of Tribbels [Mata et al., 2000, Seher and Leptin, 2000]. Only after internalisation is complete, mesodermal cells detach from the epithelium, the tube collapses and cells become fibroblasts [Clark et al., 2011]. They undergo mitosis, spread dorsally and line the basal side of the ectoderm, and then enter a second round of mitosis [Clark et al., 2011].

In mutants deficient of Fog, mesoderm can still be internalised. But instead of being invaginated as a coherent tissue, the cells lose their epithelial character and move individually, which results in a slower overall mesoderm internalisation [Parks and Wieschaus, 1991; Seher et al., 2007; Sweeton et al., 1991].

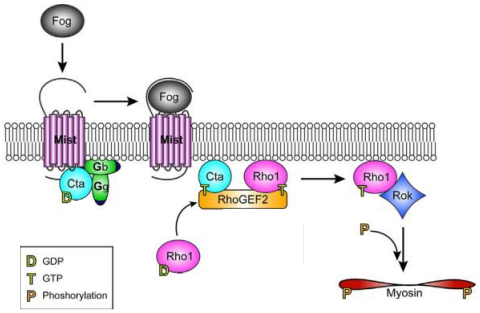

Figure3 The Fog signalling pathway in the mesoderm
Schematic representation of the Fog signalling pathway in *D. melanogaster* mesoderm. Adapted form [Manning and Rogers, 2014]

1.4. Fog regulates extension of the germband

As a regulator of GPCR signalling, Fog has also been connected not only to apical constriction in the mesoderm but also to another morphogenetic process, germband extension [Costa et al., 1994, Irvine and Wieschaus, 1994, Jha et al., 2018]. Germband extension is mainly driven by two processes, cell intercalation and invagination of the posterior midgut.

Cell intercalation is a process that describes a rearrangement of cells, e.g. a T1 transition. Four cells form such a transition for explanatory reason here termed: dorsal, ventral, anterior and posterior cell. In the initial state, the anterior and posterior cells are directly neighbouring each other, while the dorsal and ventral cells are not. Then the junction between anterior and posterior cell shrinks, causing the formation of a vertex. In this phase, all four cells are in direct neighbourhood to one another. As a next step, a new junction arises, shared by the dorsal and ventral cell. Now, the dorsal and ventral cell are in direct contact, while the formerly neighbouring anterior and posterior cells are no longer [Bertet et al., 2004, Collinet et al, 2015]. Such a neighbourhood exchange event can also be facilitated with more than four cells involved. In such an event, called rosette formation, many cells are involved in the vertex. The constriction along one axis and expansion along another remains similar to T1 transitions [Bertet et al., 2004, Collinet et al., 2015]. Through these neighbourhood exchange events, the arrangement of the cells drastically changes, and with it the dimensions of the entire tissue the cells reside in. Having previously been long in the dorsal-ventral axis and short in the AP axis, the tissue architecture has now reversed, causing the tissue to shrink along the dorso-ventral axis and extend along the AP axis [Irvine and Wieschaus, 1994]. The specific junctional remodelling is achieved by a planar polarised MyoII pool at the dorsoventral axis and a reduction of MyoII in the AP axis. This process is also regulated via GPCR signalling. Fog, expressed in low levels, binds to the GPCR Smog, and the small subunit of the G-protein, Gβ13F/Gγ1, is released [Kerridge et al., 2015] and binds to the RhoGEFs RhoGEF2 and Wireless [Kerridge et al., 2015, Garcia De Las Bayonas et al., 2019]. Wireless is specifically localised at the DV junctions of the cells [Garcia De Las Bayonas et al., 2019]. RhoGEF activation in turn causes a similar activation cascade of MyoII activation as RhoGEF2 in the mesoderm, results in a

phosphorylation of two MyoII pools, a junctional MyoII in the dorsoventral orientation and a medioapical pool. The junctional, planar polarised MyoII constricts, resulting in the vertex formation. The second constriction of the weak pool of medialapical MyoII follows this first step, exerting a pull on the AP junctions and thus causing their extension [Kerridge et al., 2015]. In addition to the specific expression of wireless, MyoII is excluded from the AP-oriented junction by a complementary expression of Par3/bazooka (enriched at the anterior-posterior junctions) and Rok [de Matos Simoes et al., 2016]. There are indications that Wireless also has an effect on AJ stability. In wireless knockdown embryos, AJs are lost from the ectoderm [Silver et al., 2019]. A third way of remodelling the cellular neighbourhood is the so called T2 transition. Here, one cell leaves the epithelium, while its neighbours remain in the tissue [Pasiliao and Hopyan, 2017]. Once the cell has left the epithelium, the remaining cells are in direct contact. This T2 transition is conceptional very different from T1/rosette formation, because in the T1/rosette formation all cells remain in the epithelium.

Additionally, to regulating cell intercalation, Fog has also been shown to be important for the invagination of the posterior midgut. In the absence of Fog, the posterior midgut fails to get internalised [Costa et al., 1994].

1.5. Mesoderm internalisation in lower flies

Even though flies share a similar overall development they can show remarkable differences in mesoderm internalisation compared to the well-studied model system *D. melanogaster*. Although all flies need to translocate the presumptive mesodermal cells into the inner of the embryo, different modes of mesoderm internalisation can be found throughout the fly order. Instead of undergoing mesoderm internalisation by invagination of a coherent tissue and forming a ventral furrow, the presumptive mesodermal cells in the midge *Chironomus riparius* (*C. riparius*) are internalised via single cell migration in a process that has been proposed to be ingression [Urbansky et al., 2016]. Ingression as a process has not been studies before in flies and not much is known about it.

Mesoderm internalisation in *C. riparius* thus is a great model to study the process of ingression and compare it to the process of invagination in *D. melanogaster* to find differences in cell behaviour between the two processes.
In the study of *C. riparius* the authors show that the mode of mesoderm internalisation can be changed genetically. In a cross-sectional view through the wild type embryo, nuclei were positioned randomly and resembled a phenotype of staggering a stochastic fashion [Urbansky et al., 2016]. The tight genetic network underlying mesoderm invagination in *D. melanogaster* is not so rigidly expressed in the presumptive mesodermal cells of a *C. riparius* embryo. Two important factors, Fog and T48, are not expressed at that stage [Urbansky et al., 2016]. Over expression of one or both factors change the nuclei staggering phenotype into a phenotype where the nuclei line up in a furrow like phenotype [Urbansky et al., 2016]. The aligned nuclei strongly resemble the furrow phenotype that can be observed in *D. melanogaster*. The expression of *fog* and/or *t48* therefore at the right space and time in the embryo seems to be sufficient to change the mode of mesoderm internalisation.

A change in mode of internalisation from single cell movement to collective cell movement needs to be connected to changes in cell behaviour. Where the changes in cell behaviour occur remains unknown and open for investigation. Since

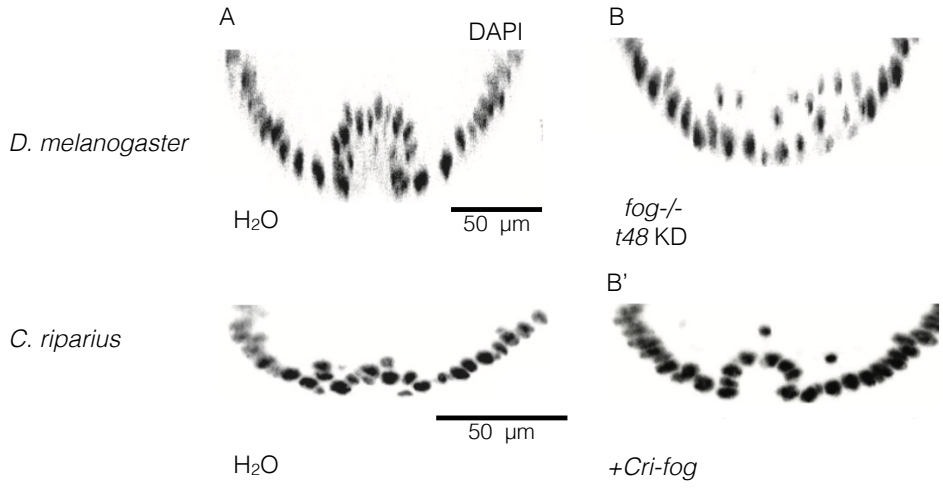

Figure4 Expression of *fog* changes mode in mesoderm internalisation.
Cross-section through the ventral side of the embryo of *D. melanogaster* (**A-A**) and *C. riparius* (**B-B'**) at a stage mid internalisation, visualising nuclei stained with DAPI. First column shows nuclear position under mock-injections (**A, B**), second column shows nuclear position after altering *fog* expression, In *D. melanogaster* via *fog -/- / t48* knockdown (**A'**), in *C. riparius* via *Cri-fog* over expression (**B'**). Scale bar 50 µm. Adapted from [Urbansky et al 2016]

mesoderm internalisation is mainly driven by apical constriction, a change in cell behaviour connected to apical constriction is very plausible. Nonetheless, other circumstances can cause the change of cell behaviour as well. Individual cell behaviour can be altered by a change in cell-cell connectivity. If *fog* over expression causes cells to be more tightly connected and to remain connected during internalisation, individual cells can affect their neighbours in their inward movement. In this case, differences in apical constriction patterns can still be present in individual cells, but the overall tissue movement is altered.

To analyse the impact of Fog on cell behaviour, a detailed description of the cell movement behaviour under wild type (wt) conditions needs to be obtained. Exactly what happens during mesoderm internalisation has never been analysed in a dynamic way in the *C. riparius* embryo. It is not known how cells behave during internalisation. Questions concerning individual cell behaviour such as onset of constriction, timepoint of internalisation, constriction pattern and cell shape remain unanswered. At the same time, the relationship between cells and the impact they might have on each other has never been analysed. Do neighbouring cells interact with one another? How closely are cells connected? Are there differences in cell behaviour when comparing the anterior and posterior border of the mesoderm? A close and dynamic examination of cell behaviour will help to answer these questions.

2. Aim

The developing animal embryo is shaped by cell behaviour in different tissues. Migratory behaviour can either be driven by independent single cells or collective cell movements. Comparing the process of mesoderm internalisation in flies reveals that both kinds of migration are used in different flies. Cellular behaviour during collective cell migration via tissue invagination is well understood, but cellular behaviour in the context of single cell ingression is barely known. The aim of this study is to gain an understanding of the cellular processes of single cell movement in the context of ingression and how cellular behaviour is modulated to facilitate invagination. As a primary aim, I want to give a detailed understanding of the process of ingression. This study gives a detailed analysis of the process of ingression and cellular behaviour during mesoderm internalisation in *C. riparius*, focusing on the apical side of the cell.

3. Results

Ingression describes a process of epithelial remodelling, in which cells detach from an epithelium and leave it individually. Ingression has been first characterised in the context of sea urchin gastrulation, where the internalisation of endoderm cells defines a hallmark of ingression cell behaviour: the formation of bottle-shaped cells. To acquire this stereotypical bottle-like shape, cells shift their centre of mass, the nucleus, to the basal side. As a consequence, the basal side of the cell rounds up, and only a thin apical extension remains in contact with the epithelium. Eventually, the cell retracts its apical extension, rounds up completely and is no longer part of the epithelium [Katow and Solursh, 1981].

3.1. *C. riparius* mesoderm cells internalise with a bottle-shaped morphology

To test whether mesoderm internalisation in the midge *Chironomus riparius* (*C. riparius)* could be characterised by the formation of bottle-shape cells, I aimed to reveal and analyse the morphology of individual mesoderm cells. The stage of mesoderm internalisation, and therefore timepoint of fixation, was set according to the progress of germband extension (GBE), following established protocol [Urbansky et al., 2016]. Embryos were fixed when the germband had extended by 10-15 percent of embryo length. To visualise cell outline in these fixed cells, different approaches were explored: to visualise cell membranes, I tested three commonly used methods, i.e. visualisation via Wheat Germ Agglutinin (WGA) [Doerflinger et al., 2010], CellMask [Sorvina et al., 2016], and FM464 [Coutelis et al., 2007]. In the *C. riparius* mesoderm; CellMask and FM464 labelled the cytoplasm, and WGA visualised the nuclear rather than the cell membrane (Figure 5).

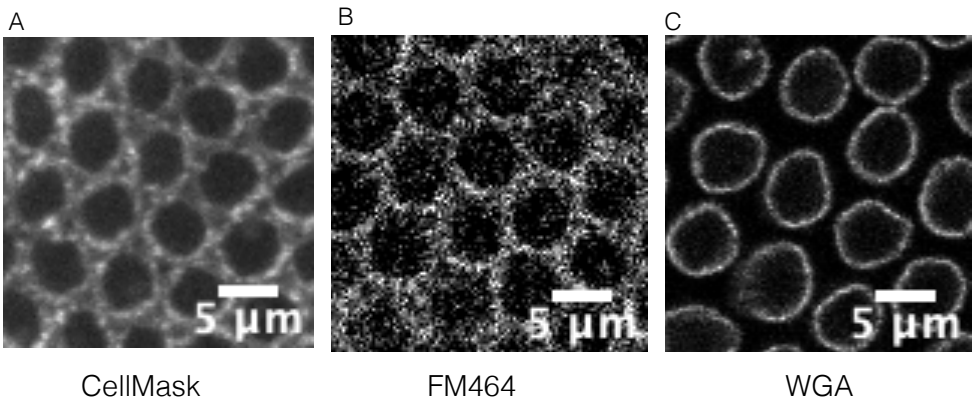

Figure5 Commercial membrane staining solutions do not work satisfyingly in *C. riparius*
Commercially available membrane staining solutions, shown in a ~5 µm subapical position. CellMask (**A**) and FM464 (**B**) show unspecific cytoplasm localisation, Wheatgerm Agglutinin (WGA) stains the nuclear membrane (**C**).

Since membrane staining was not satisfactory, I used F-Actin as a proxy for the cell outline and visualised it using fluorescently labelled Phallacidin [Urbansky et al., 2016]. The ventral side of the embryos was first imaged at high spatial resolution. Then, to obtain quantitative information of cell shape and nuclear position for each mesoderm cell, the cell and nuclear volumes (visualised by DAPI) were segmented using Illastik (Figure 6A and 6A').

Each segmented cell and nucleus was converted to a pointcloud (PC). For some cells, segmentation errors occurred, so the PC representing cells needed to be filtered for false data. This was achieved by overlaying PC of cells and nuclei (Figure 6A'' and 6A'''). Only cell PCs containing only one nucleus PC were taken for the analysis. To address whether cells assumed a bottle-like shape along their apical-to-basal axis, I generated for each cell a 2D projection that would, like a footprint, represent the 3D dimensional shape of each cell along its apical-to-basal axis (Figure 6B). These footprints were then used to differentiate columnar cells from other shaped cells: in a columnar footprint, the corresponding centre of cell mass and centroid are in roughly identical position and their ratio is close to one. By contrast, cells with an enlarged apical side (triangular cells) have a smaller value, and cells with an enlarged basal side (bottle-shape cells) have a bigger value (Figure 6B').

At 10-15 per cent germband extension, ~20 percent of cells showed a bottle-shaped phenotype, so undergoing ingression, while ~15 percent had an enlarged apical surface. The majority of cells remained in a columnar shape (Figure 6C).

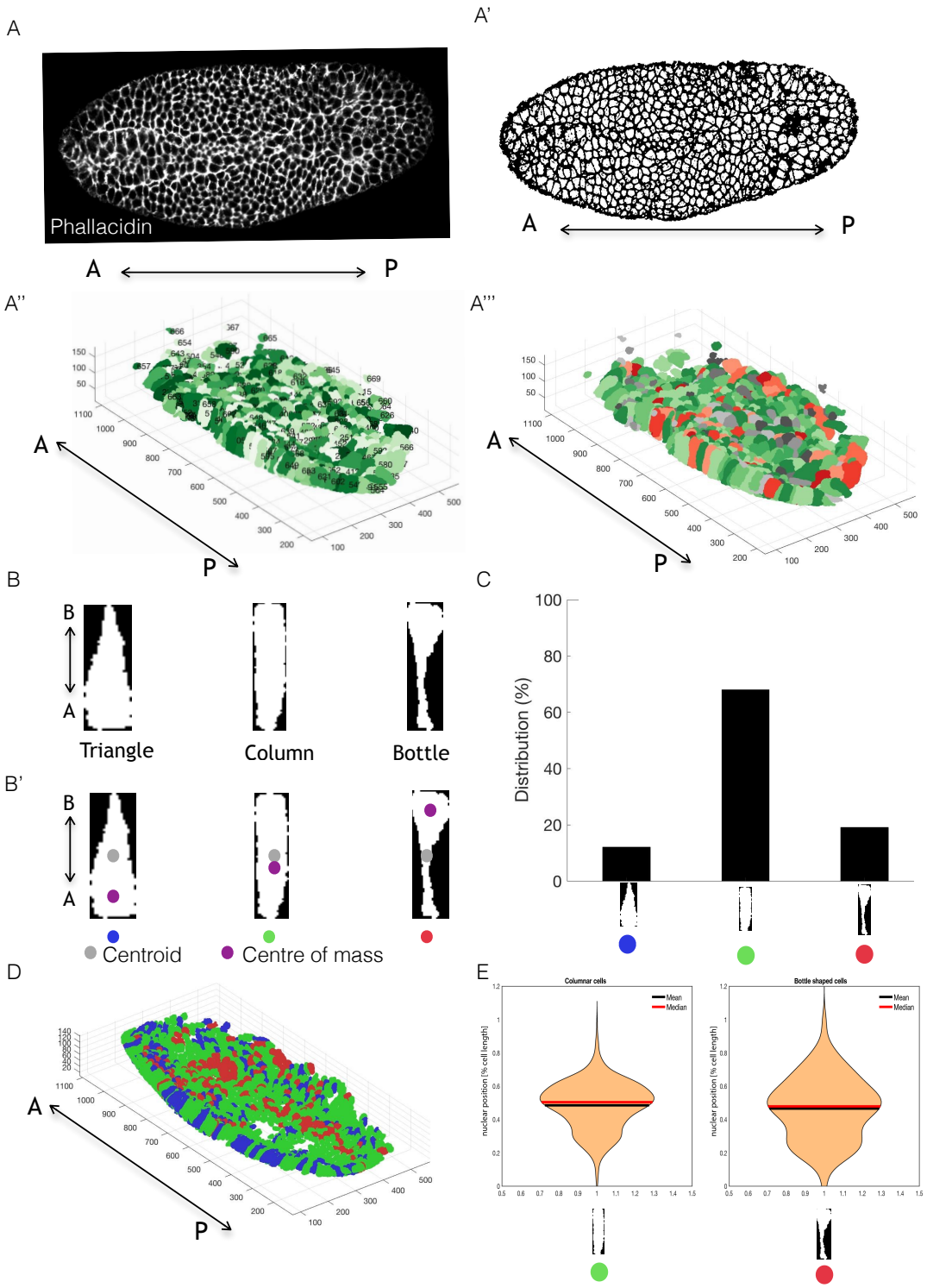

Figure6 Mesoderm cells show bottle-shape morphology
Workflow used to obtain 3D cell shape data. Embryos are fixed at 10-15 percent germband extension, stained for cell outline (Phallacidin) and nuclei (DAPI), imaged on their ventral side (**A**) and segmented with Ilastik software (**A'**). Segmented cells are converted to point clouds (**A''**) and filtered by number of nuclei (**A'''**). Color of pointclouds indicate number of nucleus point clouds: one nuclear pointclouds per pointcloud (green), more than one nuclear pointclouds per pointcloud (red), no nuclear pointclouds per pointcloud (grey).
To obtain the footprint of the cell, pointclouds are oriented along their larges axis and a 2D foot print is generated. (**B**) and categorised according to the ratio of centroid (grey dot) and centre of mass (violet dot). Triangular (enlarged apical side) cells are colour coded with blue, columnar cells with green and bottle shaped cells with red (**B'**). (**C**) The percentage of cells according to their morphology and cells in their original position coloured in the colour code of B (**D**). (**E**) Violin plots showing the position of the nucleus along the apical-basal axis of the cell for columnar and bottle shaped cells (0 percent at apical side of cell, 100 percent at basal side of the cell). n= 3 embryo, 1953 cells

For technical reasons, parts of the ectoderm were included into this analysis as well, which explains the high number of columnar shaped cells.

To ask whether cells with a particular cell shape clustered spatially in the presumptive mesoderm, cell shapes were then mapped onto the mesoderm, but no obvious pattern of shape distribution could be detected in the presumptive mesoderm (Figure 6D). While cells ingress, their nucleus will be moving basally with the cell. The nucleus is a major cell organelle, and its displacement could be the driving force in ingression behaviour. If ingression is also characterised by a nuclear drop, the position of the nucleus within a cell should differ between cells that have not stared ingression and cells that ingress, so columnar and bottle-shaped cells, respectively.

When comparing the position of the nucleus in the cell between bottle-shaped cells and columnar cells, no difference could be observed. In columnar shaped cells, the nucleus resided on average at about 48 percent cell length (0= basal, 1= apical) (n= 4 embryos, total of 948 cells), and in bottle-shaped cells, the nucleus was localised on average at about 46 percent (Figure 6E) (n= 4 embryos, 348 cells). This data shows that the nuclei did not change their relative position within the cell. Nuclear dropping therefore is not a criteria of ingression.

Taken together, the internalisation of mesoderm cells in *C. riparius* showed a typical character of cell ingression, i.e. the formation of bottle-shaped cells, which is not driven by a nuclear dropping. By finding bottle-shaped as well as columnar cells in a salt-and-pepper fashion in the mesoderm, my results furthermore suggest that ingression varies temporally between cells. Such temporal variation could be caused, for example, if cells would initiate ingression at different time points. To test this hypothesis and further characterise ingression cell behaviour, mesoderm internalisation in *C. riparius* needed to be analysed dynamically.

3.2. Establishing fluorescent reporters to study cell dynamics in C. riparius

Mesoderm internalisation is a highly dynamic morphogenetic event. To better understand this process of tissue remodelling and address the underlying principles of cell behaviour, I first needed to establish live time-lapse imaging of relevant cellular components. This required fluorescent reporters for cell membranes (via a Gap43 anchor [Kosik et al., 1988], for non-muscle Myosin II (via its small regulatory light chain *spaghetti squash* [Karess et al., 1991] and Adherens Junctions (via E-cadherin [Cavey et al., 2008]. These reporters have been established as GFP fusion constructs, where my gene of interest and eGFP encoding sequences were cloned into a mRNA expression vector. The mRNA was then transcribed in vitro, stabilised by dedicated 5' capping and 3' polyA tailing, and injected into preblastodermal embryos.

3.3. The C. riparius blastoderm diverges from tight honeycomb pattern

To test the temporal and spatial resolution of the constructs, cellular blastoderm stage embryos were analysed as the tissue is relatively static: cells are fully formed, but gastrulation has not yet begun. To estimate how much time it would take for protein synthesis and fluorophore maturation, *GAP43-eGFP* mRNA was injected at various times into pre-blastodermal embryos.

When embryos were injected when nuclei started migration to the periphery (2 hrs after deposition, 3 hours before onset of gastrulation), the resulting fluorescent signal at the membranes was highly specific and stable over a long period of time (Figure 7). For the other constructs the signal was not as bright and stable (Figure or data not shown). During cellularisation, the apical side of blastoderm cells formed a stereotypic hexagonal shape resulting in a honey comb pattern of cells, with a typical apical cell diameter of 5.84 µm (n= 3 embryos, 10 cells each). When analysed in

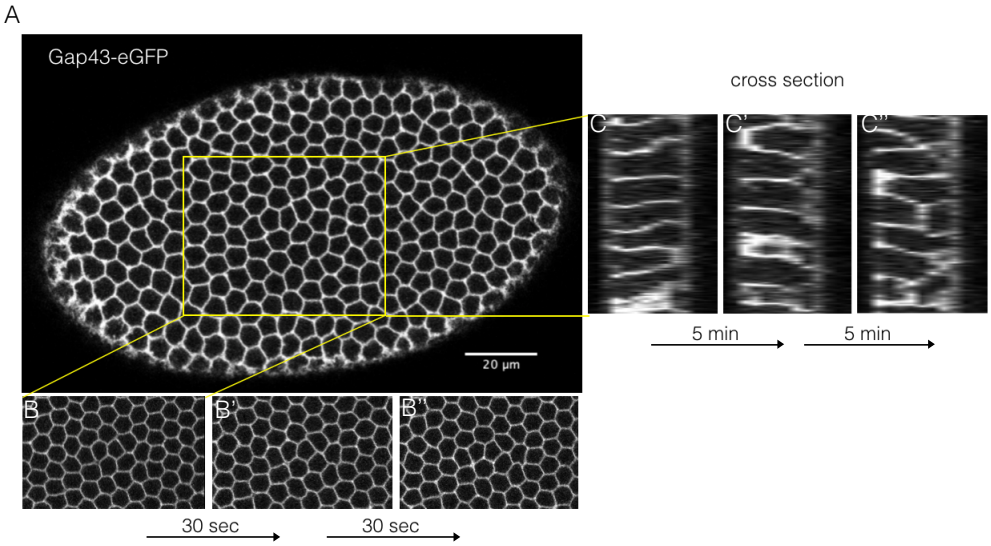

Figure7 Establishment of membrane staining in the midge *C. riparius*.
(**A**) Ventral subapical surface view after injection of a stabilised *Gap43-eGFP* reporter mRNA with fast folding dynamics visualising cell outlines in vivo. (**B-B''**) In vivo time lapse images taken every 30 seconds shown in subapical (2-3 *µ*m below apical surface) surface view. (**C-C''**) Cross sections (90° rotated) showing Gap43-eGFP with a specific and stable signal at membranes. Scale bars 20 *µ*m

detail, this honeycomb pattern appeared in the *C. riparius* blastoderm qualitatively less regular than described for *Drosophila melanogaster* (*D. melanogaster*) [Simpson et al., 2014], and cells showed distinct deviations from the honeycomb pattern in about 50% of all analysed embryos. Deviations appeared throughout the whole blastoderm and were classified into three different categories, i.e. holes, excess of membranes, and convoluted cell-cell interfaces (junctions). Most striking was the appearance of small holes between individual cells (Figure 8A), which were up to 1-2 µm in diameter. The excess of membrane could be observed by a bulging of membrane between cells in no connection to a specific position in the cell (Figure 8A). The appearance of convoluted junctions resulted in many cells with an overall asymmetric shape, which appeared in no particular order throughout the blastoderm. In these cells, membranes exhibited an unexpected curvature or twist instead of reaching from one vertex of the cell straight to the neighbouring vertex (Figure 8A).To quantify how often these features occurred in the blastoderm, cells outlines were analysed in a slightly subapical section throughout an area of about 12 by 20 cells in the blastoderm (110 x 70 µm). The selected window was on the ventral side of the embryo and reached from about 30% EL to 60% EL (0% corresponding to the anterior pole). The overall appearance of cell irregularities varied between individual embryos (n=3). The number of holes ranged from just of few to 16 holes within the indicated observation window (0.08, 0.09, 0.05 holes/cell), the occurrence of

membrane bulges was between 12 and 45 (0.2, 0.25, 0.05 bulges/cell), and convoluted membranes were observed between 24 and 80 times (0.38, 0.46, 0.11 convoluted membranes/cell).

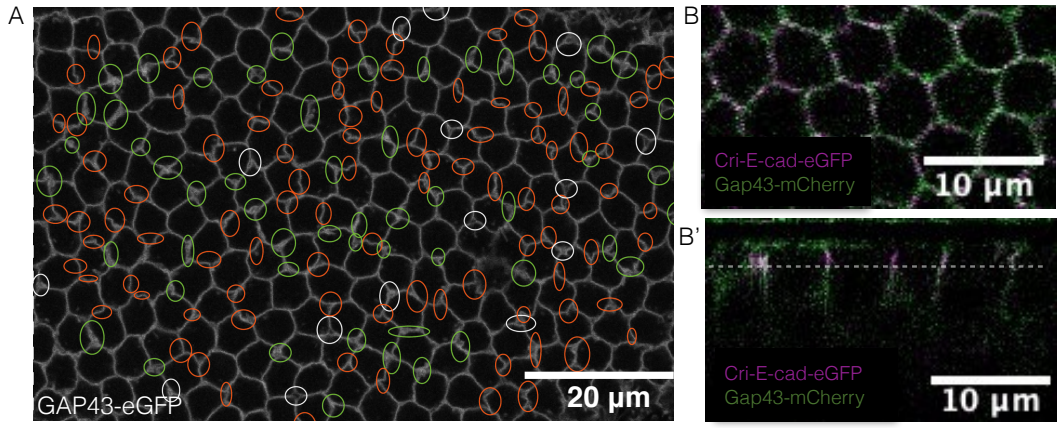

Figure8 Cells are loosely connected in the blastoderm.
(**A**) Subapical surface view of a blastoderm *C. riparius* embryo visualised with Gap43-eGFP (cell outlines) showing 3 different phenomena (1) holes between two cells (marked in white) (2) excessive membrane (marked in green) and (3) convoluted junctions (marked in orange), scale bar 20 *µ*m. *C. riparius* blastoderm embryo showing membrane with Gap43-mCherry and Adherens Junctions via Ecad-eGFP after mRNA injection in a cross section (**B**) and a subapical surface view (indicated with dashed line) (**B'**). Scale bars 10 *µ*m

Tight cell packing is maintained via Adherens Junctions (AJ) [Cavey et al., 2008]. To test whether the epithelial irregularities in the *C. riparius* blastoderm could be explained by poor cell-cell adhesion, a fluorescent reporter for E-cadherin was used. The corresponding mRNA was injected into the preblastodermal embryo and revealed spot like structures close to the membrane. While the signal was overall weak, preliminary data showed that AJs could be detected at the subapical position within the cells (Figure 8B). Their distribution at the cell outline was speckled, similar as has been reported previously for the blastoderm in *D. melanogaster* [Harris. and Peifer, 2004]. These results do not indicate major differences in E-cad mediated cell-cell connectivity in the *C. riparius* and *D. melanogaster* blastoderm. However, my analysis has been restricted to the subapical junction belt and I cannot not exclude the possibility that E-cad based adhesion along lateral cell membranes may be substantially lower in *C. riparius* than in *D. melanogaster*.

In conclusion, the *in vivo* analysis of blastoderm cell dynamics in the *C. riparius* embryo demonstrate the successful establishment of fluorescent reporters for membrane and junctional components. They characterised abnormalities in the epithelium that could indicated low cell-cell adhesiveness. While low cell-cell

adhesiveness could be related to low levels of junctional components such as E-cadherin, the subapical distribution of E-cadherin did not appear to differ qualitatively from the more adhesive blastoderm reported for *D. melanogaster*.

3.4. Setting the stage: a whole-tissue perspective on C. riparius mesoderm internalisation

Following the completion of blastoderm formation, all somatic cells showed the same morphology independent of their position in the embryo and presumptive mesoderm cells were indistinguishable from the ectoderm. Thus, to identify the mesoderm within the blastoderm, mesoderm cells were defined as those that had internalised at later stages. These cells then were tracked back through time to their position in the blastoderm. To identify the lateral border of the mesoderm domain, instead of tracking the mesodermal cells, the bordering ectoderm cells were tracked. Ectodermal cells directly adjacent to the mesoderm could be identified easily at the time of ventral closure: at this point, the ectoderm cells were characterised by being much bigger and more elongated than other ectodermal cells. Tracking these “border ectoderm” cells at either side of the ventral midline back to the blastoderm essentially defined the mesoderm anlage: all cells in between the two rows of “border ectoderm” cells were eventually internalised, while conversely none of the cells outside of the “border ectoderm” were internalised (Figure 9A and 9A’). This further supports previous interpretation in fixed data that remaining columnar cells on the ventral side of the embryo eventually become bottle-shaped cells and ingress.

To ensure that analyses between embryos were comparable also with respect to cell positions along the anterior-to-posterior axis, boundaries were defined based on specific hallmarks in the gastrulating embryo. In the anterior, the head-truck separation was visible by ectodermal cells undergoing mitosis (see also Tok, 2019). These mitotic cells were tracked and mapped in the blastoderm. The anterior boundary of the analysed mesoderm window was then set 1-2 cell rows posterior of these mitotic cells. The posterior border was set to be 12 cell rows posteriorly from the anterior border (Figure 9 B-B’’). Only embryos in which the hole length of the so defined tissue was visible over time were taking into account for the analysis.

At the onset of gastrulation, all cells in the *C. riparius* mesoderm had a comparable diameter of about 6 µm (paragraph 3.3). In the anterior, the mesoderm was about 40 µm wide and span 6-7 cells. The posterior end of the analysed area was about 65 to 70µm wide and span 12 to 13 cells (n=3; for one of these embryos only one side from the ventral midline was measurable and the data was interpolated for the whole tissue).

Following the onset of mesoderm internalisation, the anterior and posterior width of the tissue shrank continuously, albeit with different rates. At the anterior end, the border of the mesoderm anlage moved towards the ventral midline with a speed of -0.44 µm/min, while at the posterior, the speed was about -0.96 µm/min (Figure 9D).

These differences in closure speed in the anterior and posterior of the mesoderm domain scaled with the number of cells and disappeared when closure rates were normalised by the number of cells that defined the mesoderm width at its observation boundaries (Figure 9E). After about 55 minutes, all but a uniform stripe of mesoderm with a width of about 15-20 µm had internalised; shortly after, the ectoderm started to close on the ventral midline and a coherent mesoderm area was not visible anymore on the surface of the embryo (Figure 9C-C’’’).

The time it took the mesoderm from its first ventral movements until when almost all cells (> 95%) were internalised varied between embryos. For some embryos, mesoderm internalisation lasted 45 min, while for others it was up to 80 min. While all analysed embryos (n=6) had a different developmental timing, two categories could be still defined: fast developing embryos took between 45 and 60 min for mesoderm internalisation, while slow developing embryos took 70 min or longer (Figure 9F). Notably, embryos that needed a long time for mesoderm internalisation and ventral closure showed much more membrane irregularities in the blastoderm than embryos experiencing faster ventral closure.

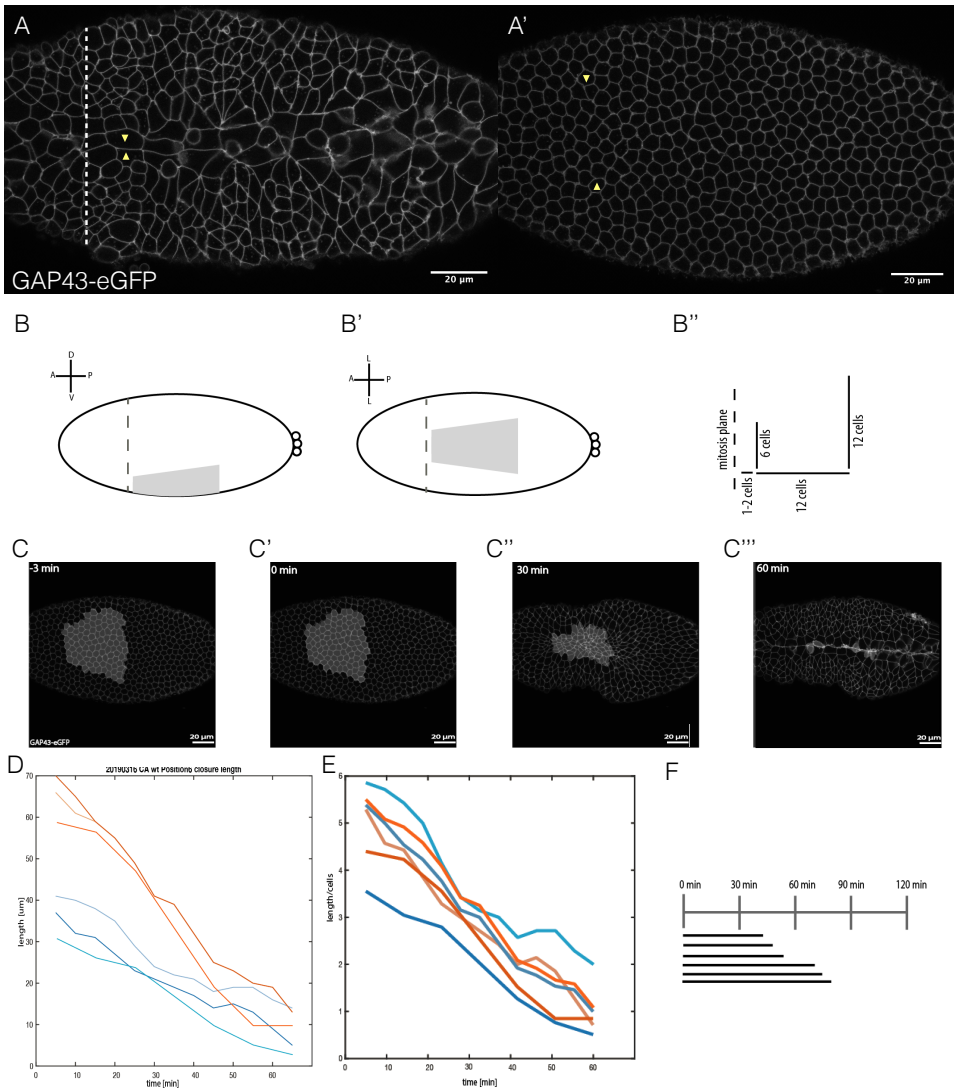

Figure9 Mesoderm tissue internalisation is homogeneous but differs in speed .
(**A-A'**) Cell of the mesoderm visualised with Gap43-eGFP shown in a subapical view after ventral closure (**A**) and in blastoderm stage (**A'**). Mesoderm is defined laterally by the bordering ectoderm cells (arrow head) that can be followed by backtracking. The dotted line indicates the head-trunk barrier, identified by mitosis events in the head region. Schematic depiction of the analysed domain of the mesoderm in a lateral (**B**) and ventral (**B'**) view. The anterior border is set 1-2 cell rows from the head-truck division, the posterior border of the domain is set at 12 cell rows posteriorly of the anterior border. Laterally the domain includes all mesodermal cell. Due to the mesoderm anlage, this results in a funnel shaped domain (**B''**). (**C-C'''**) Time series showing the process of mesoderm internalisation with mesodermal cells highlighted in white at (**C**) blastoderm stage (-3min), (**C'**) onset of mesoderm internalisation (0 min), (**C'')** mid mesoderm internalisation (30 min) and (**C'''**) shortly before end of mesoderm internalisation (60 min) when the ectoderm has started to close ventrally. (**D**) Plot showing the width of the mesoderm anlage over time (n=3). Width of the anterior domain is shown in red and width of the posterior shown in blue and after normalising width to number of cells (**E**). (**F**) Plot showing absolute time of mesoderm internalisation indicated by individual lines for individual embryos (0 min = Onset of cell movements). Two main groups can be identified (1) fast developing embryos (~ 45 to 60 min) and (2) slow developing embryos (> 70 min).

3.5. Establishing a pipeline to analyse mesoderm ingression dynamics at the single cell level

Mesoderm internalisation in *C. riparius* has previously been associated with ingression [Urbansky et al., 2016] and I could show that mesodermal cells indeed migrate via ingression (Paragraph 3.1). While cell migration via invagination has been understood very well, the cellular basis of ingression remains largely unknown. In *D. melanogaster*, single cell migration has so far only been described and qualitatively analysed in the fly notum [Marinari et al., 2012]. It has been characterised as a delamination process of individual cells, which was most prominently defined by the loss of apical area and a constant loss of cell neighbours by stochastic neighbour exchange events [Marinari et al., 2012].

To test whether these or similar features could be used to characterise mesoderm ingression in *C. riparius* required an analysis method for reliably tracking cell features. A toolkit that has been previously used to address such needs is the MATLAB software suite SEGGA (**SEG**mentation, **G**raphical visualisation and **A**nalysis; [Farrell et al., 2017]). This open source software provides a reliable method for automated cell segmentation and cell tracking. The software allows to follow segmented cells individually over time and provides an analysis of cell shape, polarity and cell movement. While the SEGGA suite internally quantifies and analyses tissue dynamics at single cell level, it outputs final results only for the complete tissue. To extract single cell data, the toolkit was modified, and variants were established that differed from the original SEGGA framework as outlined in material and methods. Briefly, the “ModTrack” variant was modified such that it allowed for the tracking output of individual cells. The “Mod1” variant was modified such that specific cells could be selected for analysis, making it possible to output measurements of cell area, number of neighbours and coordinates for cells selected by their blastoderm position. The "Mod2" variant was modified such that cells could be analysed for when a particular cell feature reached a defined threshold. Cells were colour-coded according to the time when the threshold was reached, and this colour was then mapped to the blastoderm position of the cell. The “Mod3” variant was modified such that time-dependent changes in cell features could be analysed, e.g. constriction rate as the difference of apical area between two consecutive time points. The “Mod4”

variant then allowed rates that were computed by “Mod3” to be colour-coded and visualised as a heat map. The “Mod5” variant was modified such that features of neighbouring cells were compared. In such an analysis, e.g., the apical area of a specified cell ("reference cell") was compared to the apical area of all of its neighbours. If a neighbouring cell was of the same apical area as the reference cell (or reasonably similar, with reasonably similar being defined by a user-set cut-off value), then these cells became part of a local cluster. Each cell within a local cluster then was iteratively treated as reference cell, and its neighbours were analysed for similarity in apical area. As such, a local cluster could grow until it was completely surrounded by cells that were definitely distinct in apical area from the initial reference cell. This analysis was run for each timepoint and with each cell as starting reference cell. The output of this analysis were cell maps at each timepoint of mesoderm internalisation, in which all local clusters of similar apical cell area were indicated by different coloration.

3.6. Based on single cell dynamics, the C. riparius mesoderm consists of at least two distinct populations: lateral and central mesoderm

My analysis of *C. riparius* mesoderm behaviour at the tissue level (paragraph 3.4) showed that embryos varied in the time they needed to internalise the mesoderm. These observations suggest that cell internalisation could be a non-uniform developmental process. Such a non-uniform developmental process could be caused by non-uniform constriction of mesoderm cells, e.g. by certain cells constricting earlier of faster than others. To test this hypothesis, I made use of the newly extended SEGGA toolkit and resolved the *C. riparius* mesoderm behaviour at the single cell level.

I first looked at the apical area of each individual mesoderm cell and asked how it changed over time (Figure 10A). Not surprisingly, when averaged over all cells in the

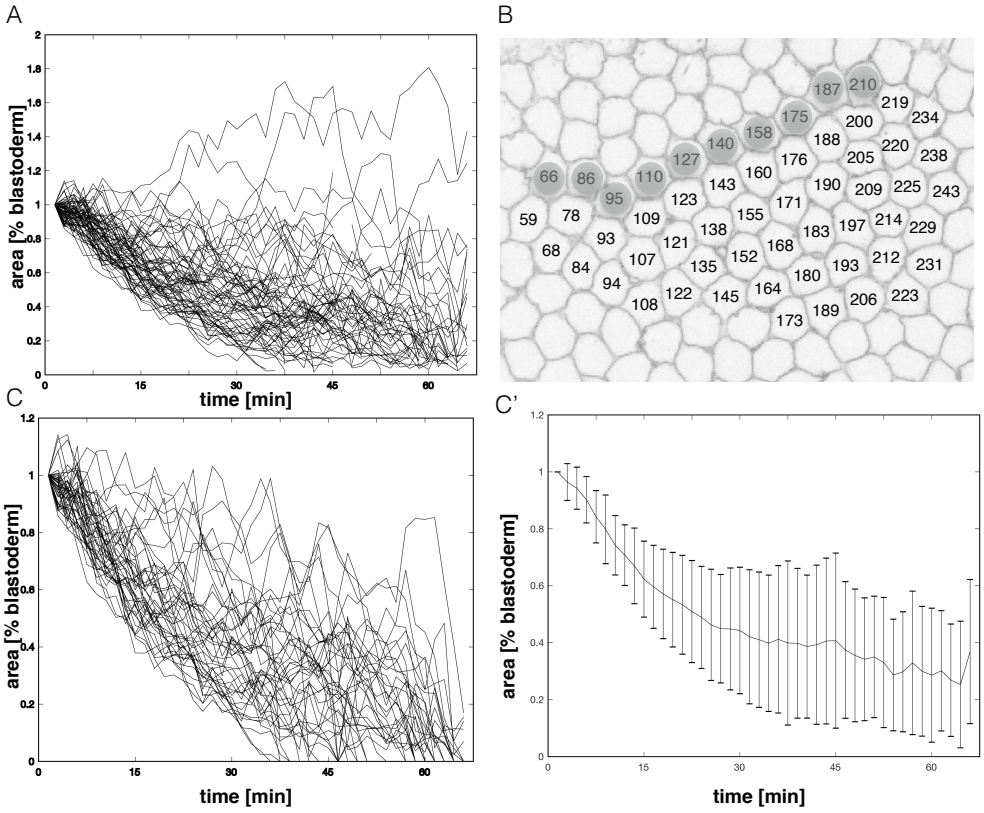

Figure10 Mesoderm consists of two populations of cells: lateral and central mesoderm
Normalised cell area of all mesoderm cells (**A**) and their position in the blastoderm, plotted are cells from one side of the ventral midline, lateral mesoderm cells are marked with a grey circle (**B**). Central mesoderm cells are plotted over time for single cells (**C**) and mean of (**C'**), error bars show standard deviation.

mesoderm, the time a cell typically needed to constrict (40-60 minutes) was about the same time the whole tissue needed to internalise (compare to Figure 9F). A first rough classification based on rate of constriction and time of internalisation then identified to two distinct populations of mesoderm cells, i.e. the lateral and central mesoderm. The lateral mesoderm was initially identified as a population of cells that had (a) an inconsistent and delayed onset of constriction and (b) was internalised very late during gastrulation. When the IDs of these cells were mapped onto the blastoderm, all cells in this population were found in the periphery of the mesoderm and in contact with the ectoderm (Figure 10B). Cells of the central mesoderm, by contrast, were identified as the remaining population of cells that constricted their apical area overall constantly. When the IDs of these cells were mapped onto the blastoderm, all cells of the central mesoderm were found in a central region along the ventral midline (Figure 10B). The classification of the mesoderm tissue in lateral and central mesoderm is known from work in *D. melanogaster* [Bhide, 2019] and suggests a conserved genetic regulation for the two cell populations.

3.7. The ingression of central mesoderm cells is characterised by a non-synchronous reduction in apical cell area

To better characterise cell ingression in the central mesoderm, a finer grained analysis of area constriction of single cells was performed. When compared to the lateral mesoderm, cells of the central mesoderm appeared as an overall homogenous pool with comparable rates of apical constriction. When compared among themselves, however, the behaviour of central mesoderm cells turned out to be rather heterogeneously (Figure 10C). A first measure for this heterogeneity was the standard deviation with which the apical area of any individual cell diverged from that of the average (Figure 10C'). When cells started apical constriction, the standard deviation was relatively low, indicating that cell behaviour was overall synchronised, meaning cells experienced the same changes in apical area over time. With time, the standard deviation increased, indicating that heterogeneity between cells increased with time (Figure 10C').

Heterogeneity in cell behaviour can be considered a hallmark of cell ingression, and it may result from cells that start to leave an epithelium individually and at an unpredictable time. Alternatively, ingressing cells may start to leave an epithelium overall collectively but at their own, individual pace. To test whether the observed ingression of central mesoderm cells was primarily characterised by cells leaving the blastoderm epithelium individually and at an unpredictable time, I determined for each cell the time of "constriction onset". For technical reproducibility, I defined constriction onset as the time when a cell had constricted its apex by more than 10 percent of its initial blastoderm area. For all central mesoderm cells, I determined the individual time point of constriction onset and then analysed how this event was distributed over developmental time. The majority of cells (almost 80 percent) reached their constriction onset within the first 10 minute after the onset of mesoderm internalisation (Figure 11A), suggesting that the onset of apical constriction was rather synchronous.

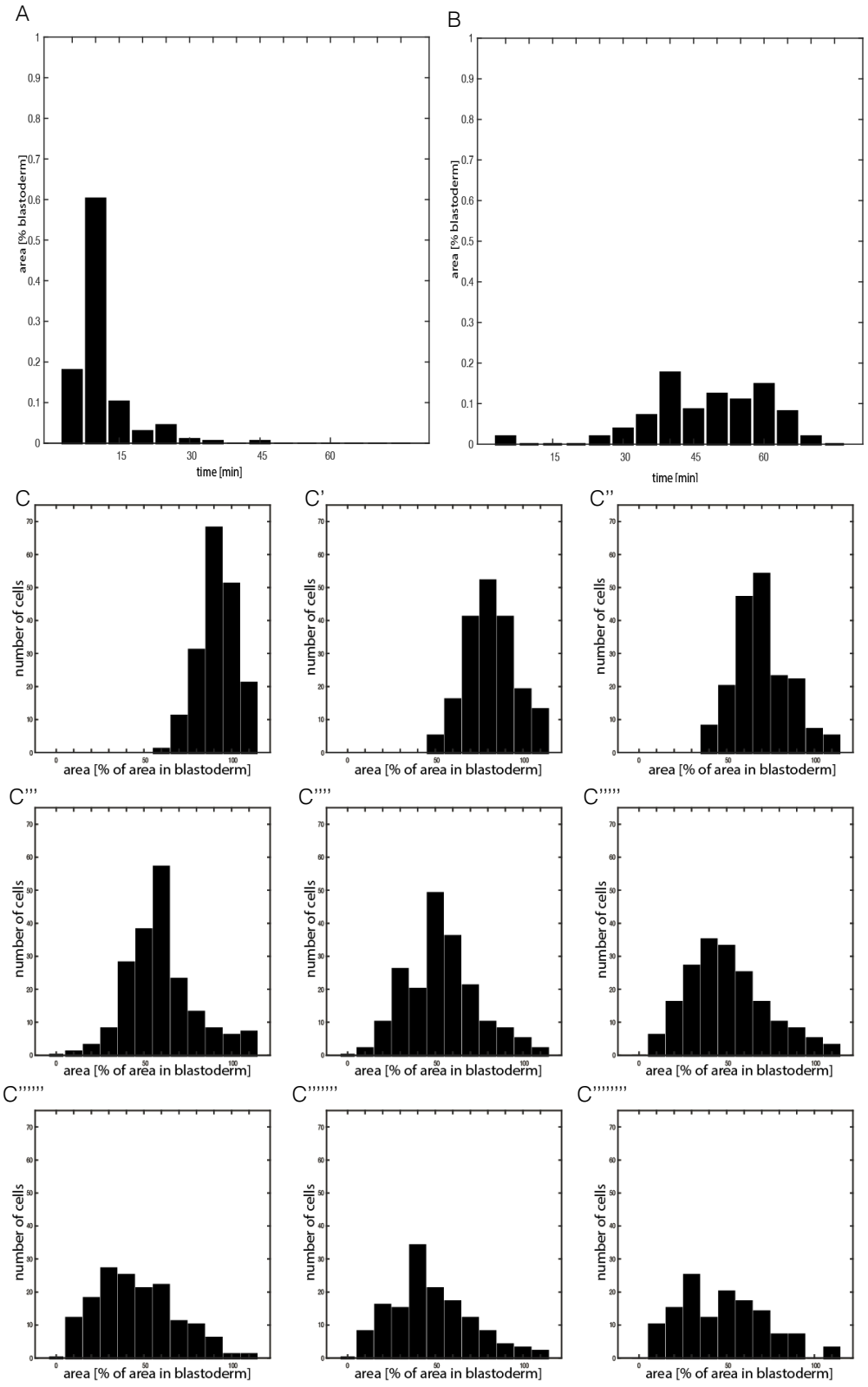

Figure11 Apical constriction is non-synchronous between cells
Distribution cell area over time at the onset of constriction (constriction of apical area by more than 10 percent) (**A**) and their timepoint of ingression (constriction of apical area by more than 10 percent) (**B**), time is binned in 5min intervals n= 2 embryos, 93 cells. (**C-C'''''''**) Distribution of number of cells over apical area in time series of 5 min intervals (**C**= 5 min after onset of ventral movement, **C''''''''**: 60 min after onset of ventral movement) n= 2 embryos, 93 cells.

Since cells started ingression more or less at the same time, the increase in heterogeneity between cells may alternatively be caused by differing in when cells ingress. To better understand possible differences in when cells ingress, I asked how much of the initial synchrony in constriction onset could be still observed at the time of cell internalisation. Analogous to onset of constriction, I defined "cell internalisation" as the time when a cell had reduced its apical area by more than 90 percent. I then determined the individual time point of internalisation for each central mesoderm cell and asked how this event was distributed over developmental time. Notably, the time of cell internalisation span an extended time period of over 50 minutes (excluding outliers), within which no clear peak of internalisation events could be determined. At any given timepoint not more than 20 percent of cells had reached the threshold defined for internalisation (Figure 11B). Taken together, these results demonstrate that that the initial synchrony in the onset of cell behaviour was lost in the progress of tissue internalisation. Ingression is therefore not a process that follows a stereotypical program once it has started.

3.8. Ingression of the central mesoderm is associated with a continuous and gradually loss of synchrony of apical area constriction interrupted by small bursts of expansion

My findings indicate that cell ingression in the central mesoderm is associated with loss of synchrony in cell behaviour. To address whether this loss of synchrony stretched continuous over the course of mesoderm internalisation or if it was lost abruptly, I aimed to reveal and quantify the degree of synchrony in cell behaviour over time. To measure the degree of synchrony in cell behaviour, I again approximated cell behaviour with apical constriction and measured the area of central mesoderm cells at defined time points, i.e. every 5 min after onset of ventral movement. For each timepoint, I compared the distribution of cells over their apical area. The differences of distribution between each timepoint will show whether loss of synchrony is gradual and continuously or switched from a high to low degree of synchrony at a defined timepoint. As shown above, this analysis recapitulated the increase of variance with time (Figure 11C-C’’’’’’’). For the first five timepoints (5-25

min), the distribution of cells showed a clear maximum. Consistent with the idea of apical constriction, at each timepoint the maxima shifted towards a smaller apical area (about 10 percent of blastoderm area every 5 min). The spread of the distribution increased with each timepoint, with less and less cells contributing to the maxima. At 30 min and later, the distribution pattern did not show such a bell shape anymore. Except for one timepoint (40 min), cells did not cluster anymore but rather showed a normal distribution. This trend also increased with time. In conclusion, this analysis shows that the loss of synchrony was a gradual process, and not a step-wise process. The further internalisation progressed, the more individualised became the constriction behaviour of the cells.

The analysis of apical area over time for each cell suggest that ingression is driven by burst of apical constriction, and that frequency and amplitude of such bursts differs between cells. However, cells have been shown to differ in when they start to constrict, and, even more substantially, in when they internalise. To support this impression, I needed to reduce this noise. Therefore, I eliminated time differences by introducing for each cell a relative time measure. This was set to 100% and covered the period between when a cell first changed its area and the last time it could be observed and tracked. This way, it was possible to compare all cells with the same relative time resolution. In individual cells, constriction behaviour was clearly variable and often interrupted by short burst of expansion. Between cells, these bursts of expansions varied in amplitude, duration, and number (Figure 12).

Taken together, the analyses of apical constriction in ingressing mesoderm cells start to outline a possibly explanation for the observed heterogeneity in the overall

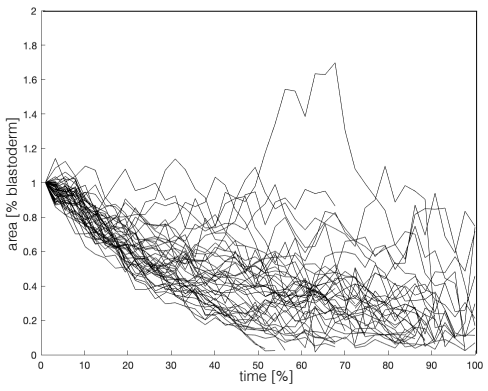

Figure12 Constriction is interrupted by bursts of expansion
Constriction pattern of individual cells with time adjusted to relative time between onset of constriction (0 percent) and timepoint of ingression (100 percent).

process. Each mesoderm cell overall constricted its apical surface. This process was interrupted by short bursts, in which cell area expanded again. So far, it seems unpredictable which cell expanded when and by how much. Under the assumption that these differences did not cancel each other out over time but instead accumulate, these small differences then led to the increase in heterogeneity that can be observed in the increase in standard deviation of apical area over time.

3.9. Ingression is characterised by apical area reduction and changes in cell surface morphology

So far, ingression has been characterised by changes of apical area. Reducing the process of ingression to the aspect of changes in apical area helped to understand that synchrony between cells was lost over time because short bursts of expansion interrupted constriction of cells, and the timing of these bursts varied between cells. The approximation of ingression by apical area was therefore a useful tool. Despite the mathematical measurement of area, the shape of a cell is also an important feature that has to be considered when characterising the apical side of a cell. Measuring the area alone does fully mirror the behaviour of the apical side of a cell. It does not reveal whether constriction is isotropic and cells constrict symmetrically/radial, resulting from an equal distribution of force over the apical surface of the cell. Or whether constriction is non-isotropic and constriction forces are spread out heterogeneously over the apical surface of the cell.

I checked for differences in apical morphology by eye and could observe substantial differences in apical shape. The apical surface of cells showed diverse shapes, such as triangular, round or rectangular. The most common shapes did not fall into one of these categories but instead were non-symmetrical (Figure 13 A-A’’’). Over the course of time, cells also changed their surface morphology. Asymmetrical surface morphology must be caused by differences in junction length, and following this line of thought, non-isotropic change of area must be caused by differences in behaviour of the junctions.
To resolve the different surface shaped further, I analysed the behaviour of individual junctions manually.

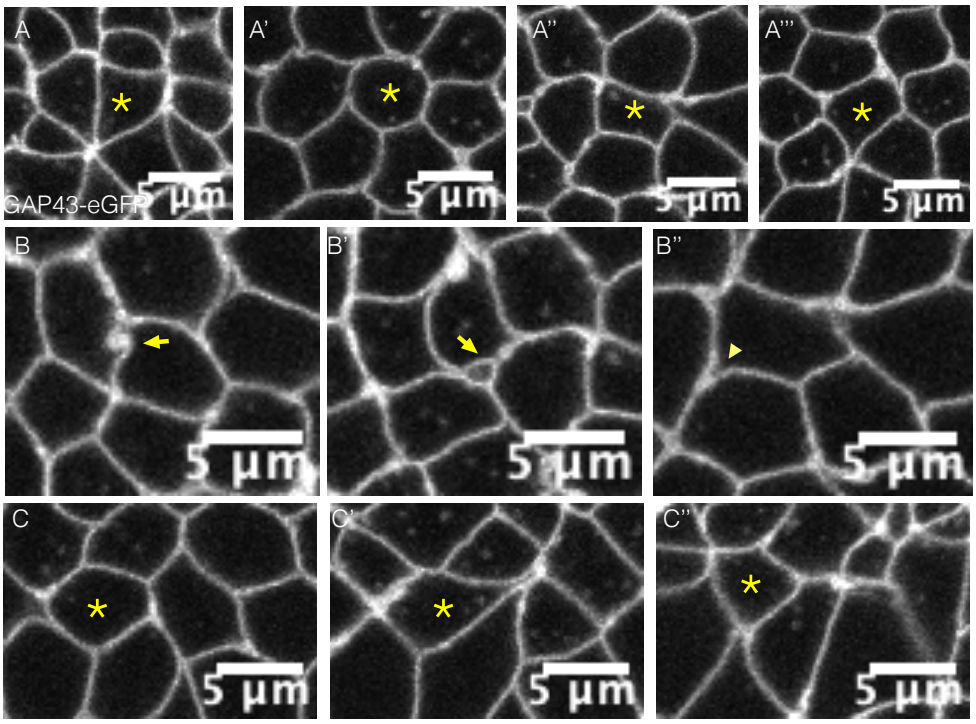

Figure13 Apical area and junction morphology are non-stereotypic
Sup apical view of cells during mesoderm internalisation. (**A**-**A'''**):Apical cell morphology diverges from stereotypically six-sided cell. Triangular (**A**), round (**A'**), rectangular (**A''**) and non-symmetric area morphologies can be found (**A'''**), cells highlighted with an Asterix. Individual junctions show signs of excessive membrane (arrow) (**B**), even to the point that holes form in between cells (**B'**). Junctions show V-shaped phenotype (arrow head) close to a vertex (**B''**).
(**C**-**C''**) Time series following the same cell being strongly deformed (**C**-**C'**: 12 min, **C'**-**C''**: 28,5 min:). Deformed cell is highlighted with an Asterix.

As expected, asymmetrical surface morphologies of cells resulted from differences in the length of junctions in the same cell. The junctions were not static but instead exhibited an extreme plasticity in their behaviour. Some junctions seemed to not be under tension. Instead of forming straight connections between cell vertex, which would indicate a degree of tension on the junctions, they were curved and convoluted (Figure 13B). In some junctions, it looked like there was excessive amounts of membrane, so that it bulged or even formed holes between cells (Figure 13B'). Then again, other junctions seemed to be under a lot of stress, so much so that they could pull their neighbouring junctions towards them. The neighbouring junctions themselves did not propagate the force they were exposed to throughout their entire length, but rather only a fraction of it became deformed. This resulted in a V-shaped phenotype, were the junctions showed a bend. Before this bend, the junction was exposed and deformed by the constricting junction, while after the bend the junctions remained in the previous orientation (Figure 13B''). The two ends of these tense junctions exhibit the stress differently, so that it looked like first one end

is under stress, then the orientation changed and the other end was being pulled together. In some cases, the tension on a junction was so high, that it could deform the entire cell. One side of the cell got pulled on heavily, so that it lost its hexagonal, or resembling, shape completely (Figure 13C-C'). This extreme experience of force was not always propagated within the same cell, so that one side looked heavily deformed while the other side remained unaffected. The immense tension could be resolved again, releasing the pull on the cell, so that it returned back to a shape similar to the one it had prior to the momentum (Figure 13C''). An overarching direction of tension in the tissue could not be observed, as junctions constricted independently of their orientation in the tissue.

In summary, the above makes clear that junctions had an independent constriction potential. This constriction potential was extremely diverse, it changed between junctions of a cell, but also in a temporal manner in the same junctions. This independent junction constriction seemed to be the main driver of changes in cell surface morphology. This analysis shows that the process of ingression is a combination of apical area reduction and anisotropic changes in surface morphology. The changes in surface morphology result from independent junction remodelling, causing an asymmetric surface shapes at the apical side of the cell.

3.10. Ingression is a combined process of apical constriction, cell surface morphology and change in neighbourhood

I have shown that ingression in the mesoderm of *C. riparius* is a process combined of apical area reduction and remodelling of surface morphology. Cells executed both features in a stochastic manner that does not allow to make predictions about the apical area and shape of a cell at any time during the process.

Individual cell movement has been described before in the fly notum [Marinari et al., 2012]. It has been shown that cells leave the tissue they reside in in a process referred to as delimitation. To reduce overcrowding, cells leave the tissue via a combination of apical area reduction and change in neighbourhood. A computational model showed further that cell anisotropy promotes delimitation. Once cells leave the

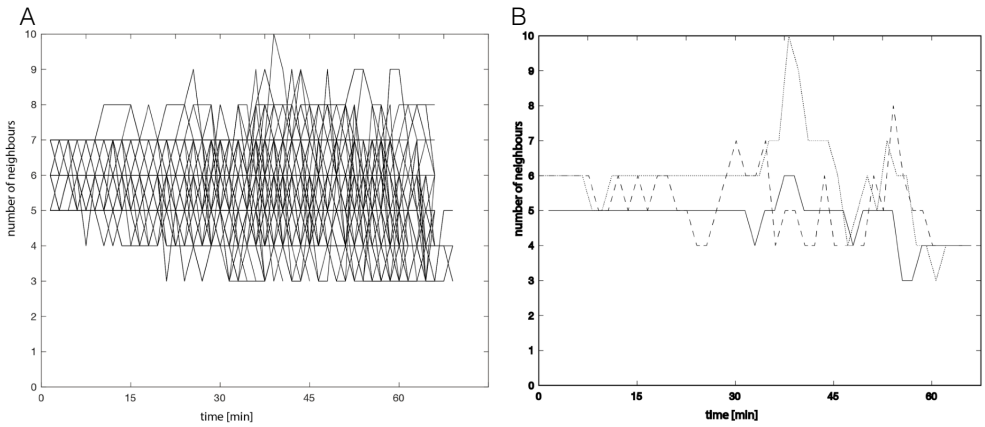

Figure14 Number of cell neighbours fluctuates over the course of time
Number of cell neighbours of individual cells over time (**A**) with three examples of extreme phenotypes of change in number of neighbour: some cells temporally have up to ten neighbours (dotted line), down to three neighbours (continues line) changed the number of neighbours frequently (dashed line) (**B**).

tissue, they undergo cell death [Marinari et al., 2012].
Migrating cells in the mesoderm are not programmed to undergo cell death like the cells of the notum do, but I wanted to see if the process of leaving the tissue shows similarities between *C. riparius* mesoderm and *D. melanogaster* notum. For the mesoderm, I could already show that ingression consists of apical constriction (Paragraph 3.5 -3.7) and anisotropic surface shapes (Paragraph 3.8). It remains to be investigated whether mesoderm cells also experienced a changing neighbourhood arrangement simultaneously to ingression.

The SEGGA tool provided information on the number of neighbours a cell has, which allowed me a qualitative, dynamic analysis of the direct neighbourhood of a cell. The cells in the *C. riparius* presumptive mesoderm indeed experienced a change in number of neighbours.
At the beginning of mesoderm internalisation, cells frequently switched between a state of having 5, 6 or 7 neighbours. At about 10 min after onset, this fluctuation increased and more often, the number of neighbours includes 4 or 8 cells (Figure 14A). Illustrated in Figure 14B are three examples of extreme cases, where number of neighbour either went up to 10, down to 3 or fluctuation was very heavy. All cells experienced a change in number of neighbours, but the frequency and extremes differed between cells.

Concluding from these results, it can be stated that ingression in the context of *C. riparius* presumptive mesoderm was always facilitated by a combination of apical constriction and a change in number of neighbours.

3.11. *Mesoderm cells ingress and intercalate simultaneously*

The frequent changes in number of neighbours indicates that the mesoderm is a plastic tissue, which gets remodelled during the process of mesoderm internalisation. Such tissue remodelling in the gastrulating fly embryo can be found in the extending germband [Irvine and Wieschaus, 1994]. Through cell intercalation via T1 transitions and rosette formation, the ectoderm tissue converges in its dorsoventral axis and extends in the anterior-posterior axis. To see if cell intercalation also happens in the mesoderm in *C. riparius*, I manually followed the junctions during the process of cell ingression and analysed whether or not they were involved in a neighbour exchange event (NEE).

NEEs happened frequently and the number of junctions involved in a NEE was extraordinarily high along the non-anterior-posterior (AP) junctions. Of about 100 cells (102 vs 108 cells per embryo), 102 or 137 junctions were involved in a NEE, resulting in 1 and 1.26 NEE per cell, respectively (Figure 15A). These NEEs occurred throughout the process of ventral closure/mesoderm internalisation, as early as 3 min after onset until ventral closure was almost complete (57 min) (Figure 15B). The difference in occurrence of NEE per cell in the different embryos showed again that mesoderm internalisation is a stochastic process in *C. riparius,* and embryos varied in their development. Additionally, to T1 transitions and rosette formation, T2 transitions can also be found in the ingressing mesoderm (Figure 15C-C''). This is not surprising as I could show earlier that the timepoint of ingression varies between

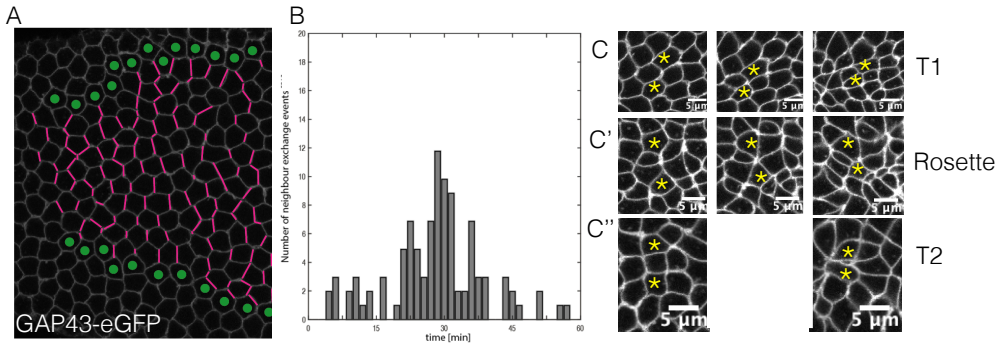

Figure15 Cells frequently exchange their neighbours
(**A**) Junctions of mesoderm domain visualised with Gap43-eGFP, membranes highlighted in pink will be involved in a neighbour exchange event over the course of mesoderm internalisation, green dots mark cells of the ectoderm, enclosing the mesoderm domain at both sides. Distribution of number of neighbour exchange events over time (**B**), with examples of the three neighbour exchange events T1 transition (**C**), rosette formation (**C'**) and T2 transition (**C"**). Two cells are highlighted with an Asterix that gain direct neighbourhood through the neighbour exchange event.

cells (paragraph 3.6). Naturally, when a cell ingresses, its previous neighbours gain a new neighbourhood arrangement.

A co-occurrence of apical constriction and neighbour exchange via T1 transitions and rosette formation has not been shown previously in *D. melanogaster* wt conditions. Cells either constrict their apical area or intercalate. The process of mesoderm internalisation in *C. riparius* therefore is based on a so far not reported phenomenon, namely the co-existence of two seemingly exclusive mechanism of cell shape changes. In *D. melanogaster*, both processes a temporally and spatial separated. First, the ventral cells constrict apically and get internalisation, and then cell intercalation in the ectoderm begins as part of the extending germband. The two processes depend on a different distribution of MyosinII (MyoII) in the cell. Apical constriction is driven by a strong medioapical pool of MyoII that constricts the cell isotropically [Martin et al., 2009]. On the contrary, for cell intercalation, a junctional, planar polarised pool of MyoII has been reported, that accumulates at the dorsoventral junctions. This pool of MyoII is responsible for the constriction of individual junctions [Kerridge et al., 2016]. Medioapical MyoII is also involved in cell intercalation, as it drives junction extension along the anterior-posterior axis (AP), but this pool is much weaker than the medioapical pool in constricting mesoderm cells or the junctional pool at the dorsoventral junctions. With apical constriction and cell intercalation happening at the same time in the same cells, strong pools of MyoII localisation should also be found simultaneously in a medioapical and a junctional position in the cell. I looked at MyoII endogenous localisation with a fluorescent

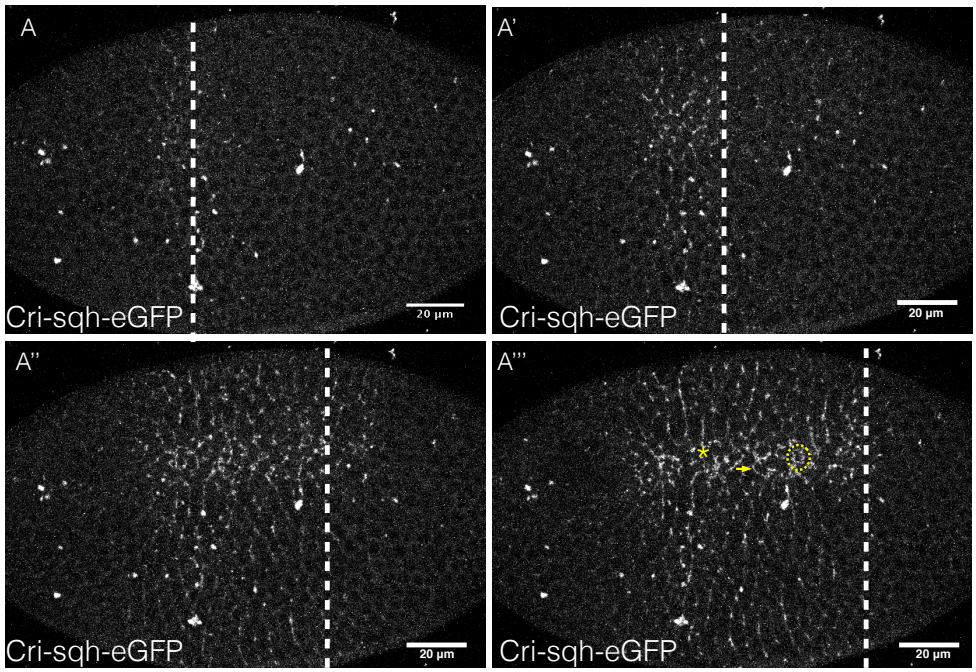

Figure16 Junctional MyoII can be found stochastically in the mesoderm
Maximum projection of Cri-sqh-eGFP at the ventral side of the embryo. Time series shows a wave-like expression pattern form anterior to posterior (**A-A'''**) the dotted line indicates wave front Cri-sqh-eGFP signal can be found as speckles (Asterix), elongated structures (arrow) and round structures (surrounded by dotted circle), scale bar 20 *µ*m

reported fused to the small regulatory light chain of MyoII, *sqh* (paragraph 3.2). Preliminary data on MyoII localisation in the apical side of the presumptive mesodermal cells hint to support this hypothesis of two pools of MyoII in the cells.

The MyoII signal could first be detected at the anterior end of the mesoderm tissue, where it formed speckles at the apical side of the cell (Figure 16A). The appearance in speckles moved in a wave towards to posterior end, which took 35 min for the whole mesodermal tissue to show MyoII staining (Figure 16A'-A'''). These speckles could be the medioapical pool of MyoII. In addition to these speckles, elongated structures of MyoII could be found, which might be the junctional MyoII pool. Interestingly, the junctional MyoII pool was not organised in a planar polarity manner as it was in the ectoderm. This junctional pattern was sometimes so that it looked like the MyoII signal outlined the hole cell circumference in a radial polarity (Figure 16A''').

To make definite statements about the medioapical or junctional character of MyoII, a co-labelling of MyoII and the cell membrane needs to be made. From this, it

will be easy to identify the localisation of MyoII and verify the hypothesis of two strong MyoII pools in the same tissue.

3.12. Mesodermal cells experience a displacement along the anterior-posterior axis as well

As stated before (paragraph 3.9), cells in the mesoderm show two different cell behaviours at the same time, ingression and cell intercalation. Cell intercalation has been described before and studied in the extending germband of the gastrulating fly embryo [Collinet et al., 2015]. Here, cell intercalation causes a deformation of the tissue. When cells constrict their dorsoventral junctions and extend new junction is an anterior-posterior direction and maintain their area, this is reflected also in the tissue morphology. The tissue converges in the dorsoventral axis and extends along AP.

The influence of cell intercalation on tissue morphology in the presence of apical constriction has not been studied. In the *C. riparius* mesoderm, intercalation is accompanied by apical constriction, so the area is not maintained. An expansion of the tissue therefore does not necessarily have to follow the convergence of the tissue in this case. The constriction of the mesoderm tissue along the dorsoventral axis has been shown above (Figure 9C-D). To observe a potential expansion along AP, I tracked the centre of the apical area of individual cells for both the anterior and posterior population as proxy for the tissue expansion. The cells showed a strong displacement towards the ventral midline, which was expected. Additionally, they also experienced divergence along the AP axis (Figure 17A). These cell tracks showed that also in the context of mesoderm internalisation in *C. riparius*, T1 transitions and rosette formations correlated with a convergent-extension of the tissue. Surprisingly, the extension of the tissue was much more pronounced in the posterior population than in the anterior population.

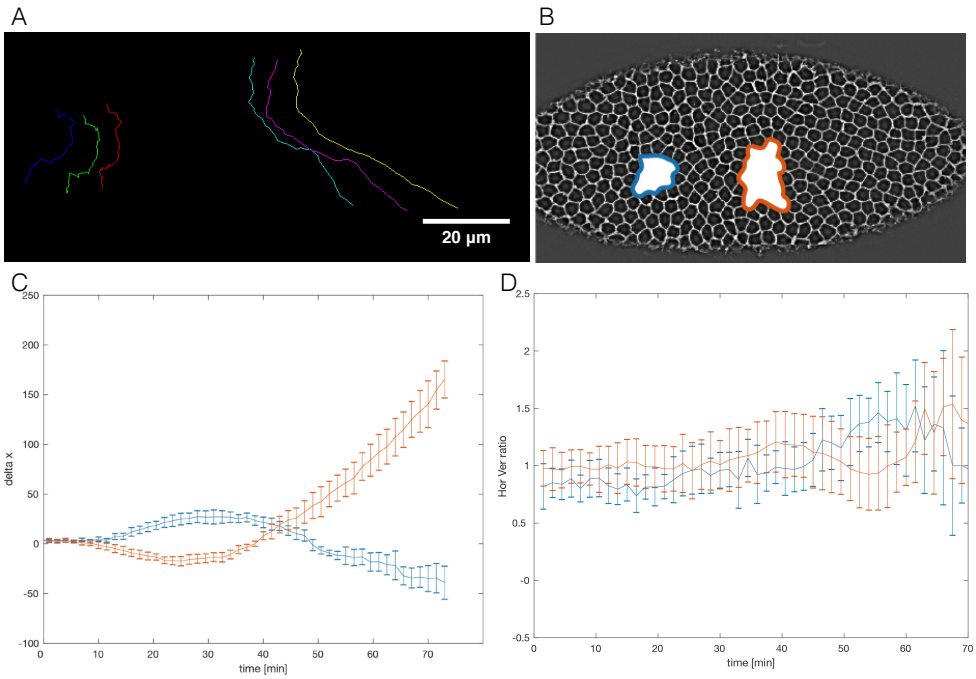

Figure17 Cells experience unequal displacement along the anterior-posterior axis
Individual cell tracks (**A**) from an anterior and posterior population highlighted in (**B**), anterior population represented in blue, posterior population represented in red. (**C**) Mean and standard deviation of Δ X coordinate normalised to X coordinate in blastoderm, during mesoderm internalisation, anterior population in blue, posterior population in red. Mean and standard deviation of cell stretching visualised by the ration of the horizontal vs vertical axis of each cell, the value of 1 meaning that both axis are of equal size (**D**).

To capture the differences in the displacement of cells along the AP axis between the two cell populations a more quantitively analysis needed to be established. I referred back to the single cell data obtained by the SEGGA analysis. Additionally, to data on apical area, SEGGA also provides information about the position of each cell with the x coordinate presenting the position of a cell along the AP axis, and the y coordinate specifying its position along the dorsoventral axis. I defined two populations of cells, each spanning over three rows of cells, one at the anterior border of the analysed mesoderm domain and one at the posterior (Figure 17B). I normalised the X coordinate of each cell to its position in the blastoderm and compared the mean of the normalised x coordinate of the two populations over time. Any anterior movement of cells resulted in a decrease of the delta x value, and posterior movement increased it.

Very early on, about 5 min after the onset of mesoderm internalisation, the displacement of the cells started. Surprisingly, this first AP directed movement of the populations was towards each other. This was shown by the anterior cells being displaced towards the posterior (increase of the values) and the posterior cells towards the anterior (decrease of the values). About 30 min after onset of ventral

movement, a change in direction of cell displacement could be observed. From this point on, the anterior population was experiencing a displacement towards anterior, and the posterior population towards posterior. The displacement of the posterior population was stronger than that of the anterior and differences between the two populations also increased over time. Finally, the two populations had diverged from one another by ~200 a.u. (Figure 17C).

These findings show two things. First, prior to the extension, the tissue also temporally constricted along the AP axis. The constriction of the tissue along AP could be caused by the apical constriction of ingressing cell. Secondly, the anterior and posterior population indeed differ greatly in the displacement along the AP axis.

The differences in tissue expansion could result from differences in cell morphology. It is possible that cells in the posterior elongated more along the AP axis than cells in the anterior. An accumulation of elongated cells could lead to a tissue elongation. The cell tracking and SEGGA analysis were done via tracking the centre of a cell. The position of the area centre does not indicate the morphology of the cell. Possible differences in cell stretching were not taken into consideration.

To test the hypothesis that the difference in tissue displacement were caused by differences in cell morphology in the anterior and posterior population, I considered the ration between horizontal (along the AP) axis and vertical (along dorsoventral) axis of the cells. If a cell was not stretched in any direction, the ration should be 1, an elongation of cells in AP caused the value to increase, while an elongation along the dorsoventral axis would decrease the value of the ration. For both populations, the horizontal-to-vertical ration of cells remained without great changes for most of the ingression process. In the anterior population, cells did not experience a stretch, as the ratio was close to one. In the posterior population, cells were first stretched along the dorsoventral axis but gradually lost such a stretch and the ratio became closer to one. After about 45 min after first ventral movements had started, cells started to experience more stretches, but never diverged far from a value close to one (Figure 17D). Concluding from this data, the differences in AP extension of the presumptive mesoderm tissue did not result from cellular deformations.

If the differences in AP displacements between the two cell populations is not driven by the cells of the mesoderm themselves, an external tissue must influence

mesoderm cells in their displacement behaviour and be responsible for the differences along the mesoderm tissue. Two possibilities come to mind, either a tissue anteriorly of the mesoderm inhibits extension in this direction and the mesoderm tissue has to evade in the only direction possible, posteriorly. Or, an external force is pulling on the mesodermal tissue from its posterior end, and this force is not propagated equally through the tissue. In the gastrulating fly embryo, evidence for both these scenarios can be found. Anteriorly to the mesoderm the head-truck separation can be found. In *C. riparius*, this is defined by a ring of mitotically active cells around the embryos (Figure 9A and Tok, 2019). In the posterior, the process of GBE sets in, beginning with the invagination of the posterior midgut. Both processes might have an impact on mesoderm tissue extension. The head-trunk separation might serve as a physical barrier, inhibiting mesodermal tissue from expanding further. The invagination of the posterior midgut at the same time might pull the mesodermal tissue towards the posterior pole of the embryo. How exactly the tissues interact with one another is not known. A precise description of the developmental timeline of all processes of gastrulation in *C. riparius* needs to be generated to be able to correlate different movements temporally. Once the temporal order is understood, precise experiments can be planned to understand the interplay between different gastrulation movements.

3.13. Influence of Folded Gastrulation (Fog) on mesoderm internalisation in C. riparius

Previous analyses of mesoderm internalisation in *C. riparius* highlighted a major difference to mesoderm internalisation to *D. melanogaster* in that the process appeared to be independent of *fog*-controlled GPCR signalling (see introduction). Furthermore, the injection of *fog* mRNA and ectopic activation of GPCR signalling in the early *C. riparius* embryo substantially altered the morphogenetic process and led from a process of single cell movements to collective cell movements [Urbansky et al., 2016]. These analyses had been carried out in fixed embryos based on the analyses of nuclei that served as faithful proxies of cell position. The authors resulted in a working model in which randomised apical constriction was the main cause for single cell movements in the *C. riparius* mesoderm, and *fog*-induced GPCR signalling resulted in collective cell movements by a speeding up and harmonising apical cell constriction. My analyses of cell dynamics in the *C. riparius* mesoderm now indicate that cell-cell connectivity and the randomised junction remodelling play a critical role in mesoderm cell ingression, which suggests that injected *fog* in *C. riparius* may alter cell and tissue behaviour beyond the previously proposed harmonisation of apical constriction. To address this possibility, I revisited the effects of *fog* injection on *C. riparius* mesoderm formation using my newly established in vivo imaging toolkit.

3.14. Blastoderm is more tightly packed in C. riparius embryos with ectopic fog expression

In comparison with wt embryos (Figure 8A), the blastoderm in *fog* over-expressing embryos showed only very few irregularities in the membrane alignment and divergence from the honeycomb pattern. As mentioned before, two different phenotypes in respect to cell arrangement could be found in the wt blastoderm. Slow developing embryos showed many sites of membrane irregularities, fast developing embryos had a more honeycomb-like blastoderm cell arrangement. From the three kinds of membrane abnormalities, all could be found also in the *fog* over expression background (Figure 18) but with a much reduced occurrence. Holes between two

cells were found only scarcely (0.008, 0 holes/cell) and also the number of spots of excessive membrane were much reduced (0.03, 0.008 bulges/cell). The most abundant membrane irregularity was still the phenomenon of convoluted junctions, yet this was also much reduced compared to the slow developing wt embryos (0.14, 0.05 convoluted membrane/cell) (compare paragraph 3.3). This shows that cells are tighter packed than under wt conditions of slowly developing embryos.

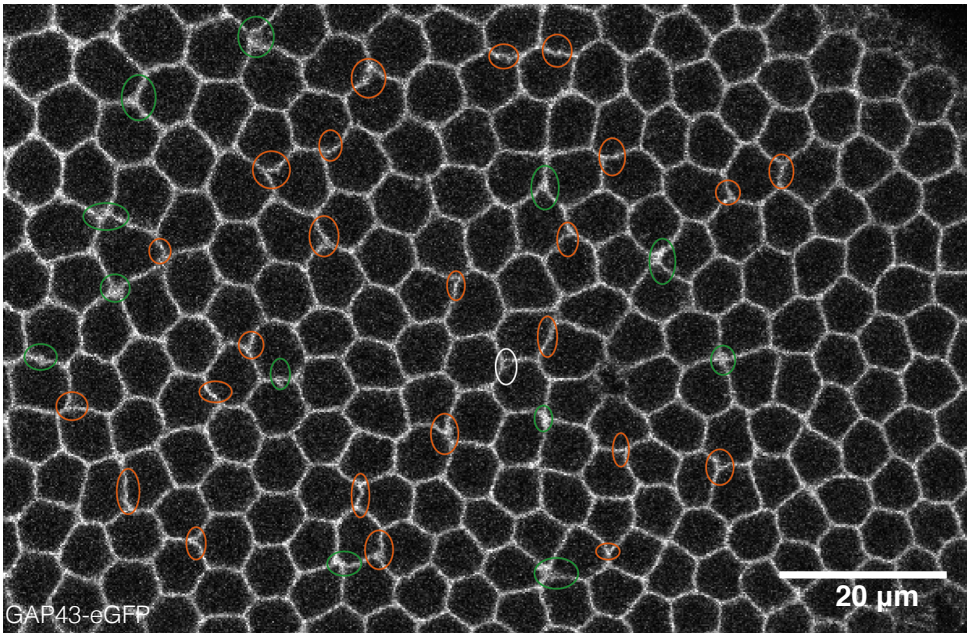

Figure18 Cells are tighter packed in the blastoderm upon *fog* over expression
Subapical view of the blastoderm embryo, co-injected with *Gap43-eGFP* mRNA(membrane label) and *Cri-fog* mRNA showing 3 different phenomena (1) holes between two cells (marked in white) (2) excessive membrane (marked in green) and (3) junctions which do not form a straight line between two vertexes (marked in orange).

3.15. Mesoderm internalisation is overall faster after ectopic fog expression

As expected, the mesoderm anlage was unaffected by *fog* overexpression. Using the above described method of backtracking (Figure 9A) reveals that the mesoderm anlage was of the same dimensions as in wt embryos. At the anterior boarder (35 µm in width) 6-7 cells span the mesoderm anlage in the dorsoventral axis, and 11-13 cells at the posterior border (55 µm) (Figure 19A). Similar to what can be observed in the wt (Figure 9D), independent form the number of cells spanning over the

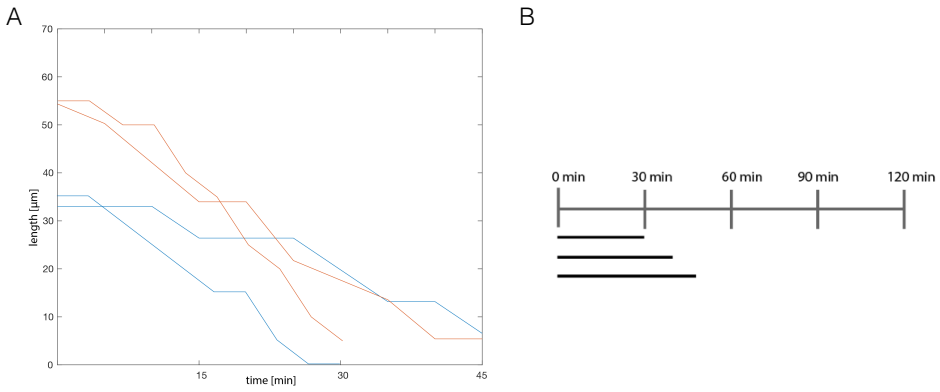

Figure19 Mesoderm internalisation is faster upon *fog* over expression
(**A**) Width of the mesoderm domain at the anterior (blue lines) and posterior border (red lines). Two embryos were analysed, the graph for the anterior and posterior plotted over time (n=2).
(**B**) Plot showing absolute time of mesoderm internalisation indicated by individual lines for individual embryos (0 min = Onset of cell movements).

presumptive mesoderm, ventral closure was happening simultaneously along the AP axis. From this I can conclude that the core process of ventral closure was unaffected by *fog* over expression and differences in mesoderm internalisation were not caused by a difference in prepatterning and tissue anlage.

The process of mesoderm internalisation over all was faster than under wt conditions, where mesoderm internalisation took 45 to 80 min (Figure 9F). It took between 30 and 48 min (n=3) for the presumptive mesoderm tissue to get internalised in *fog* over expressing embryos (Figure 19B), making it on average considerably faster than wt embryos. This data is constant with the observations drawn from wt analysis, namely that embryos with a tighter cell packing in the blastoderm stage experience faster mesoderm internalisation.

3.16. Fog does not cause a harmonisation of apical area constriction

Fog over expression has been shown to have a significant impact on mesoderm internalisation [Urbansky et al., 2016]. Upon *fog* over expression the mode of mesoderm internalisation changes from single cell movement to collective cell movement. The switch could be facilitated by a harmonisation of apical constriction. If all cells constrict their apical area simultaneously, following the same constriction

pattern, the stochasticity of cell ingression could be turned into a coherent tissue invagination.

The close examination of apical constriction in the wt phenotype revealed that *C. riparius* cells indeed show little signs of homogeneous apical constriction. Cells constricted their apical area asynchronously and all followed an individual constriction pattern (paragraphs 3.7 and 3.8). If the assumption mentioned above is correct, *fog* over expression should bring order to the apical constriction behaviour of cells. To gain a rough overview of apical constriction in a *fog* over expression background, I looked at the mean of apical area over time. The process of mesoderm internalisation was in general faster than under wt conditions (Figure 9F), which should be recapitulated also in the speed of constriction of the individual cells. Indeed, it took on average about 30 min for a cell to constrict its apical area and vanish from the surface of the embryo. Many cells diverged from the mean though, resulting in a high variance of apical area at all time points (Figure 20A). This analysis shows already, that *fog* over expression did not homogenise the overall constriction mechanism of mesoderm cells. *Fog* over expression still might have an influence on a specific aspect of constriction which was not captured in the rough analysis. I therefore looked at onset of constriction, timepoint of internalisation and individual constriction pattern of cells and compared them to the data obtained from wt.

First, I wanted to see if apical constriction began in all cells at the same time. Just like in the wt analysis, I analysed cells for when they constricted their apical area by 10 percent and looked at the distribution of when cells reached this threshold (see paragraph 3.7). Compared to the wt situation, where about 80 percent of cells reached this threshold within the first 10 min of constriction (Figure 11A), the distribution of cells in a *fog* over expressing background was much wider spread. Only about 55 percent of cells reached the threshold within the first 10 min, the remaining cells all reached the threshold with a wide distribution (Figure 20B). Fog therefore did not have a harmonising effect on the onset of constriction in cells. In fact, the opposite is the case. The internal synchrony of when to begin apical constriction that can be found in wt embryos was lost after *fog* over expression.

Next, I analysed the timepoint of internalisation, defined as a cell having reduced its apical area by 90 percent (see paragraph 3.7), and looked at the distribution of

when cells fell under the threshold. The timepoint at which cells got internalised varied greatly between different cells. Cells were normally distributed, with the majority of cells, ~50 percent, getting internalised between 25 and 35 min after onset of ventral movement. The remaining cells were spread in a normal distribution (Figure 20C). Comparing this distribution pattern to the one of the same analysis in wt (Figure 11C) revealed that there is no difference between the two phenotypes. Under both conditions, the distribution was wide spread and showed no distinct maxima, indicating little synchrony between the cells.
Comparing the synchrony of cells at the onset of constriction and at the timepoint of internalisation shows that the low, but present synchrony at the beginning of the process was completely lost at the end of it. Just like for the wt, the question resulting from the observation in of loss of synchrony is if synchrony was lost gradually or if it was lost at a specific timepoint.

For a better temporal resolution of the increase in heterogeneity, I looked at the distribution of cell area in 5 min intervals (Figure 20 D-D’’’’). The more the process progresses, the more the distribution of cells was spreading. 5 min after onset of ventral movement, less than half the cells had started constriction, and the ones that did had not constriction much yet. Thus, the cells therefore still clustered together. With every new 5 min time point, this clustering of cells got more and more diffused. Already 15 min after onset of ventral movement, no such cluster was detectable anymore, cells were distributed normally. Another 10 min later, so 25 min after onset of ventral movement, cells were almost equally distributed in relations to their apical area. These analyses show that the increase of heterogeneity between onset of constriction and timepoint of internalisation was gradual and continuously, just like in the wt (Figure 11C-C’’’’’’’), the degree of heterogeneity did not change dramatically between two timepoints.

Finally, I checked whether the constriction pattern of individual cells was homogenised in the presence of Fog. To determine the constriction pattern and compare it between cells, I changed the time scale from absolute time in min to a relative time scale, set individually for each embryo between first timepoint of constriction to last measurable timepoint, just like for the wt analysis (paragraph 3.8). Looking at apical area changes over the relative time showed that the variance between individual cells remained high. Constriction was interrupted by bursts of

expansion, that varied in their frequency and amplitude drastically between individual cells (Figure 20E). From this analysis is became clear that Fog did not smoothen the constriction pattern of cells.

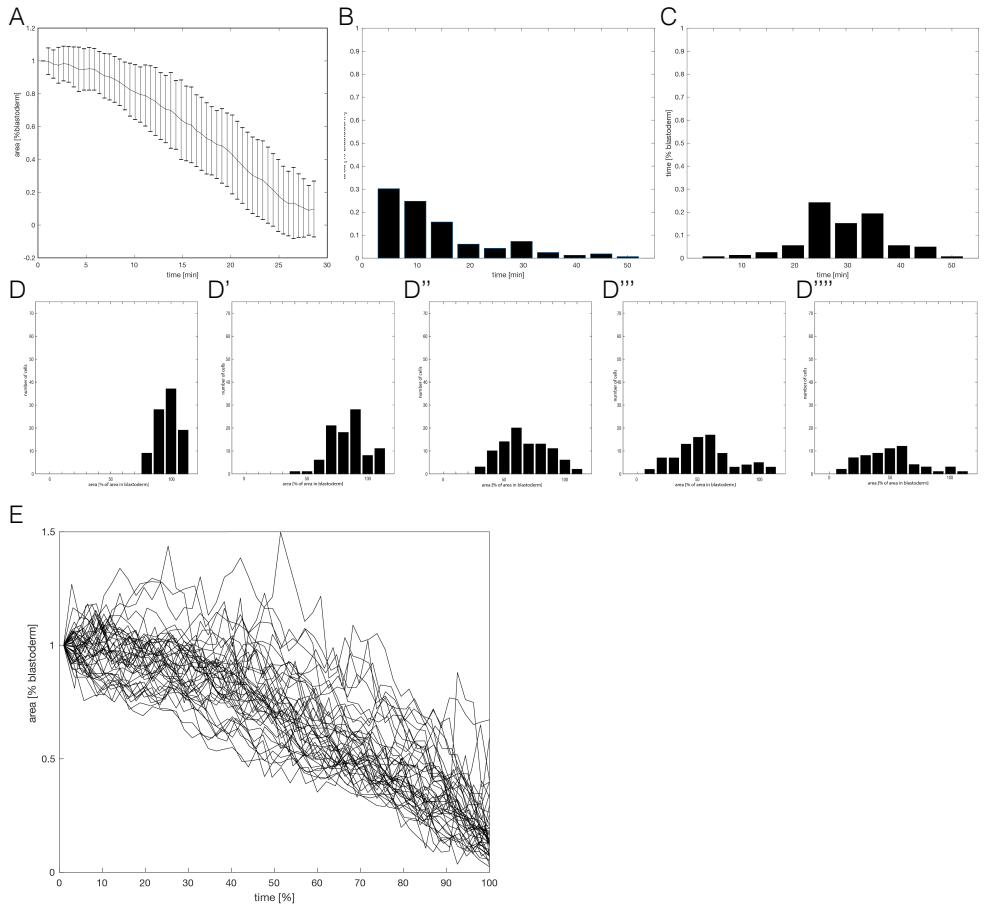

Figure20 Fog does not harmonise apical constriction
Apical area constriction of individual mesoderm cells normalised to their apical area in the blastoderm. Apical area constriction of cells is on average fast, but standard variation is constantly high (**A**). Distribution of cell for when they start apical constriction (constriction of apical area by more than 10 percent) (**B**) and timepoint of internalisation (constriction of apical area by more than 90 percent) (**C**) over time. Distribution of cell area, each plot shows a 5 min intervals (**D-D''''**). (**E**) Constriction pattern of individual cells, relative time set for each cell individually from timepoint of constriction (0 percent) to ingression (100 percent).

In conclusion, these analyses on apical constriction show clearly that *fog* over expression did not have an ordering impact on apical area constriction. Apical constriction did not become more homogeneous compared between cells in the presence of Fog and wt. The idea of gaining a collective cell movement through homogenising the apical constriction has to be dismissed. In my in depth wt description I could show that apical constriction was not the only cellular behaviour which is happening in the ingressing *C. riparius* mesoderm. Cells were additionally changing their neighbours frequently and experienced a displacement along the AP

axis of the embryo (Figure 15 and 17, respectively). During the entire process of mesoderm internalisation, cells were loosely packed and showed signs of low cell-cell connectivity.

The over expression of *fog* might have an influence on one of these tissue characteristics. A change in cell behaviour independent of apical constriction might be responsible for the change in the mode in internalisation in *C. riparius* from single to collective cell movements.

3.17. Junction remodelling is more homogeneous in the presence of Fog

In the wt *C. riparius* mesoderm, cells were often asymmetric in shape and were loosely packed, which was likely caused by a great difference in individual junctions appearance (Figure 13). Over expressing *fog* had a visible effect on the junction behaviour. While in the wt, some junction showed a phenomenon of excessive membrane, sometimes even to the degree of forming holes between single cells, this was greatly reduced in *fog* over expression. No holes were formed between cells during mesoderm internalisation and the junctions did not show signs of excessive membrane. Only occasionally, junctions were convoluted or showed the V-shape phenotype, the latter mainly in connection with a T1 transition. This resulted in cells that were more angular and more symmetrical cells. Interestingly, cells occasionally aligned in multi-cellular clusters, in which cells had almost rectangular junctions and thus were almost aligned in both horizontal and vertical direction (Figure 21). These arrangements were held in place for about 5 min and then get resolved again.

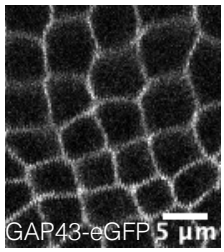

Figure21 Fog causes straighter junctions and more symmetrical cells.
Example of mesoderm cells after co-injection of Gap43-eGFP(membrane label) and *Cri-fog* mRNA scale bar 5 μm

These results show that heterogeneity of the junction remodelling was reduced upon *fog* over expression, and junctions seemed to be under higher tension. This caused junctions to be more oriented in a straight line form one vertex to another. This in turn resulted in cells with more symmetrical apical area morphologies and a tighter cell packing in the tissue.

3.18. Number of neighbour exchange events is not reduced by fog over expression

Cell neighbour exchange happened frequently in the mesoderm cell in *C. riparius* wt (Figure 15). Since Fog has been shown to be important in the context of cell intercalation in the ectoderm in *D. melanogaster* [Kerridge et al, 2016], over expression of *fog* might have an influence on NEEs in *C. riparius* as well. Tracing individual junctions again, like in the wt analysis, revealed that the frequency of NEE did not decrease in the *fog* over expression background. NEE per cell was either at a rate of 1.21 NEE/cell, comparable to the frequency in one wt embryo (Figure 15), or even increased to 1.6 NEE/cell. The NEE also occurred earlier, directly after onset of ventral movement (1 min) and throughout the process (Figure 22), until almost the point of ventral closure. All three types of NEE, T1, rosette and T2 occurred in the fog over expression background as well.
Comparing two *fog* over expressing embryos with different phenotypes makes it difficult to judge the impact of Fog on NEEs. More embryos have to be analysed before a clear statement about the influence of Fog on NEEs in the *C. riparius* mesoderm can be made.

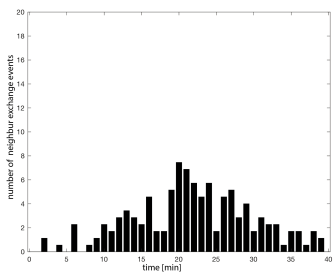

Figure22 Neighbour exchange is not reduced by Fog expression
Distribution of number of neighbour exchange events over time.

An increased number of NEEs hint at the overall tissue architecture as being more plastic. This is contradictory with the analysis of cell und junction morphology. NEEs need to be analysed more in detail, e.g. the spatial resolution of NEEs, to understand the process better and connect it to the other observed phenotypes in a *fog* over expressing embryo.

3.19. External force is more uniformly propagated in the tissue

I could show that cells were tighter packed in the blastoderm and remained in such a way over the course of mesoderm internalisation (Figure 18 and 21). A tight cell packing can have an influence on the propagation of an external force, as it might be transmitted more smoothly through the tissue when the junctions are under tension. If this is the case, the differences in posterior displacement of anterior and posterior cell populations should be reduced when *fog* is over expressed.

There were differences when comparing the data between the different *fog* over expressing embryos, so I focus here primarily on the embryo with the more pronounced phenotype, as the other one resembled the wt phenotype. The first difference compared to the wt phenotype is the reduction of a 2 phased process of constriction along the AP axis followed by an elongation. Instead, a direct and continuous displacement towards the posterior could be observed in the whole tissue (Figure 23A and B). Both, anterior and posterior cells, were primarily (first 5 min) displaced with the same speed, and then the speed of displacement was slowed

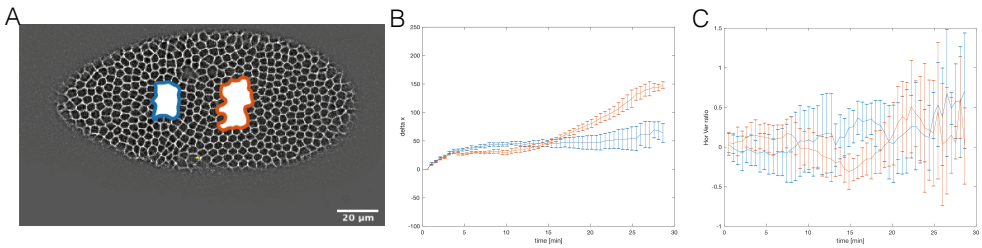

Figure23 Fog causes coherent tissue displacement towards posterior
The change of displacement along the AP axis of the embryo of cells from two populations of the embryo, highlighted in (**A**) anterior population in blue, posterior population in red. Mean and standard deviation of AP-coordinate of each cells in the population compared to its AP-coordinate in the blastoderm over time (**B**). Ratio of horizontal to vertical axis of each cell over time, averaged over the corresponding population (**C**).

down and almost stagnated for about 5 min. It is to be mentioned here, that the posterior population experienced a stronger impulse to stagnate, so that the relative displacement towards posterior was greater in the anterior population. At again a five minutes interval of stagnation, the posterior population experienced a heavy and steady posterior displacement. In contrast to this, the anterior population of cells remained in a weaker displacement slope, but equally steady. This resulted in a divergence of the two populations in respect to their total posterior displacement at the end of mesoderm internalisation. Yet, the difference of delta x, meaning displacement in the X coordinate (paragraph 3.12), between the anterior and posterior population was smaller in the *fog* over expression compared to the wt. Under both conditions, the external force, mostly likely the onset of GBE, set in after about half the time needed until the mesoderm was internalised completely. At the end of mesoderm internalisation, the posterior displacement was at a comparable level (150 a.u. in fog, 160 in wt) for the posterior population, yet a great difference could be found in the anterior population (60 vs -20 a.u.). This shows that the anterior cell population was displaced much more towards the posterior in the presence of Fog. In contrast *fog* over expression had no effect on the posterior population.

The difference between both conditions lets me hypothesis the following: Under wt conditions, cells are more plastic, due to individual junction remodelling. This buffers out the posterior displacement of cells induced by an external force in the posterior which pulls strongly on the cells. Towards the anterior, the force is lost. The sum of cell and junction deformations that happen between the posterior and anterior population counterbalances a propagation of the external force.
In contrast to this, the force is propagated much more smoothly in the cells expressing *fog,* facilitated by the tighter cell packing in the tissue and less deformations of cells and junctions. This propagation is so strong that it overshadows the movement towards the anterior in the anterior population.
I raise the hypothesis, that the differences in posterior displacement between wt and *fog* over expression are caused by a tighter cell packing, resulting in a propagation of the external force through the mesoderm tissue. To be able to do so, I have to exclude that posterior displacement is as false refection of changes in cell stretching along AP (see paragraph 3.12). Just like in the wt, I compared the ratio between horizontal and vertical axis for cells in the anterior and posterior population.
Small changes in the ration of horizontal vs vertical axis could be observed early on

between the two populations but the orientation of the stretch changed frequently in both populations. At the end of mesoderm internalisation, the anterior population was stretched more along the AP axis, but this elongation happened only during the previous 5 min (Figure 23C).

Overall, the cell stretching showed no great difference between the anterior and posterior population. Additionally, no difference between wt and *fog* over expression could be observed in the way cells stretched their apical area. It is unlikely, that the small changes in cell morphology play a major role in tissue displacement. This strengthens my hypothesis that the homogeneous posterior displacement of the cells resulted from increased cell packing and less cell deformation.

3.20. Nuclear position is unaffected by Fog

As mentioned before, during the process of mesoderm internalisation, the nuclei experience a basal dropping in the cells [Kam et al., 1991]. Not much is known about the mechanism. The nuclear drop might be driven genetically or physically, as a result of cell shape changes. My pipeline to analyse the position of the nucleus in a cell can be used to determine whether the over expressing *fog* had an influence on the nuclear dropping mechanism. If nuclear position changed within the cell, the expression of *fog* would be the first link to a genetic network underlying nuclear dropping.

Just like in wt, embryos were fixed at 10-15 percent GBE and stained for membrane and nuclear signal. Cells were segmented and grouped into three categories, columnar, bottle shaped or enlarged apical area (see paragraph 3.1). When looking at the percentage of cells according to their category, it becomes clear that the number of columnar cells, so not yet having begun ingression, was reduced compared to the wt. Both, the number of bottle shaped cells and cells with an enlarged apical area had increased (Figure 24A). This indicates that the process of mesoderm internalisation was more progressed over all. When mapping the cell shape back onto the position of the cells, more bottle-shaped cells can be observed in the ventral part of the embryo (Figure 24B).

To determine whether there is a difference between the nuclear position in internalising cells themselves between wt and *fog* over expression, I looked at the position of the nucleus in the bottle shaped cells. In both phenotypes, nuclei resided in the same position along the apical-basal axis (wt: 46, fog: 45 percent cell length, n= 3 embryos, 317 cells) (Figure 24C-C', compare to Figure 6E). This clearly shows that *fog* over expression did not have a direct impact on the position of the nucleus in the cells.

Nuclear dropping might still be regulated via a genetic network, but Fog does not act in it.

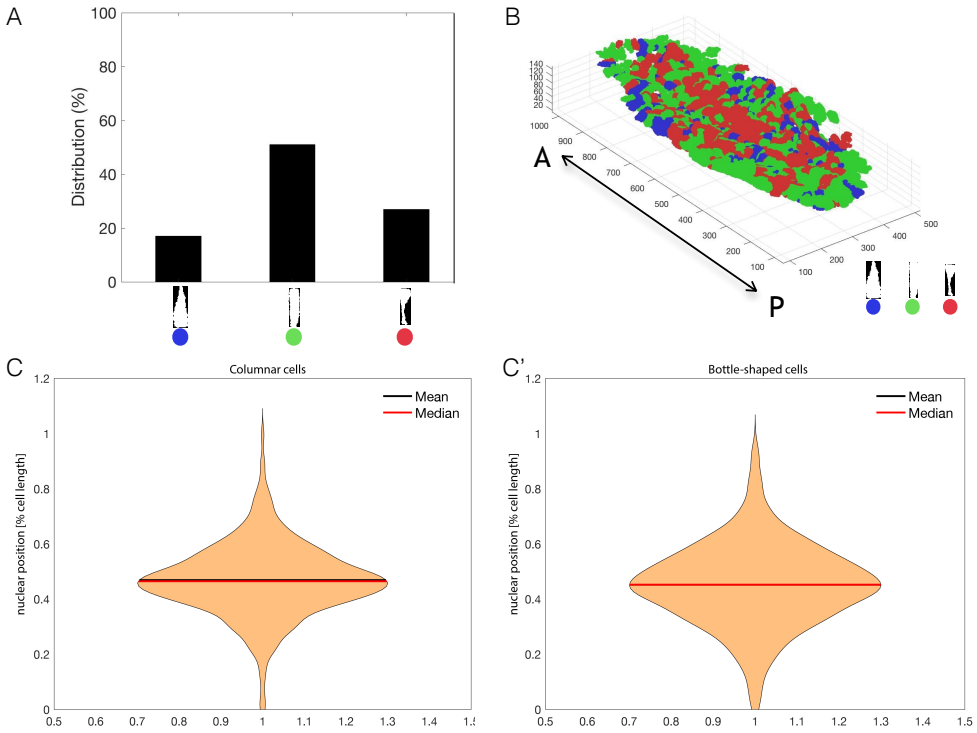

Figure24 Nuclear position is not effected by *fog* over expression
Pointclouds representing cells of the ventral and ventrolateral region of a *fog* over expressing embryo, fixed at 15 percent GBE. Cells are grouped and colour coded in three categories (1) increased apical surface (blue) (2) columnar (green) (3) bottle shaped (red) **(A**). Percentage of cells according to groups, cells in their original position coloured in the colour code of A (**B**). Position of the nucleus of in columnar cells (**C'**) and bottle-shaped cells (**C")**, 0 percent at apical side of the cell, 100 percent at basal side of the cell. n= 3 embryos, 1268 cells

4. Discussion

In this thesis, I characterised the morphogenetic movement of mesoderm internalisation in the midge *Chironomus riparius* (*C. riparius*) on a cellular level. The establishment of the first protocol for life imaging of cell components, such as cell membrane or Adherens Junctions (AJs), was successfully achieved as a prerequisite. Data on dynamic cells movements revealed that mesoderm internalisation is indeed a process of ingression with a salt-and-pepper-like fashion of temporal differences between cells. This difference in cell behaviour is caused by an accumulation of small bursts of expansion interfering with constriction of the apical area. In addition, there are indications suggesting that loose cell-cell contacts and a high heterogeneity in junction mobility cause the stochasticity in ingression behaviour between cells.

The secretion protein Folded gastrulation (Fog), a ligand to the G protein coupled receptor (GPCR) pathway, has previously been shown to affect mesoderm internalisation and to change cell movements from single cell to collective cell movement [Urbansky et al., 2016]. In this study, I investigated the impact of *fog* over expression on cellular behaviour. *Fog* over expression does not result in a homogenisation of apical constriction between cells, as has previously been hypothesised. Instead, I found evidence that in the presence of early *fog* expression, heterogeneity of junction mobility is reduces and cell-cell contact is tightened. Cell internalisation is thus not just a cell autonomous process anymore, but cells interplay and “pull each other inwards”, causing the process to resemble a coherent tissue movement.

4.1. Presumptive mesodermal cells do not act as a coherent tissue

Fly gastrulation is a good model to study differences in morphogenesis. Even though the species are very diverged, the basic hall marks of early development are similar between species, differing only in detail.

Comparing the development of *C. riparius* to *Drosophila melanogaster* (*D. melanogaster*), such differences are already present very early on. Even before the onset of gastrulation, the blastoderm in the two species differs. While cells in the higher flies are organised in a strong honeycomb pattern [Simpson et al., 2014], blastoderm in *C. riparius* is much less tightly packed. Cells frequently “jiggle in their position” and change their neighbours temporarily. Between the cells, the cell-cell connections are not very strong, so that cell membranes are convoluted and even from small holes in between cells. These membrane irregularities also form constantly during the process of mesoderm internalisation. Additionally, cells change their neighbour frequently, which indicates that the mesoderm is a plastic and deformable tissue. This hypothesis is supported by the fact that an external force is not propagated equally through the tissue. The fact that cells in the presumptive mesoderm are individual “entities” that do not form a coherent tissue explains why cells are internalised via ingression as single cells instead of invagination as a tissue.

4.2. Differences in apical constriction come from heterogeneous MyosinII pools

Ingression is primarily characterised by the stereotypic bottle-shaped cell morphology with a reduced apical area. I was able to show that cells in the C. riparius mesoderm also transform into bottle-shaped cells and can therefore truly be labelled as ingressing. This transformation is driven by apical constriction and not a basal drop of the nucleus. The process of apical constriction differs between cells resulting in an asynchronous ingression of individual cells. I showed that the differences in apical constriction appear because constriction is interrupted by short bursts of expansion that vary between cells. In addition, cells do not constrict their apical surface homogeneously. In fact, each junction can show a different degree of constriction and might even elongate temporarily. This causes the apical cell shape to become asymmetrical. Preliminary data of MyosinII (MyoII) localisation shows that MyoII is also heterogeneously distributed at the single cell junctions. In D. melanogaster apical constriction has been associated with a medioapical pool of MyoII that constricts the cell surface, and a second, junctional pool of MyoII, which

stabilises the constrictions [Martin at al., 2009]. I associate the speckled MyoII on the ventral side of the embryo with the medioapical pool of MyoII. This pool of MyoII is inconsistently appearing and disappearing in the cells. This indicates that the medioapical pool of MyoII does not continuously drive apical constriction. This might be the reason for the short bursts of expansion in the apical area.
The heterogeneous distribution of MyoII at the junctions in C. riparius may result in an uneven stabilisation of constriction. Junctions with high MyoII localisation stabilise the constriction much better than junctions with weak MyoII localisation. The potential for junction remodelling differs not only between junctions of one cell, but also in junctions of different cells. No obvious pattern can be observed in the MyoII localisation throughout the whole mesoderm tissue.

4.3. Presumptive mesoderm might be disrupted by other gastrulation processes

The process of mesoderm internalisation is much slower in *C. riparius* than in *D. melanogaster*. Before mesoderm internalisation is completed, cells start to be displaced not only ventrally but also along the anterior-posterior axis, which I interpret as onset of germband extension (GBE). Additionally, cells undergo neighbour exchange events (NEEs). Both phonemes are not present in the *D. melanogaster* mesoderm during the internalisation process [Rauzi et al., 2015, Jodoin and Martin, 2016]. Both these processes might interfere with a smooth and fast mesoderm internalisation via ingression. NEE is characterised as a two-step process, constriction of junctions along one axis and extension along another. While the constriction phase might positively influence apical constriction, the extension phase might interfere with it. In the *D. melanogaster* ectoderm, neighbour exchange is dependent on the planar polarity of a cell. I could not find indications for a strong planar polarity in the *C. riparius* presumptive mesoderm. This opens the possibility that NEEs are regulated very differently between the mesoderm and ectoderm, by a factor that is not known yet.

Similarly, the onset of GBE may disrupt homogeneous cell behaviour on a tissue level. I demonstrated that cells from the posterior population are affected more by the

onset of GBE than cells from the anterior population. It is not known how onset of GBE influences ingressing cells. I hypothesise that the speed of ingression is reduced when cells move in two directions at the same time, compared to in just one direction. A link between NEEs and GBE is also possible. In *D. melanogaster* NEEs are an essential driver of GBE [Collinet et al., 2105]. In the case of the ingressing mesoderm, no indications for this can be found. NEEs start before onset of GBE and do not increase in number while GBE takes place. I hypothesise that NEEs in the *C. riparius* mesoderm are therefore not directly related to GBE but instead are a characteristic of the mesoderm cells themselves.

4.4. Fog over expression causes homogenisation of junction behaviour and a higher cell-cell connectivity

From work in *D. melanogaster* and *C. riparius* it has been shown that the G-protein coupled receptor (GPCR) signalling ligand Folded gastrulation (Fog) has the potential to affect the mode of mesoderm internalisation [Urbansky et al., 2016]. Over expression of *fog* in the *fog*-deficient *C. riparius* embryo causes a phenotype that shows a higher degree of organisation of nuclei with respect to one another. They show a “pearls on a string” phenotype, forming a shallow furrow, which was referred to as invagination. Vice versa, inhibiting *fog* together with the anchor protein *t48* [Kölsch et al., 2007] expression in *D. melanogaster* causes a loss of coherent tissue invagination and cells are internalised stochastically resembling ingression, as shown by the position of the nuclei.

Here I focus on the impact of *fog* on the *C. riparius* presumptive mesoderm. Three different possibilities could cause this phenotype of furrow formation on a cellular level.

1. Under wt conditions, cells start constricting their apical area all at different times. This is likely induced by a self-excitation potential of the GPCR Mesoderm invaginating signal transducer (Mist) [Manning and Rogers, 2014]. Once activated, the process of apical constriction could run smoothly in all cells. In the presence of *fog*, a uniform activation of the GPCR pathway might be induced. A coordination of

constriction onset might be sufficient to cause a homogeneous constriction in all cells.

2. Building on the first hypothesis, it is possible that cells all begin the process of apical constriction at the same time but then follow an individual pattern of apical constriction, causing some cells to constrict faster than others. It is possible that constriction relies on iterations of Mist self-excitation, activating MyoII anew each round. Differences in the turnover rate of excitation could lead to differences in constriction patterns. Introducing Fog to the system could induce a stronger activation of MyoII, and thus overshadow the nuances in self-excitation of Mist.

3. Cells are so loosely connected that they undergo ingression completely independently. Overexpression of *fog* induces tighter cell-cell connections. Temporal differences would still be present between cells, but cells would not ingress individually anymore. Rather, ingressing cells would stay connected and pull neighbouring cells inwards with them.

As a first step, I checked whether *fog* over expression changes the composition of mesoderm anlage and tissue behaviour. As expected, mesoderm anlage is unaltered by *fog* over expression. The two transcription factors Twist and Snail are identity-giving genes [Leptin, 1991]. They lay upstream of Fog in the genetic cascade and thus are unaltered by *fog* over expression. This analysis also revealed that mesoderm internalisation is not massively changed due to *fog* over expression. The funnel shaped anlage remains unchanged, with the same simultaneous closure in anterior as posterior part of the mesoderm domain. Temporally, *fog* over expression leads to a speed-up of the internalisation process.

Systematically, I tested for the three possible ways how Fog might influence cell behaviour.

1. Fog homogenises the onset of constriction. I defined onset of constriction as the timepoint at which cells have constricted their apical area by 10 percent and looked at the distribution of when cells reached this threshold. As expected, not all cells reached the threshold at the same time, but about 80 percent of cells reached it in a time span of 10 min. After introducing *fog* to the system, instead of narrowing the distribution span, it increased, with only 50 % reaching the threshold in the 10

min time window. This shows that *fog* does not coordinate the onset of apical constriction and the hypothesis can be discarded.

2. Fog signal causes homogeneous constriction. When I over expressed *fog*, the process of mesoderm internalisation is faster, both on the tissue scale level as well as in terms of the constriction rate of individual cells. Differences in apical constriction over time, therefore are reduced compared to wt, because the process is more compressed temporally. When looking at the individual constriction patterns of the cells, a high variance was still observed. Constriction was frequently interrupted by short bursts of expansion. Fog over expression therefore does not lead to a more homogeneous constriction pattern.

I could show that in the wt, constriction is not uniform in the cell. Junctions have a high degree of autonomous remodelling capacity causing asymmetrical cell shapes. In the presence of Fog, the junctions are less convoluted and apical cell morphology is more symmetrical. The direct reason for this cannot be gleaned from the data presented in this study. It is likely that the over expression of *fog* induces a stronger force in the medioapical pool of MyoII. A strong medioapical pool of MyoII might overshadow differences in junctional MyoII and thus reduce the autonomous remodelling capacity of the junctions. The hypothesis can neither be accepted nor discarded at this point.

3. Fog causes a tighter cell-cell connection. I could show that cells in a wt background are only loosely connected, even to a point where holes form between cells. When over expressing *fog*, the cells show far fewer of these membrane abnormalities. I interpret this as an indication for a higher cell-cell connectivity. Another important finding favouring this interpretation is the displacement towards the posterior, which is most likely due to the onset of GBE. In a wt embryo, GBE acts as an external force that pulls on the mesodermal cells. This pull is strongly visible in the posterior population of mesodermal cells being translocated towards the posterior but cannot be observed the anterior population. The mesodermal cells do not propagate the pulling force. I believe that this is because the cells are not tightly connected. Any external force is dissipated in the loose cell-cell connection and the constant “jiggling of cells” that can be seen in the high fluctuation of cell neighbours and the convoluted junctions.

Introducing Fog to the system changes this phenotype. Cells of the anterior pool of presumptive mesodermal cells experience a stronger posterior displacement, likely because cells are connected more tightly and the external force is propagated more strongly. A stronger cell-cell connectivity must be caused by an alternation in the behaviour of AJs. Fog signalling could influence AJs behaviour in two ways. (1) Fog has a direct influence on AJ distribution through a yet unknown mechanism and equalise the presence of AJs at all junctions. In this case, all junctions of a cell will be connected uniformly to the neighbouring cells, leaving little room for abnormalities in the junction shape. (2) Fog reduces AJ endocytosis. It has been shown that AJs are disassembled in cells expressing *snail*, yet an active MyoII pool protects the AJs from being turned over [Weng and Wieschaus, 2016]. Fog sets a cascade in motion that will activate MyoII. An increased or more stable activation of MyoII can result in a stronger protection of AJs from endocytosis. At this point, differentiation between both explanations is not possible.

The frequency of neighbour exchange in the *C. riparius* mesoderm in the presence of Fog does not yet clearly fit to the hypothesis of enhanced cell-cell contact. To undergo cell intercalation, cells need to be loosely connected at the shrinking junction and strongly connected at the extending junctions. A uniform distribution of AJs would lower the potential of cells to intercalate. Before making assumptions on a connection between an increase in cell-cell connectivity and an increase in neighbour exchange events, a detailed analysis of the latter is required. So far, only the temporal aspect of neighbour exchange events has been analysed. A resolution in space still remains to be done. In addition, possible changes in AJ distribution and stability in the presence of Fog have to be proven.
An alternative hypothesis for the change in posterior displacement of cells has be considered as well, independent of cell-cell connectivity.

Fog has also been shown to be an important driver for posterior midgut invagination [Costa et al., 1994]. A ubiquitous expression of *fog* might have an effect on this process itself. It is possible that an increase in Fog signalling causes a stronger and/or faster invagination of the posterior midgut, resulting in an increase in force that is acting on the mesoderm tissue. In this scenario, the strong force of the invaginating posterior midgut may influence the entire embryo and thus also cells from the anterior mesoderm population.

4.5. Summary

In the *C. riparius*, presumptive mesoderm is internalised via single cell ingression. Ingressing cells differ in the process of apical constriction, likely introduced by a diversity of independent junction remodelling. Low cell-cell connectivity and frequent neighbour exchange cause the cells to ingress individually instead of via the formation of a coherent tissue. Introduction of Fog to the system in early developmental stages increases the cell-cell connectivity and causes a harmonisation of junction behaviour. This results in a faster and more homogeneous internalisation process.

4.6. Perspective: from ingression towards invagination

A simultaneous internalisation of all mesodermal cells could have multiple benefits for the subsequent development of the embryo. First of all, invagination correlates with higher developmental speed [Urbansky et al., 2016]. The presented data here supports this idea. It is possible that more tightly connected cells pull neighbouring cells inward with them. It can be hypothesised that each individual cell thus does not need to build up all the energy needed for ingression itself but can rely on more energy efficient ways of internalisation as a group of cells.

The data presented indicates that the transition from ingression to invagination is a multi-step process. Stronger cell-cell connections, equally distributed MyoII at the junctions and a strong medioapical pool of MyoII, inhibition of neighbour exchange events and a decoupling of mesoderm internalisation and germband extension all needed to evolve until mesoderm could be invaginated as efficiently as in *D. melanogaster*. Here, I show that the early expression of *fog* could serve as a driver for one or more of such steps in the evolution. Even before the onset of gastrulation, *fog* expression has an impact on cell-cell connectivity. Cells are much more tightly packed than under wt conditions. This effect of Fog might be conserved through the insect class. In the flour beetle *Tribolium castaneum*, loss of *fog* causes holes to form in the blastoderm [Benton et al., 2019].

In addition to being responsible for tighter cell-cell connections, Fog has been shown to regulate apical constriction. When the medioapical pool of MyoII constricts, the force is transmitted equally to all junctions of the cells. This reduces the apical area and a second pool of MyoII at the junctions stabilises the new cell shape [Martin et al., 2009]. Repetitive rounds of this constriction mechanism cause a ratchet-like constriction pattern. In the *C. riparius* mesoderm, MyoII is unequally distributed at the junctions, with some junctions showing significant MyoII localisation and others showing no or little MyoII localisation. I believe that this is the reason for the inhomogeneous constriction. Junctions do not stabilise the constriction induced by the apical pool equally. Three steps need to be achieved in order to go from a phenotype found in *C. riparius*, asymmetric constriction, to the one found in *D. melanogaster,* symmetric constriction. First, all junctions need to have accumulated the same amount of MyoII at them to guarantee an equilibrium of force. Second, a medioapical pool of MyoII needs to be localised in the cells, which can build up enough force to pull on the boarder of the cells and constrict its apical side. Third, the force built up by MyoII must be anchored evenly across AJs. This can only be achieved by an even distribution of AJs at the junctions.

As stated above, the presence of neighbour exchange events is a great difference in mesoderm internalisation between the two flies but is not found naturally in the invaginating tissue of *D. melanogaster* [Jodoin and Martin, 2016]. It is not fully understood yet how neighbour exchange is regulated genetically in the ectoderm tissue in *D. melanogaster*. A planar polarisation of MyoII seems to be important for cell intercalation. The absence of such planar polarised MyoII in the *C. riparius* mesoderm hints at a different genetic regulation of cell intercalation in the two tissue. The absence of cell intercalation in the *C. riparius* mesoderm could be caused by either a missing expression or an active repression of unknown regulating factors. In addition to a genetic regulation, NEEs might be inhibited in the *D. melanogaster* mesoderm by the equal distribution of junctional MyoII. A directed constriction and extension of specific junctions might not be possible. Consequently, the stochastic localisation of junctional MyoII in the *C. riparius* mesoderm might favour NEEs. Junctions with high MyoII localisation might constrict faster than others, and junctions without MyoII localisation might extend more easily, resulting in effective cell intercalation.

Lastly, over the course of evolution, a mechanism was put into place to temporally separate mesoderm internalisation and onset of GBE. Preliminary data existing in the lab shows that this separation might have a substantial effect on the mode of internalisation. Interfering with the terminal system, i.e. injection of dsRNA against *torso*, completely inhibits germband extension [personal communication with Dr. Silvia Urbansky]. It appears that in this context the mesoderm forms an extremely deep furrow as it is being internalised. How exactly ventral furrow formation and onset of GBE are connected is not understood.
In conclusion, I believe that a transition from ingression to invagination could be induced experimentally in the *C. riparius* mesoderm by a simultaneous combination of higher cell-cell connectivity, a redistribution of MyoII, a reduction in the number of neighbour exchange events and an inhibition the onset of GBE.

4.7. Outlook

This study gives a detailed cellular description of cell shape changes during ingression of the mesoderm. It reveals that other processes are occurring simultaneously in the mesoderm, i.e., neighbour exchange and posterior displacement due to the onset of GBE. How other processes interact with ingression is not addressed, yet.

To set the stage to study how onset of GBE can influence mesoderm internalisation, the temporal sequence of the two processes needs to be understood. To this end, it will be helpful to have an in-toto view on the embryo. Using light sheet movie SPIM microscopy, a visualisation of the process of mesoderm internalisation and GBE can be obtained, and the two processes can be set in relation to one another on a temporal and spatial level. Using RNAi against components of the terminal system, e.g. *torso*, will inhibit the invagination of the posterior midgut [Collinet et al., 2015]. Mesoderm internalisation can thus be studied. Comparing data from wt and *torso* deficient embryos will highlight the consequences of onset of GBE on mesoderm internalisation.

I have shown that ingression happens simultaneously with cell intercalation in the same cells. Such a co-occurrence has not been described before. This gives the

unique opportunity to study how neighbour exchange influences the ability of cells to internalise. There is evidence that NEEs can be reduced genetically in *D. melanogaster.* In the absence of a specific RhoGEF, called Wireless, the occurrence of NEEs are strongly reduced [Garcia de las Bayonas et al., 2019]. In a recently started project, influence of Wireless on NEEs in *C. riparius* is being tested. It will be interesting to see whether reducing *wireless* in *C. riparius* also reduces NEEs, like in *D. melanogaster*, and if so, how this influences mesoderm internalisation.

On a cellular level, it will be interesting to investigate further the cellular components MyoII and E-cadherin, as an indicator of AJs. The localisation of MyoII in the cell - junctional versus medioapical - needs to be understood properly in the wt. Only then can the hypothesis of how fog influences MyoII behaviour be analysed comprehensively. Moreover, the behaviour of AJs needs to be studied in detail. In this work, I show with membrane data that the cell-cell connectivity during the process of mesoderm internalisation in the *C. riparius* cells is strongly reduced compared to cells of the *D. melanogaster* embryo. I wonder if this is due to either a reduced number of AJs compared to *D. melanogaster* or an inhomogeneous distribution of them. Following up on this, it is not clear how the AJs behave during the process of ingression in *C. riparius*. In the process of mesoderm invagination in *D. melanogaster* it has been shown that the AJs experience a shift from a subapical to an apical position [Weng and Wieschaus, 2016]. This is believed to be one reason for the wedge like cell shape of invaginating cells. In *C. riparius*, cells do not become wedge-like, but instead bottle shaped. Where AJ are positioned in these cells, and when their endocytosis occurs remains to be investigated. I postulate that the over expression of *fog* causes tighter cell-cell connectivity and that this in turn induces cells to act as a coherent tissue. AJ distribution and/or stability should then be affected in the context of *fog* over expression.

5. Materials and Methods

5.1. Material

5.1.1. Chemicals

Name	Company	Catalogue Number
Agar	Roth	5210.2
Agarose	Peq-Gold	35-1020
Ampicilin	Sigma	A9518
Bleach	DanKlorix	
CellMask	Thermo Scientific	C10046
Chloroform/Isoamylalcohol	Sigma	25666
DAPI	Molecular Probes Life Technologies	D1306
Dinatriumhydrogenphosphat	Grüssinu	12133
DNA ladder ready mix	Thermo Scientific	SM1173
dNTP	Sigma	D7295
EDTA	Applichem	A3553
Ethanol	Sigma	52603
Ethidiumbromide	Roth	2218.2
Ethylenediaminetetraacetic Acid	Sigma	34549
FM464	Thermo Scientific	T13320
Formaldehyde	Sigma-Aldrich	252549
Gel Loading Dye	NEB	10047936
Glacial acetic acid	Merck	607002006
Glycerol	Sigma	54997
Hablocarbonoil 27	Sigma-Aldrich	8773
Hablocarbonoil 700	Sigma-Aldrich	8898
Haptane	Roth	8654.3

Name	Company	Catalogue Number
Isopropanol	Sigma	69694
Methanol	Sigma-Aldrich	322415
Natriumactate	Grüssing	1131
Natriumchlorid	Sigma	31434
NTP	Thermo Scientific	R0481
Phallacidin	Invitrogen	B607
Phenol/Chloroform/IAA	Roth	A156.1
Potasium Acetate	Grüssing	12001
Potasium Chloride	Applichem	A3582
Potassium dihydrogen phosphate	Applichem	3620
RNase Inhibitor	Roche	11801800
Sodium Dodecyl Sulfat	Roth	CN30.2
Tris base	Roth	4855.2
Tryptone	Sigma-Aldrich	T9410
Tween-20	Sigma	P1379
Wheat Germ Agglutinin	Thermo Scientific	W11261

5.1.2. Media and Solutions

Media	Composition
LB	Tryptone 10g/l Yeast Extract 5g/l Sodium chloride 10g/l
LB-Amp Plates	Tryptone 10g/l Yeast Extract 5g/l Sodium chloride 10g/l Agar 15g/l Ampicillin 50µg/

Media	Composition
Lysis Buffer	NaOH 8g/l SDS 10g/l ad 1l H_2O
Neutralisation Buffer	$C_2H_3KO_2$ 3M
PBS	NaCl 80 g KCl 2g Na_2 HPO_4 14.4g KH_2PO_4 2.4g ad 1l H_2O
PBT	PBS (1x), Tween-20 0.1%
Resuspension Buffer	Tris base 6.06 g/l Na_2EDTAx2 H_2O RNase A 100mg/l ad 1l H_2O
SOC	Tryptone 20 g Yeast extract 5 g NaCl 0.5 g ad 1l H_2O
TAE	Tris base 242 g/l Glacial acetic acid 5.71% EDTA 50mM

5.1.3. Kits

Name	Company	Catalogue Number
Capping-Kit	Cellscript	C-SCCS1710
PolyA-Kit	Cellscript	C-PAP5104H
QIAquick Gel Extraction	Qiagen	28706
TOPO TA cloning Kit	ThermoScientific	450641

5.1.4. Organisms

Chironomus riparius
Escherichia coli

5.1.5. Enzymes and Buffers

Name	Company	Catalogue Number
Antarctic Phosphatase	NEB	M0289S
Antarctic Phosphatase Reaction Buffer	NEB	B0289S
AvaII	NEB	R0153S
CalI	NEB	R0197S
Cutsmart Buffer (10x)	NEB	B7204S
DNase Turbo	ThermoScientific	AM2238
EcoRI	NEB	R3101S
Gibson Assembly mix	NEB	E2611
HF Buffer (5x)	NEB	B0518S
HindIII	NEB	R0104S
iProof Polymerase	Biorad	1725300
NotI	NEB	R3189S
PacI	NEB	R0547S
Proteinase K	Invitrogen	25530-015
RNA Polymerase SP6	Ambion	00830286
SacI	NEB	R3156S
T4 ligase	NEB	M0202S

Name	Company	Catalogue Number
T4 ligation buffer	NEB	B0202S
XbaI	NEB	R0145S

5.1.6. Plasmids

Plasmid	Stock number	Origin
eGFP with 5' insertion site in pSP	LP 538	Benton et al., 2013
eGFP with 3' insertion site in pSP	LP 537	Benton et al., 2013
GAP43-eGFP in pSP expression Vector	LP 595	Invitrogen Gene Art Quality Assurance Documentation 12ABHG2P Ref number: 1256268
Cri-E-cad in pSP expression Vector	LP554	5' RACE cDNA library
Cri-sqh in pSP expression Vector	LP596	5' RACE cDNA library
Cri-E-cad in pCR2.1 TOPO Vector	LP540	5' RACE cDNA library
Cri-sqh in pCR2.1 TOPO Vector	LP 575	5' RACE cDNA library

5.1.7. Primer

Primer	Stock number	Sequence
GAP43 forward	SL0932	CAACTTTGGCAGATAAAATGCTGTGCTGTATGCGCCGC
GAP43 reverse	SL0933	CGGAGCCGGCGGAGCCGCCAATCTTCTGGTCC

Cri-sqh forward	SL0906	CTCAACTTTGGCAGATAAAATGTCATCAAGGAAGAC
Cri-sqh reverse	SL0907	CCTCGCCCTTGCTCACCATTTGTTCATTCTCATTTTC
Cri-E-cad forward	SL0869	GCTCAACTTTGGCAGATAAAATGGGAACATCTAAGAATATG
Cri-E-cad reverse	SL0870	CTCGCCCTTGCTCACCATGGAAATTCTCCATCCTTCATC
Gibson Vector (LP 537) forward	SL0868	TTTATCTGCCAAAGTTGAGC
Gibson Vector (LP 537) with linker forward	SL931	GGCTCCGCCGGCTCCGCCGCCGGCTCCGGCGAGGTGATGGTGAGCAAGG
Gibson Vector (LP 537) reverse	SL0871	CCATGGTGAGCAAGGGCG
eGFP in 3’ forward	SL 751	GCTCAAGCTTGAATACAAGCTTGCTTGTTCTTTTTGCAGAAGCTCAGAATAAACGCTAACTTTGGCAGATACCTTAATTAAGCGGCCGCCATGGTGAGCAAGGGCGAGG
eGFP in 3’ reverse	SL 738	GTCCTCTAGATTACTTGTACAGCTCGTCCATGCC
eGFP in 5’ forward	SL 758	GCTCAAGCTTGAATACAAGCTTGCTTGTTCTTTTTGCAGAAGCTCAGAATAAACGCTCAACTTTGGCAGATACCAAATGGTGAGCAAGGGCGAG
eGFP in 5’ reverse	SL 747	GCTCTCTAGACCATGGGGCGGCCGCCTTGTACAGCTCGTCCATGC

5.1.8. Disposables

Name	Company	Catalogue Number
Cover slip	Marienfeld	0101122_214
Dry yeast	RUF, Aldi	
Filter paper	Machery-Nagel	MN 615 1/4
Glass capillaries	Hilgenberg	

Name	Company	Catalogue Number
Microscope slide	Roth	H878
Needles	Harvard apparatus	30-0019, GC100F-10
Parafilm	Sigma-Aldrich	P8299
Parsley	Tro-Kost	
Petri dish	Grainer Bio-one	632181
Reaction tube 0.5 ml	Eppendorf	30124332
Reaction tube 1.5 ml	Eppendorf	30125150

5.1.9. Instruments

Agarose gel documentation	Mitsubishi Biometra P93
Electroporator	MicroPulser BioRad
Heatblock	Mixing Block MB-102, Bioer
Incubator	Incubation Shaker Model G25, New Brunswick Scientific Co. Inc., Edison, USA
Injector	Eppendorf FemtoJet Express
Spectrophotometer	DS-11+, DeNovix
Needle puller	Flaming, Brown Micropipette Puller Sutter Instrument CO., model P-97
Tabel top centrifuge	Eppendorf Centrifuge 5417R
Thermocycler	S1000 Biorad, Hercules, CA, USA
Vortex	Vortex Mixer 7-2020, neoLab

5.1.10. Microscopes

Binocular	Zeiss Stemi 2000
Confocal	Leica SPE, Leica SP8
Stereoscope	Zeiss Axio Vert.A1

5.1.11. Software

Software	Company
Geneious 6.1.6	Biomatters Limited, New Zealand
Ilastik	Interactive Learning and Segmentation Toolkit Sommer C., Strähle C., Köthe U., Hamprecht F.A.
Illustrator CS6	Adobe, USA
ImageJ	http://fiji.sc/ImageJ
Matlab R2016a	The MathWorks, Inc., Natick, Massachusetts, United States
Matlab R2018b	The MathWorks, Inc., Natick, Massachusetts, United States
SEGGA	Segga: a toolset for rapid automated analysis of epithelial cell polarity and dynamics. Farrell, D. L., Weitz, O., Magnasco, M. O., and Zallen, J. A

5.2. Methods

5.2.1. Summary

Cloning and RNA synthesis

The expression vector pSP35T [Amaya et al., 1991, Urbansky et al., 2016] was modified for mRNA generation. Via primer overhangs, *Chironimus riparius* (*C. riparius*) specific Koszac sequence was added after the 5'UTR. Coding sequence of eGFP was inserted via conventional restriction digests with XbaI and HIndIII. For insertion of other coding sequences of specific genes, a small fragment containing recognition site for PacI and recognition site for NotI was inserted via primer overhangs either between Koszac sequence and eGFP or between eGFP and 3'UTR. For the later case, the stop codon from eGFP was eliminated via prime overhangs. (primer pairs:5'-

GCTCAAGCTTGAATACAAGCTTGCTTGTTCTTTTTGCAGAAGCTCAGAATAAACG
CTAACTTTGGCAGATACCTTAATTAAGCGGCCGCCATGGTGAGCAAGGGCGAG
G/5'-GTCCTCTAGATTACTTGTACAGCTCGTCCATGCC and 5'-
GCTCAAGCTTGAATACAAGCTTGCTTGTTCTTTTTGCAGAAGCTCAGAATAAACG
CTCAACTTTGGCAGATACCAAATGGTGAGCAAGGGCGAG/5'-
GCTCTCTAGACCATGGGGCGGCCGCCTTGTACAGCTCGTCCATGC)
This resulted in vectors suitable for simple generation of fusion constructs with eGFP at 5' or 3' site.
Cri-Ecad and *Cri-sqh* (small regulatory light chain) were identified from transcriptome sequences (comp2297_c0_seq1 and comp492_c0_seq1, respectivly), full length coding sequence was amplified from 5'-RACE generated cDNA library. The sequences were cloned into a commercially available pCR2.1-TOPO® vector via TA overhand (ThermoFischer Scientific). *Cri-Ecad*, *Cri-sqh* and GAP43 (Invitrogen Gene Art Quality Assurance Documentation 12ABHG2P Ref number: 1256268) full length coding sequence were cloned into the modified expression Vector pSP-eGFP via Gibson cloning. A linker sequence (received from Yu-Chiun Wang, RIKEN Center for Developmental Biology, Japan) between sequence *of eGFP* and gene of interest for introduced via primer overhang. Primer pairs: *GAP43* 5'-
CAACTTTGGCAGATAAAATGCTGTGCTGTATGCGCCGC/
5'-CGGAGCCGGCGGAGCCGCCAATCTTCTGGTCC,
sqh 5'-CTCAACTTTGGCAGATAAAATGTCATCAAGGAAGAC/
5'-CCTCGCCCTTGCTCACCATTTGTTCATTCTCATTTTC
Cri-ecad 5'-GCTCAACTTTGGCAGATAAAATGGGAACATCTAAGAATATG/
5'-CTCGCCCTTGCTCACCATGGAAATTCTCCATCCTTCATC
backbone
5'-GGCTCCGCCGGCTCCGCCGCCGGCTCCGGCGAGGTGATGGTGAGCAAGG/
5'-CCATGGTGAGCAAGGGCG
mRNA was generated in vitro using the RNA Polymerase SP6 (Ambion), and stabilised using with 5' capping via ScriptCap Cap 1 Capping System and 3' PolyA tailing via Poly(A) Polymerase Tailing Kit (both CellScript).
All molecular cloning steps were performed as described previously (Sambrook and Russell, 2014) or according to user manual.
Detailed description of all processes below.

Injection and fixation and Microscopy

The laboratory strain of *Chironomus riparius* [Klomp et al., 2015] was cultured as described before [Caroti et al., 2015]. For full shape cell analysis, embryos were injected either with water as control, or *Cri-fog1*, fixed and stained with Phallacidin (F-Actin) and DAPI (nuclei) as described [Urbansky et al., 2016]. For life imaging, embryos were aligned on a cover slide and injected with *GAP43-eGFP* mRNA, *sqh-eGFP*, GAP43-mCherry plus *Cri-ecad-eGFP* (1:1), *GAP43-eGFP* plus *Cri-fog1 (1:1).* Fixed samples were imaged as described previously [Urbansky et al., 2016]. Life imaging was performed in time lapse recordings in 10 µm volume with 1 µm sections on a Leica SP8 or Leica SP5 Confocal microscope.

Detailed description of all processes below.

Image processing and analysis

Detailed description of all processes below.

5.2.2. Molecular work

Generation of Plasmids

For this work, I was involved in generating the following plasmids: eGFP with 5' insertion site in pSP (LP 538), eGFP with 3' insertion site in pSP (LP 537),*GAP43-eGFP* in pSP Vector (LP 595), s*qh-eGFP* in pSP Vector(LP596), *Cri-ecad-eGFP* in pSP Vector(LP554), *Cri-ecad* in pCR2.1 TOPO Vector(LP540), s*qh-eGFP* in pCR2.1 TOPO (LP 575).

Modification of expression vector

The expression Vector pSP35T was modified to facilitate high trough put cloning of fusion constructs. Two clones were generated, containing an *eGFP* sequence with an insertion site either in 5' or 3' orientation. Sequences of pSP and *eGFP* were obtained from clones previously present in the lab (pSP35T: Urbansky et al., 2016, eGFP: Caroti et al., 2018)

C. riparius specific Koszac sequence [Klomp et al., 2015] was added via primer overhang. Primers additionally contained an insertion site for subsequent cloning

steps. This insertion site contained a recognition site for the restriction enzymes PacI and NotI and XbaI and HindIII recognition site for conventional cloning.

Extraction of sequence for gene of interest

For *Gap43* the sequences were already present in the lab, but as inserts in different plasmids (plasmid LP318, originally received from Invitrogen Gene Art Quality Assurance Documentation 12ABHG2P Ref number: 1256268). To extract the sequence of interest, the plasmid was linearised NotI. Restriction digest was set up as following, and incubated for 40 min at 37 °C. The restriction enzyme was then inactivated by heat inactivation for 20 in at 80 °C.

Sequence for *Cri-E-cad* and *Cri-sqh (*small regulatory light chain of MyosinII*)* was amplified from cDNA via PCR (see below). Sequences were identified by blasting coding sequence of the corresponding gene in *Drosophila melanogaster* against *C. riparius* transcriptome. The sequences were identified as comp2297_c0_seq1 for *Cri-E-cad* and comp492_c0_seq1 for *Cri-sqh*.

Plasmid	0.5 µl
Restriction enzyme	1 µl
10 x cut smart buffer	3 µl
H_2O	ad 30 µl

Dephosphorisation with Antarctic Phosphatase

Since the DNA fragment of interest come from preexisting plasmids, religation in the original conformation needed to be inhibited. This was achieved by dephosphating the DNA fragments at the 5’ and 3’ ends, so spontaneous religation was inhibited. In order to do so, 3 µl of 10x Antarctic Phosphatase Reaction Buffer was added together with 1 µl Antarctic Phosphatase to 30 µl linearised plasmid, incubated tor 30 min at 37 °C and inactivated by heat inactivation for 5 min at 65 °C.

DNA amplification and clean up

DNA was amplified using Polymerase chain reaction (PCR). The following components were mixed together in 0.5 ml reaction tube.

5x HF Buffer	4 µl (6 for vector)
dNTPs	0.5 µl
Primer forward	0.5 µl
Primer reverse	0.5 µl
DNA template	1 µl
iProof Polymerase	0.2 µl
H_2O	ad 20µl (25 µl for vector)

If the fragments were of correct size and of high quantity, they were cleaned from the agarose gel using the “QIAquick Gel Extraction” Kit accoring to the provided manual.

TOPO TA cloning

Cri-E-cad and *Cri-sqh* sequence were primarily cloned into a TOPOII vector. For this the PCR product was cleaned up with the QAIquick gel extraction kit following instructions. Because PCR did not provide A-overhangs necessary for TOPO TA cloning, a A-tailing step was performed, by mixing following components and incubation for 20 min at 72 °C.

F100 Buffer	2 µl
Clean PCR product	10 µl
ATPs	0.5 µl
F100 Taq	0.2 µl
H_2O	ad 20 µl

Next, ligation was performed with 4 µl PCR product, 1 µl pCR2.1 TOPO TA vector, 1 µl salt solution for 5 min at room temperature. For the transformation, the ligation was diluted 1:4, and of this 0.5 µl was used (see below). For faster selection, 40 µl X-gal was added to the LB-AMP plate and was let dry prior to adding transformed cells.

Restriction digest and ligation

To generate modified pSP35T with eGFP sequence and insertion site, PCR products for backbone and eGFP insert were digested with XbaI and HindIII at 37°C for 2 hours and enzymes were inactivated at 80 °C for 20 min.

DNA	1 µl
Restriction enzyme	1 µl
10x Cut smart buffer	5 µl
H_2O	ad 50 µl

Vector	3 µl
Insert	1 µl
T4 Buffer (10 x)	2 µl
T4 ligase	0.2 µl
H_2O	ad 20 µl

Ligation was carried out with 1:3 ration of vector and insert and incubated at room temperature for 1 hour. 2 µl of ligation mix was used for transformation.
2 µl of ligation mix was used for transformation.

Gibson Assembly of plasmids

Sequences used for in vitro transcription were ligated via Gibson cloning, it allows for scarless assembly of DNA fragments. Via primer overhang a linker sequence (received from Yu-Chiun Wang, RIKEN Center for Developmental Biology, Japan) was added before the eGFP sequence.

For cloning of *GAP43-eGFP* in the pSP vector, 250 ng of *GAP43* DNA and 50 ng of the pSP vector were mixed with 27 µl Gibson Assembly master mix,for the *Cri-sqh* clone, 200 ng of the *sqh* DNA and 66 ng of the pSP vector were mixed with 1 µl H_2O and 10 µl Gibson Assembly master mix. *E-cad-eGFP* was assembled with 60 ng vector and 150 ng *Cri-E-cad* DNA. The mix was incubated for 40 min at 50 °C in a thermocycler with a heated lid at 105 °C.

Electrocompetent cells

For proper plasmid uptake, bacteria cells needed to be made permeable. One single colony was used to inoculate 100 ml LB medium, which was incubated over night at 37 °C, rocking at 200 rpm. This pre-culture was then used to inoculated 37 °C warm LB media with of 8 ml of pre-culture in 800 ml LB medium. Under unchanged conditions, cells were grown until a value of 0.6-0.8 measured with a photometer at OD600nm was reached. Cells were then cooled down on ice for 15 min and harvested by centrifugation. After the supernatant was discarded, the pellet was resuspended in 20 ml ice cold H_2O. Once the cells have been resuspended, the volume was increased to 400 ml by ice cold H_2O and centrifuged again. The pellet was then resuspended in 20 ml ice cold H_2O, volume filled up to 200 ml and again centrifuged. The pellet was then resuspended in 30 ml ice cold 10 % Glycerol and distributed to 4 50 ml Conical Centrifuge Tubes. The tubes were filled up to 50 ml with ice cold 10 % Glycerol and again centrifuged. The pellet was resuspended in 4 ml 10% Glycerol and distributed in 40 µl aliquots into pre-cold 1.5 ml reaction tubes. Aliquots were then shock-frozen with liquid nitrogen and stored at -80 °C.

All pipetting steps were performed at 4 °C, to reduce temperature changes. All centrifugation steps are performed for 30 min at 4000 rpm at 4 °C.

Plasmid amplification in bacteria and isolation

Assembled DNA plasmids were amplified in bacteria. For this, electrocompetent *E. coli* cells were thawed on ice, and plasmid as well as a cuvette were cooled down. The Gibson assembly mix was diluted by 1:3 and of this dilution, 1 µl was added to 40 µl *E. coli* cells. After electorporation, 1000 µl preheated (37 °C) SOC solution was

added and all incubated for 1 h at 37 °C while gently rocking at 200 rpm at 37 °C. 100 µl were then plated on a LB plate containing the selection factor Ampicillin and incubated over night at 37 °C. The next morning, single colonies were picked with a sterile, wooded tooth pick and transferred into a liquid LB+Ampicillin medium, in which they were again cultured over night under gentle rocking conditions (200 rpm at 37 °C). Cells presumably containing the plasmid of interest were harvested in a 1.5 reaction tube by gentle centrifugation at 4000 rpm for 2 min. The supernatant was discarded, and the pellet resuspended in 200 µl cold resuspension buffer. The cells were lysed by incubating them in 200 µl Lysis Buffer for 2 min. The lysis reaction was stopped by adding 200 µl neutralisation buffer, after which the mixture was centrifuged for 15 min at 14 000 rpm. DNA was dissolved in the supernatant, which was transferred into a new reaction tube, where it was precipitated by adding 500 µl 100 % Isopropanol and an incubation step of 10 min, followed by centrifugation for 15 min at 14 000 rpm. The supernatant was discarded, and the pellet washed with 75 % EtOH. After letting the pellet air dry, it was eluted in 30 µl Elution Buffer.
For a rough estimate whether or not the isolated DNA consisted of the plasmid of interest, a test digest was performed for each clone. For *GAP43-eGFP* in pSP, the plasmid was digested with AvaII, for the *sqh-eGFP* clone, ClaI and SacI were used and *Cri-E-cad-eGFP* with EcoRI In all cases, digestion was executed using the following ingredients and incubated for 60 min at 37 °C. Inactivation of the plasmid was done by heat inactivation for 20 min at 80 °C or 65 °C, receptively. 5 µl were analysed on a 1 % Agarose gel for correct band size.

DNA plasmid	1 µl
Restriction enzym	1 µl
10x Cut smart buffer	5 µl
H_2O	ad 50 µl

For an in-depth quality check, the plasmids were commercially sequenced using the SP6 primer and the sequence was checked for alignment using the Geneious software “map to reference” tool.

mRNA *in vitro* transcription

DNA linearisation

From the obtained plasmids mRNA was transcribed. In order to do so, the plasmid needed to linearised beforehand. The following linearisation mix was assembled.

Cleaned DNA Template	10-20 µg	5 µl
EcoRI	10-20 units	5 µl
CutSmart Buffer	10x	5 µl
H_2O		ad 50 µl

The plasmid is linearised at 37 °C for 1 h, after which the enzyme is inactivated via an incubation step of 20 min at 65 °C. To clean the DNA from the restriction enzyme, 2 µl Proteinkinase K and 5 µl SDS (10 %) is added and all is incubated at 50 °C.

DNA clean up via Phenol/Chloroform and precipitation

Before transcription, the linearised DNA fragment needs to be cleaned off all residues from previous steps. For this Phenol/Chloroform extraction is used. The mixture containing the DNA of interested is filled up to 200 µl with nuclease-free water and 1 volume of Phenol/Chloroform/IAA, mixed vigorously by vortexing and then phase separated by centrifugation for 5min at 15 000 rpm. The upper phase is transferred in to a fresh reaction tube, and one volume of Chloroform is added again. The solution is vortexted, centrifuged (5min at 15 000 rpm), and the upper phase again transferred into a new reaction tube. For precipitation, 1/10 volume NaOAc and 3 volumes of 100 % EtOH is added and incubated over night at -20 °C. The next day, the solution is centrifuged for 20 min at 15 00 rpm at 4 °C, the supernatant is discarded, the pellet washed with 70 % EtOH, centrifuged again for 5 min at 15 000 rpm and the supernatant discarded again. The DNA pellet is resuspended in 10 µl nuclease-free water, centrifuged again for 30 min at 15 000 rpm at 4 °C. The DNA pellet washed again with 100 % EtOH, centrifuged again for 30 min at 15 000 rpm at 4 °C. The supernatant discarded and the pellet resuspended in 10 µl nuclease-free water. Quality of the cleaned DNA was checked on a 1 % agarose gel.

In vitro transcription

For in vitro transcription, the following components were added together and then incubated for 4 h at 37 °C.

linear DNA	5 µl
10x Transcription Buffer	8 µl
RNase inhibitor	2 µl
NTP	40 µl
RNA Polymerase Sp6	2 µl
H_2O	24 µl

After transcription, the DNA is degraded by adding 8 µl Turbo DNase and incubated together for 20 min at 37 °C.

RNA clean-up via Phenol/Chloroform and precipitation

Clean RNA is obtained by another Phenol/Chloroform extraction and precipitation. The procedure is similar to DNA clean up via Phenol/Chloroform and precipitation described above, with the following changes. Volume is filled up to 300 µl, one volume of Phenol/Chloroform/IAA, and 1/10 volume of NH_4OAc was added. After centrifugation and upper phase transfer, another Phenol/Chloroform/IAA step was executed. To increase the volume of the aquatious phase, 100 µl of H_2O was added, and then 400 µl Phenol/Chloroform/IAA. Clean up procedure then follows as for DNA. To precipitate the RNA, one volume of Isopropanol p.a. was added and all incubated over night at -20 °C. The RNA pellet, obtained by centrifugation at 15 000 rpm at 4 °C for 30 min, was washed with 80 % EtOH, and spun down again for 5 min at 15 000 rpm at 4 °C. The pellet was then resuspended in 10 µl 1x Capping buffer, of which 0.5 µl were used to analyse the RNA quality on a 1 % Agarose gel.

Stabilisation of RNA via capping and extended A-tailing

To stabilise the in vitro transcript RNA, a cap and long A-tail was added to it. To cap the RNA, the following components were added together and incubated for 45 min at 37 °C.

RNA (not heat denaturated)	9.5 µl
h20	24 µl
GTP	5 µl
SAM	1.25 µl
RNase inhibitor	1.25 µl
2'O-Methyltransferase	2 µl
10 x Capping Buffer	5 µl
Capping enzym	2 µl

Without another purification step, A-tailing was proceeded. The following components were added and incubated at 37 °C for either 60 min (if RNA fragments is larger than 730 bases or 120 min (if RNA fragments is smaller than 730 bases).

capped RNA	50 µl
RNase inhibitor	0.3 µl
10 x Poly-A Buffer	6.6 µl
ATP (10mM)	6.6 µl
Poly-A Polymerase	2.5 µl

mRNA	Concentration
GAP43-eGFP	1.66 µg/µl
Cri-sqh-eGFP	3.1 µg/µl
Cri-E-cad-eGFP	1.27 µg/µl
GAP43-mCherry	982 ng/µl

The so stabilised RNA was cleaned and precipitated again as described above. After the pellet was washed with 80 % EtOH, it was air dried at room temperature and resuspended in 25 µl clean H_2O. Concentration was measured using the Nanodrop Spectrophotometer, and if concentration was above 1000ng/µl, aliquots of 0.5 µl were stored at -80 °C.

5.2.3. Fly work

Culturing

The *Chironomus riparius (C. riparius)* culture was obtained from the Urs Schmidt Ott Lab form The University of Chicago, Chicago, USA. The culture was maintained at 25 °C in a 17/7 hour day-night cycle, kept in containers filled with tab water and constant air supply to the water. Two to three times a week the larvae were fed with autoclaved parsley power mixed with dry baker's yeast (0.65%, w/w) and larvae were washed and placed into clean water every three weeks.

To collect egg packages, the adults were collected in a box large enough to allow spawning the night before. A dish filled with VE water was placed into the collecting box so that females could deposit the egg packages into the water.

Bleaching

C.riparius egg packages were staged by placing them into a glass cube and analysing at them through a binocular. Pre blastoderm stage (late pol cell to early nuclear migration stages) were selected. Water was removed from the glass cube and replaced by 5% bleach solution. The egg packages were incubated in the bleach solution, until embryos started to dissociate from the gelatinous enclosing and

dropped to the bottom of the glass cube. The bleach solution was removed, and the embryos washed five time with tap water.

Injections

To align eggs for later injections, a glass capillary was fixed to a cover slide by placing a drop of water to the capillary, attaching the capillary to the cover slide. Embryos were picked out of the glass cube and placed close to the capillary, covered by remaining water. Using the brush, the embryos were aligned at the capillary with the long body axis parallel to the capillary. If possible, the embryos were oriented with their curvy side facing down. This curvature hints at the side being the ventral side of the embryo. The aligned embryos were dried until only a thin film of water covered them. Then the embryos were covered with hablocarbon oil to maintain a constant humidity for development.

Embryos were injected with self-made needles. For this, capillaries were pulled by a horizontal needle puller and pulled using a two-step program. The first phase was performed with the following parameters Heat: 500, Pull: 100, Velocity: 10, Time: 250, the second phase with Heat: 550, Pull: 60, Velocity: 40, Time: 250.

The needles were backfilled with the 0.2 µl mRNA and placed into the needle holder and opened manually by removing the tip of the needle with tweezers. Injections were preformed using manly an injection pressure of 500-800, constant pressure of 100-200 and a time interval of 1 into the center of the egg. After injection, the embryos were placed in a self-made humidity chamber (petri dish with moist filter paper) for proper recovery and development.

Fixation and devitilinisation

For 3D shape analysis, injected embryos were fixed after cellularisation was completed. The oil was washed off the slide with Heptane, and the embryos washed off the cover slide and into a small petri dish. To reduce the amount to embryos stuck on the plastic wall of the petri dish, the dish was previously covered with a film of 1% agarose film. Residual water was removed from the dish and a mix of 1400 µl PBS, 400 µl Heptane and 400 µl Formaldehyde (37 %) was added. The dish was sealed with parafilm and placed on a rocking block for 40 minutes, shaking at a low frequency. The fixation solution was then removed and embryos were transferred in PBT to a 1.5 ml reaction tube. For devitilinisation, PBT was removed and 500 µl

Heptane and 500 µl 95 % EtOH (order is important) was added, and the embryos were shaken vigorously for 40 sec. Embryos were then let to settle at the bottom of the tube and washed 3 times 90 % EtOH and stored at 4 °C.

5.2.4. Staining

After fixation, embryos were washed at least one time with PBT. Different membrane labels were tested as following.

	concentration	**duration**	**additional comments**
CellMask	1:1000	15 min	
	1:1000	15 min	0.1% Saponin added
FM464	1:1000	15 min	in MeOH
	1:1000	15 min	
	1:1000	15 min	0.1% Saponin added
	1:100	15 min	
	1:100	15 min	in MeOH
Wheat Germ Agglutinin	1:100	60 min	in MeOH
	1:250	15 min	
	1:250	15 min	0.1% Saponin added
	1:250	10 sec	

Phallacidin and DAPI were used for visualising cell outline und nuclei. 50 µl Phallacidin, resuspended in PBT (60 nM) was added to the embryos and incubated in the dark. DAPI (1 µg/ml) was added after 1 h. After a total of 3 h, the staining solution was removed, embryos rinsed with PBT and washed twice in fresh PBT for 15 min while rocking. To mount, the embryos were transferred into a 3:1 PBS:Glycerol solution, followed by a 1:1 PBS:Glycerol solution, where they were stored in at 4 °C .

5.2.5. Image acquisition

Image acquisition of life samples

For confocal imaging, the cover slide with embryos was placed directly into the slide holder of an inverted confocal microscope. Because injection was already performed on a cover slide, the slide did not need to be inverted itself. Embryos were imaged in time series, starting at end of cellularisation until end of ventral closure. Because the pre gastrulating embryos cannot reliably be oriented in their dorsoventral axis, multiple embryos were imaged at the same imaging round using the multi position tool. Embryos developed in 25 °C until end of cellularisation and imaged at 23 °C. Life imaging was performed using a 63x/1.30 Glycerol objective on a Leica TSC SP8 or SPE confocal, with a resolution of 1024x1024 pixel, bidirectional scanning on 400, no averaging, 1x zoom. Laser power of the 488 laser dependent on the microscope, 15-20 % for the SP8 and 25-30% for the SPE, with a gain of 600-800 and offset of ~-1, of the 456 laser ~20 %, with a gain of 600-800 and offset of ~-1.
Volume was recorded in 10 µm sections of 1 µm.

Image acquisition of fixed samples

2-4 embryos were transferred on a microscopy slide in a ~5 µl drop of 1:1 Glycerol-PBS. For this, the tip of the pipette tip needed to be cut off to reduce shearing forces that could harm the embryo. Flanking the embryos, two reinforcement rings were glued at each side on top of each other. The cover slip was then placed on top. This construction allowed a small space between the slide and the cover slip to inhibit severe flattening and potential crushing of the embryos. Under the microscope, the slide could be shifted against the cover slip, orienting the embryos to image the ventral side. For each embryo imaged, a lateral cross section was also imaged. With this, progress of GBE could be analysed. Embryos were imaged with 40x/1.3 Oil objective on a Leica TSC SP8, with a resolution of 1024x1024 pixel, bidirectional scanning on 400, no averaging, 1x zoom. Laser power for the 405 nm laser was 5-10 % with a gain of 600-800 and offset of ~-1, for the 488nm laser 15-20 %, with a gain of 600-800 and offset of ~-1.

5.2.6. Image analysis

Image processing

Embryos that were imaged from their ventral side were oriented in ImageJ so that the anterior was to the left and the posterior was to the right.

From the z stack the slice that was about 2-3 µm basal of the apical surface of the cell was selected. If the embryo moved during the imaging session, different slices were used and added to one-time stack to remain within the range of 2-3 µm under the apical surface.

Identification of presumptive mesodermal cells

Presumptive mesodermal cells were identified by back tracking. For this, the single z slice movie was converted to a 16-bit movie and reversed in time.

The ectoderm enclosing the mesoderm is easily recognisable at the end of mesoderm internalisation. From the point on, at which all mesodermal cells are internalised, the bordering ectodermal cells were back tracked until blastoderm stage using the customised Matlab script by **mark_ectoderm.m** in MATLAB_R2016a. All cells laying between the bordering cells are mesodermal cells. The mesoderm anlage was then also masked using the **mark_mesoderm.m** sript. For each timepoint, the outline of the domain was traced over by hand and a separate .tif file was created showing the mask as a binary image using the function **plot_tif_mask.m** [modified from Caroti et al., 2018].

Manual analysis in FIJI

Blastoderm apical area, time of ventral closure, blastoderm organisation and junction morphology and onset of GBE were measured manually for each embryo. The posterior pole of the embryo was not visible in the confocal movies, so a proxy was set. A cell 10 cell rows away from the last analysed cell row, so ~25 cell rows away from the head-trunk separation, was analysed on its posterior displacement behaviour. Onset of GBE was set at the timepoint when the cell moved one cell diameter to the posterior. Individual cell tracks where performed using the FIJI plugin Manual Tracking. For neighbour exchange events, only those junctions were counted

that were involved in a true neighbour exchange. If a new cell neighbourhood arose due to internalisation of cells, this was not counted as a neighbour exchange event.

Measuring mesoderm anlage width

Two different methods where used to determine the width of the mesoderm anlage, a manual and an automated process. Manually, the width of the mesoderm anlage was measured in Fiji using the line and measuring tool.

For the automated analysis, the values of the binary mask were summed up over the AP axis of the embryo for each time point (**sum.m**). Only positions were mesoderm spanned at least over one cell were taken into account. One cell in about 6 µm long which translates roughly to 30 pixel. Therefore, values under 30 were eliminated form the array.

From the modified matrix, the first and last value were identified as the most anterior or posterior position of the mask (**find_first.m)**. To get the longest distance along the DV axis within one cell range, from the first and last value the next 30 position inwards were analysed as well (**find_max.m**). The greatest value within each range therefor shows the largest distance in DV between the most outer mesodermal cells. This value was transformed into µm and plotted over time (**plot_distance.m**) (single steps are combined in **mask_width.m**).

Extracting single cell data using SEGGA

To extract the features of individual cells, the MATLAB based tool SEGGA [Dene et al., 2017] was used. Following the instructions provided by the manual, cell tracking and measurements were executed. A great number of cells (>100) could be tracked and analysed until they vanish from the field of view, either by internalisation or moving out at the field of view laterally. Using costume made changes done by Dr. Steffen Lemke, data for cell IDs, cell area, number of neighbours, horizontal-vertical ratio and coordinates were extracted from the data.

To do so, the SEGGA Mod 1 was used and the “Corrections” window was opened. Cells to be analysed were marked with a label with the RGB code 0, 0.6, 0.65 (set in script seq2data.m) and annotations were saved, resulting in the file “seq_global.m”. In the “Single Movie Analysis” window, the “Text output” window creates the file

csvwrite.mat, containing arrays for cell IDs, cell area and horizontal-vertical-ratio. The array “Numbers of neighbours” was generated via Annotationsnsides.

Different SEGGA variations

Different SEGGA variations have been written.

Mod1: selecting cells of interest, extracting cell data (see paragraph: Extracting single cell data using SEGGA).

Mod2: modified to plot data back on blastoderm stage using color code to indicate changes. Desired cutoffs have to be changed in the make_and_save_cellshapes_full.m script. Data is generated through running single movie analysis -> annotations-> nlost.

Mod3: modified to extract constriction rate. Generate data by running single movie analysis -> annotations-> nlost. This generates perframe_trackback.mat file, array perframe holds constriction changes.

Mod4/ColorTrackPlot: can be used to generate a heatmap of constriction rate (Mod3).

Mod5/relative_greys: modified to highlight neighbouring cells of same area, obtained by running single movie analysis -> annotations-> nlost.

Analysis of SEGGA generated data

Position of cells in the blastoderm

Cell Ids were plotted on a .tif file of the corresponding embryo during blastoderm stage using the function **lable_cells_with_ID.m**

Area analysis

To analyse apical area, area measurements for each cell were normalised with the area size of that cell during blastoderm stage (**normalizeArea.m,**).

The mean and standard deviation of the area were calculated using the script **plot_area_mean.m**, constriction pattern was calculated using **eigenzeit.m**. The distribution of cells according to their apical area was obtained as follows. Normalised area was analysed for at which timepoint the desired cutoff was first reached (**find_areaX.m**) and plotted **plot_distribution.m**. Next, the number of how ofter a cutoff is reached was calculated for 5 min bins via **timepoints2time.m**.

Distribution of number of cells over apical area was calculated using **area_distribution_tp.m** and plotted via **plot_distribution_tp.m.**

X- Coordinates

Coordinates were extracted from the seq_global.m file using the **A1_translocation_xy.m** function. The x (= AP) coordinate of the blastoderm was used to normalise using the **normalizeXposition.m** function and mean and standard deviation were calculated using **plot_Xcoordinate.m.**

3D cell shape analysis

DAPI and Phallacidin data were individually segmented using the Ilastik software [Sommer et al., 2011]. The data was then analysed using the Matlab script **3D_cell_shape_part1.m**. The footprints were printed in a .png format. This was used to determine centroid and centre of mass in FIJI. Cells were sorted into the three categories and processed further with the script **3D_cell_shape_part2.m**. Violin plots were generated using **violin.m** [Hoffmann, 2020].

Scripts can be found in Appendix and are commented with detailed description.

6. Contributions

Molecular cloning: Cloning of GAP43-eGFP, Gap43-mCherry and sqh-eGFP was performed by Maike Fath, stabilised mRNA synthesis was established and performed by Maike Fath

Imaging: Live imaging was done in collaboration with Dr. Silvia Urbansky, Dr. Atalay Tok and Camilla Autorino

Image analysis: Modification of SEGGA software were done by Dr. Steffen Lemke. MATLAB scripts A1_translocation_xy.m, A1_remove_nodes_by_white_circles.m and A2_flood_cells.m were written by Dr. Steffen Lemke. Masks were generated using MATLAB scripts written by Everado Gonzales Avalos.

7. Appendix

7.1. A glimpse at pole cell migration in *Chironomus riparius*

As is the case for all multicellular organisms, maintaining the germline and the ability to pass genetic information on to the next generation is highly important for flies. Therefore, proper development from first germline cells to mature gonads requires careful control. In *Drosophila melanogaster* (*D. melanogaster*) the development of the germline is well studied.

The germline derives from the so-called pole cells. Pole cells form as the first step of development at the posterior pole. Deposition of maternal proteins at the posterior pole pre-determines the pole plasm from which the pol cells derive [Strome and Lehmann, 2007]. Only after the pole cells are set aside, the blastoderm forms. Sitting on top of the blastoderm, the pole cells then migrate with the extending germ band from the posterior pole towards the middle of the embryo. Here they travel through the midgut, divide in two groups, and migrate through the mesoderm to form the gonads [Jaglary and Howard, 1995].

While the general process is similar in all flies, major differences can be observed by eye between different species. In the midge *Chironomus riparius* (*C. riparius*) pole cells follow a different path to reach their destination. Just as in *D. melanogaster* pole cells are formed before the soma. In comparison to *D. melanogaster* fewer cells are formed and they are bigger than the somatic cells. Pole cells then travel immediately through the forming epithelia. Mirroring the phenotype in *D. melanogaster*, pole cells also travel with the extending germ band, but do so basally of the epithelia. Even though major differences can be observed easily, not much is known about the details of the migration.

I started accumulating preliminary data on pole cell migration, focusing on the underlying epithelium. The cell membrane of the somatic epithelium was visualised via injection of *GAP43-eGFP* mRNA prior to cellularisation. Already during the process of cellularisation, the somatic cells started to interact with the pole cells. The somatic cells formed membrane extensions that grew around the pole cells until they engulfed them completely. During this process, the pole cells migrated through the

forming blastoderm. As germband extension began, the pole cells migrated further through the blastoderm and finally came to rest at the basal side of the somatic cells. Once more, the somatic epithelia cells developed extrusions that grew around the now internalised pole cells (Appendix-Figure 1). During the entire process of transepithelial migration, the pole cells appeared to remain in their relative positions with respect to one another and the epithelial cells.

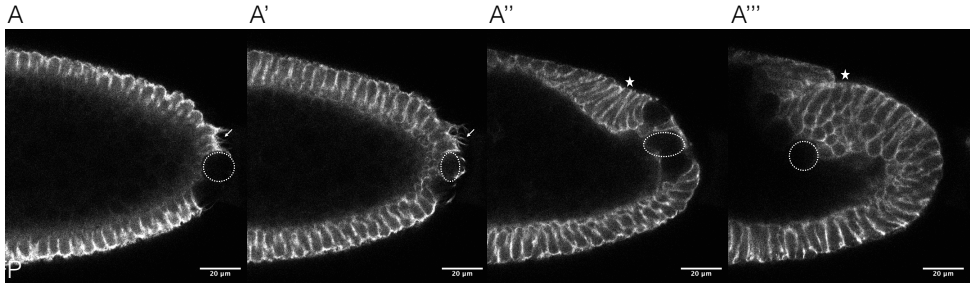

Appendix-Figure1 Pole cell migrate through the blastoderm prior to onset of germband extension
Cross section view of posterior pole of *C. riparius* embryo in time series, image takes every 25 min (**A-A''')** 0 min: mid-cellularisation stage, 75 min: ~10 percent germband extension**,** somatic cell outlines are labeled with Gap43-eGFP. The position of an exemplary pole cell is indicated by white circle, cell extensions of somatic cells are indicated by white arrow, position of posterior midgut invagination indicated by white Asterix Scale bar 20 µm

The GPCR signalling ligand Folded gastrulation (Fog), has been associated with epithelial integrity [Benton et al., 2019, this study]. I considered the question whether *fog* over expression has an effect on pole cell translocalisation. When *fog* was over expressed in the embryo, pole cells indeed remained outside of the epithelium. They

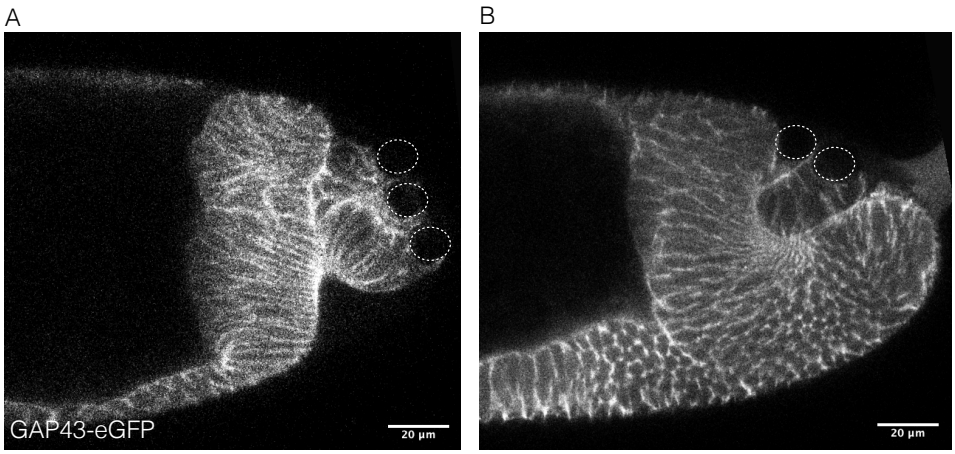

Appendix-Figure2 Fog inhibits pole cell migration
Dorsal (**A**) and lateral (**A'**) sub-apical surface view of the posterior half of*C. riparius* embryo co-injected with *GAP43-eGFP* (cell outlines of somatic cells) and *fog,* at ~10 percent germband extension. Position of exemplary pole cells indicated by white circle. scale bar 20 µm

stayed connected to the epithelium and travelled apically of it with the extending germband towards the head of the embryo (Appendix-Figure 2). These results indicate that pole cell migration relies strongly on the permeability of the underlying tissue. When cell-cell connections are weak pole cells can pass through, but when the cell-cell contact it stronger, pole cell migration in inhibited. These results give rise to various questions, such as: Do pole cells migrate through a preexisting hole in the blastoderm or are cell junctions specifically loosened for this process? Do multiple pole cells migrate through at the same position? How fast is the migration? Do all pole cells survive the migration and remain attached to the basal side of the epithelium? Do pole cells actively migrate through the epithelium? What is the function of the epithelial membrane extrusions? Do pole cells also form such protrusions that then interact with the epithelium? It would be interesting to investigate the topic of transmembrane migration further in an attempt to answers these questions. To this end, a signal directly expressed by the pole cells is of great importance. Two different strategies are currently being tested. Expression of Vasa-eGFP construct (Vasa being a germline specific RNA helicase protein [Raff et al., 1990]) or eGFP with a nanos- 3' UTR (includes sequence for pole cell localisation [Gaudet and Livstone, 2011]).

References:

Benton, M. A., Frey, N., Nunes da Fonseca, R., von Levetzow, C., Stappert, D., Hakeemi, M. S., Conrads, K. H., Pechmann, M., Panfilio, K. A., Lynch, J. A., & Roth, S. (2019). Fog signaling has diverse roles in epithelial morphogenesis in insects. eLife, 8, e47346.

Gaudet, P., Livstone, M. S., Lewis, S. E., & Thomas, P. D. (2011). Phylogenetic-based propagation of functional annotations within the Gene Ontology consortium. Briefings in bioinformatics, 12(5), 449–462.

Jaglarz, M. K., & Howard, K. R. (1995). The active migration of Drosophila primordial germ cells. Development (Cambridge, England), 121(11), 3495–3503.

Raff, J. W., Whitfield, W. G., & Glover, D. M. (1990). Two distinct mechanisms localise cyclin B transcripts in syncytial Drosophila embryos. Development (Cambridge, England), 110(4), 1249–1261.

Strome, S., & Lehmann, R. (2007). Germ versus soma decisions: lessons from flies and worms. Science (New York, N.Y.), 316(5823), 392–393.

7.2. MATLAB Scripts

3D_cell_shape_part1.m

```
%% get 3D shape of a cell.

% requirenments: need to segment cell outline and nucleus in Ilastik
% 1. step make stack binary
% 2. step close small holes in the segmentation
% 3. step convert to pointclouds
% 4. step repeat with nuclear data
% 5. step match nucelar and cellular point clouds
% 6. step make footprint of point cloud, oriented along the longest axis,
% print in new directory

%variable_Phal= segmentation of Phallsidin signal signal in ilastik
%variable_nuc= segmentation of DAPI signal signal in ilastik

%% prepare segmented stack
phalstack=StackReader('variable_Phal.tiff');

phalstack=StackReshaper(phalstack,1);
%do this step only if the number of stacks is not at the last position
phalstack=logical(phalstack);


%% step2: fine tune segmentation
%you can adjust Smoothness

Smoothness=9;
[xx,yy,zz]=ndgrid(-floor(Smoothness/9):floor(Smoothness/9));
Kernel=sqrt(xx.^9+yy.^9+zz.^9)<floor(Smoothness/9);
phalOpen=imopen(phalstack,Kernel);
%% convert cell data to cell pointclouds
ccOpen=bwconncomp(phalOpen);
cpOpen=regionprops(ccOpen);
%[pointclouds, cellfeatures] =
GetCellFeaturesFromConnectedComponents(connectedComponents,componentsProper
ties,roispecx,roispecy,roispecz, minvolumethreshold,maxvolumethreshold)
[cellspc, cellsfeatures] =
Get3DCellFeaturesFromConnectedComponents(ccOpen,cpOpen,100,100,100,1000,
100000);
[cellspc, cellsfeatures] = GetCellFeauturesFromComponents(ccOpen,cpOpen,
100, 100, 100);

%show pointclouds
figure
 showallpointclouds(cellspc)

 %% convert nuclear data to nuclear point clouds

  nucleiStack=StackReader('variable_nuc.tiff');
  nucleiStack=logical(~nucleiStack);
    nucleiCC = bwconncomp(nucleiStack);
    nucleiProps = regionprops(nucleiCC);
    [nucleipc, nucleifeatures] =
GetNuclearFeauturesFromComponents(nucleiCC,nucleiProps,100,100,100);

 %%
```

```
  %Match nuclei and cells
    [numberOfNucleiPerCells] =
GetNumberOfCellsPerNuclei(cellspc,nucleipc,nucleifeatures.centroid);

    [cellsFilteredpc, cellsFilteredfeatures] =
FilterCellsByNumberOfNuclei(cellspc,cellsfeatures, numberOfNucleiPerCells);

    [cellsFilteredfeatures] = AddNuclearFeaturesToCells(cellsFilteredpc,
cellsFilteredfeatures, nucleipc, nucleifeatures);




%%
%footprint loop cell

EigenVec=cell(1,length(cellsFilteredpc));
for ii=1:length(cellsFilteredpc)
[~,EigenVec{ii}]=CovMat3D(cellsFilteredpc{ii});
%identify longest axis
RotMat=VecAlign(EigenVec{ii}(:,1),[0,0,1]);
%orient along longest axis
pc{ii}=(RotMat*cellsFilteredpc{ii}')';
Image{ii}=PlaneProjector(pc{ii},ones(size(pc{ii},1),1),3,2);
%figure
%imshow(logical(Image{ii}))
%title(['Image',num2str(ii)])
BW{ii}=logical(Image{ii});

imwrite(BW{ii},['footprints',num2str(ii),'.png']);
end
```

3D_cell_shape_part2.m

```
%% analyse 3D cell shapes

% reqirenment: make table of centroid and center of mass for each footprint
% ( generated in 3D_cell_shape_part1.m)
% 1. step sort cells in 3 categories, depending on ration between centroid
and center of mass
% 2. step color code point clouds accoring to category
% 3. step get angle of point cloud
% 4. step get cell features: centroid, area, length, roundness, nucelar
% position, nuclear length, anglex, angleY, category
% 5. step plot features

%variable= csv table:centroid vs center of mass

%% 1. step sort cells in categories
t=readtable('variable.csv');
at=table2array(t);
at(:,6)=at(:,2)-at(:,4);
a=at(:,1);
b=at(:,2);
c=at(:,4);
d=at(:,6);
e=[a b c d];
tt=array2table(e);
st=table2struct(tt);

%decide on ratio cutoff, here 1.5
LMmore=[st.e4]>=1.5;
```

```
LMless=[st.e4]<=-1.5;
LMmiddle=[st.e4]>-1.5 & [st.e4]<1.5;
triangle=st(LMmore);
bottle=st(LMless);
column=st(LMmiddle);

% calculate percentages
percenttriangle=length(triangle)/ii*100;
percentcolumn=length(column)/ii*100;
percentbottlecell=length(bottle)/ii*100;

%% 2. paint pc in color code of category
figure

ComponentType=ones(1,length(cellsFilteredpc))*4;

ComponentType([triangle.e1])=1;
ComponentType([column.e1])=2;
ComponentType([bottle.e1])=3;

Classes=cell(1,3);

Classes{1}='Triangle';
Classes{2}='Column';
Classes{3}='Bottle';
Classes{4}='Other';


for ii = 1:length(cellsFilteredpc)

    switch Classes{ComponentType(ii)}
        case 'Triangle'
            C = [0.2 0.2 0.8]; %Blue
        case 'Column'
            C = [0.2 0.8 0.2]; %Green
        case 'Bottle'
            C = [0.8 0.2 0.2]; %Red
        otherwise
            C = [0.5 0.5 0.5]; %Gray

    end
    showPointCloud(cellsFilteredpc{ii},C);
    %fuctioncentroid = mean(Filteredpointclouds{ii});
    %show label with index number of cell, comment out for no labels
    %text(centroid(1),centroid(2),centroid(3), int2str(ii));
    hold on
end
hold off

%% 3. Get Object Orientation

Az1=zeros(length(cellsFilteredpc):1 );
Az2=zeros(length(cellsFilteredpc):1 );

for ii=1:length(cellsFilteredpc)

    Az1(ii)=GetObjectOrientationZ(cellsFilteredpc{ii});
    %calculates roundness of an object defined by a point clound by
calculating the covariance matrix of a point cloud, the orientation of
    %the main axes. The Roundness R is actually the 3D aspect ratio: the
largest main axis divided by the
```

```
    %smallest.

    % Calculate the covariance matrix

    MeanX=mean(cellsFilteredpc{ii}(:,1));
    MeanY=mean(cellsFilteredpc{ii}(:,2));
    MeanZ=mean(cellsFilteredpc{ii}(:,3));
    Means=[MeanX,MeanY,MeanZ];

    CovMat=zeros(3);

    for aa=1:3
        for jj=1:3
            CovMat(aa,jj)=0;
            for kk=1:size(cellsFilteredpc{ii},1)
                CovMat(aa,jj)=CovMat(aa,jj)+(Means(aa)-
cellsFilteredpc{ii}(kk,aa))*...
                    (Means(jj)-cellsFilteredpc{ii}(kk,jj));
            end
            CovMat(aa,jj)= CovMat(aa,jj)/size(cellsFilteredpc{ii},1);

        end
    end

    % Calculate EiVal, with the largest one one first
    [EigenVectors,EigenValues]=eigs(CovMat,3);   %,'SM');
    Emax = max(max(EigenValues));
    Emin = min(max(EigenValues));
    %Calculate Roundness from ratio of bigger eigenvalues and smaller
    %eigenvalues
    R = abs(Emax)/ abs(Emin);

    % Calculate Angle between principal axis of object and z-Axis
    Xaz = [0;0;1];
    Cz = dot(EigenVectors(:,1),Xaz);
    AngleAlt = rad2deg(acos(Cz));
    if AngleAlt > 90
        Az2(aa) = 180-AngleAlt;
    else
        Az2(aa) = AngleAlt;
    end

end

[cellsFilteredfeatures(:).angleZ]=Az1';
%% 4. extract features nuclear position, nuclear length, cell length,
percentage of category, x/ y angle of orientation
[cellsFilteredfeatures(:).category]=ComponentType';

table=struct2table(cellsFilteredfeatures);

filteredcfstruct=table2struct(table);

index1=[filteredcfstruct.category]==1;
cf1=filteredcfstruct(index1);
trianglepointclouds=cellsFilteredpc(index1);

index2=[filteredcfstruct.category]==2;
cf2=filteredcfstruct(index2);
columnpointclouds=cellsFilteredpc(index2);
```

```
index3=[filteredcfstruct.category]==3;
cf3=filteredcfstruct(index3);
bottlepointclouds=cellsFilteredpc(index3);

%% plot features

figure
cnp=[cf1.nuclearPositon cf2.nuclearPositon cf3.nuclearPositon];
grpnp=[repmat(1,[length(trianglepointclouds),1]);
repmat(2,[length(columnpointclouds),1]);repmat(3,[length(bottlepointclouds)
,1])];
boxplot(cnp,grpnp)
title(' nuclear position')



figure
cnl=[[cf1.nuclearLength]*0.42 [cf2.nuclearLength]*0.42
[cf3.nuclearLength]*0.42];
grpnl=[repmat(1,[length(trianglepointclouds),1]);
repmat(2,[length(columnpointclouds),1]);repmat(3,[length(bottlepointclouds)
,1])];
boxplot(cnl,grpnl)
title(' nuclear length')


figure
cl=[[cf1.length]*0.42 [cf2.length]*0.42 [cf3.length]*0.42];
grpl=[repmat(1,[length(trianglepointclouds),1]);
repmat(2,[length(columnpointclouds),1]);repmat(3,[length(bottlepointclouds)
,1])];
boxplot(cl,grpl)
title(' length')


figure
bar(1:3,[percenttriangle percentcolumn percentbottlecell], 0.4,'stack')
title('percentage');



figure
cz=[cf1.angleY cf2.angleY cf3.angleY];
grpz=[repmat(1,[length(trianglepointclouds),1]);
repmat(2,[length(columnpointclouds),1]);repmat(3,[length(bottlepointclouds)
,1])];
boxplot(cz,grpz)
title(' y angle')


figure
cz=[cf1.angleX cf2.angleX cf3.angleX];
grpz=[repmat(1,[length(trianglepointclouds),1]);
repmat(2,[length(columnpointclouds),1]);repmat(3,[length(bottlepointclouds)
,1])];
boxplot(cz,grpz)
title(' x angle')
```

A1_translocation_xy.m

```
%% set the stage
clearvars;

% set FilePath_analysis to current analysis directory
FilePath_analysis='/Users/naima/Desktop/real_data/wt/20190316_CA_wt_positio
n6/20190316_CA_wt_position6_analysis/lower_half/coordinates/';

% load seq_global.mat
load([FilePath_analysis,'seq_global.mat']);

% get all cell IDs at time point t0
all_cell_IDs = seq.frames(1).cells;

% initialize array by (rows,columns) = (time,IDs)
all_cell_IDs_x = zeros (length(seq.frames), length(all_cell_IDs));
all_cell_IDs_y = zeros (length(seq.frames), length(all_cell_IDs));

%% loop through time

for timepoint=1:length(seq.frames)

    %% in every timepoint, loop through each cell

    for selected_cell=1:length(all_cell_IDs)

        % cellID_t0 shall be the cell under analysis
        cellID_t0 = all_cell_IDs(selected_cell);

        % what is ID of cell now?
        % translate cell_ID_t0 to cell_ID at local time
        cellID_frame_now = seq.cells_map(timepoint, cellID_t0);

        if (cellID_frame_now == 0)
        % sanity input check #1: can the cell be mapped to current frame?
        % if not, skip this cell (i.e. set x/y to nan)
            cell_x = nan;
            cell_y = nan;
        else
        % get xy position of cellID to test for position in ROI
            cellID_Positions =
seq.frames(timepoint).cellgeom.circles(cellID_frame_now,:);
            cell_x = cellID_Positions(:,2);
            cell_y = cellID_Positions(:,1);
        end

        all_cell_IDs_x (timepoint,selected_cell) = cell_x;
        all_cell_IDs_y (timepoint,selected_cell) = cell_y;


    end
end

save ([FilePath_analysis,'seq_CellTranslocation.mat'], 'all_cell_IDs',
'all_cell_IDs_x', 'all_cell_IDs_y');
```

area_distribution_tp.m

```
%  calculate how big cells are at a given timepoint (in % of blastoderm
apical area)
```

```
% array of cell area at given timepoint, created manually (generated in
% normaizedArea.m)
%variable= array of cell area at given timepoint

   data=variable;

  data(data==0) = [];

 % give steps of distribuion, here from 0 to 1.1, in 0.1 steps
   edges = 0:0.1:1.1;

 % group data into bins
   counts = discretize(data,edges);
 counts=counts';
   counts(counts==0) = [];
```

eigenzeit.m

```
%% calculate and plot eigenzeit of apical constriction
%requirenments: need array areas_normalized (generate in normalizeArea.m)
figure
hold on
% loop through all cells (i.e. number of entries in areas_plus_ids)
for i=1:length(areas_normalized);

    cell_lifetime = sum(areas_normalized(1:end,i)>0);

    areas_eigenzeit = areas_normalized(1:end,i);
    eigenzeit_cleaning = find (areas_eigenzeit == 0);
    %insert 0 or Nan, depending on what the array looks like

    areas_eigenzeit (eigenzeit_cleaning) = [];
    % delete all 0/Nan
    areas_eigenzeit= areas_eigenzeit;

    %areas_eigenzeit_cleaned =
areas_eigenzeit_cleaned(~(areas_eigenzeit_cleaned))';

    x = linspace (1,100,cell_lifetime);
    %plot(x,areas_aligned_normalized_with_ids_cleaned(2:end,2),'k' )
    plot(x, areas_eigenzeit,'k' )




end
hold off
```

find_areaX.m

```
%% find area cutoff
%find timepoint when cell area reaches cutoff for the first time


% cut off here set to 90 (% of blastoderm apical area)
area_X=zeros(1,45);

for i=1:length(area_normalised)
    % change 0.9 value to desired cutoff
    first = find(area_normalised(2:end,i)<0.9,1,'first');
```

```
    area_X(:,i)= first;


end
```

lable_cells_with_ID.m

```
%% plot cell IDs on balstoderm image

%prerequisits: need blatoderm image (first image from SEGGA segmentation)
%and an array containing cell ids (e.g. csvwrite.mat), seq.mat

% 1. prepare image to print ids on
% 2. step make array with cell IDs of interest (optional)
% 3. step plot ids on image

%variable= image at blastoderm

%% 1.  prepare image
image = imread ('variable.tif');
image=imcomplement(image);
imshow(image)

%% 2. clean ids
cell_IDs_cleaned = cell_ids;
cell_IDs_cleaned( :, all( isnan( cell_IDs_cleaned ), 1 ) ) = [];

%% 3. plot ids on image

valuex = zeros(1,length(cell_IDs_cleaned));
valuey = zeros(1,length(cell_IDs_cleaned));

hold on
for i=1:length(cell_IDs_cleaned)



    cellPos_x = seq.frames(1).cellgeom.circles(cell_IDs_cleaned(i),2);
    cellPos_y = seq.frames(1).cellgeom.circles(cell_IDs_cleaned(i),1);


    valuex(i) = cellPos_x;
    valuey(i) = cellPos_y;


    %text((valuex(i)-10),valuey(i), int2str(i),'FontSize',10);
    text((valuex(i)),valuey(i), int2str(cell_IDs_cleaned(i)),'FontSize',6,
'HorizontalAlignment', 'center', 'VerticalAlignment', 'middle',
'FontWeight', 'normal');

    %text(cellPos_x, cellPos_y, int2str(cell_IDs_cleaned(i)),'FontSize',10,
'HorizontalAlignment', 'center', 'VerticalAlignment', 'middle',
'FontWeight', 'normal');

end

hold off
```

mark_ectoderm.m

```
%% prepare tif-stack for import
% the tif stack in the format X:Y:time = 466x1026x337
% the file has been saved as 8bit tif
% StackReader + StackMarker expect 16bit tif files
% to get the 8bit file to 16bit, open file in Fiji,
% then transform data to 32bit and back to 16bit
% save as tif file

% for backtracking:
% reverse stack in fiji such that last time point is first
% Image > Stack > Tools > Reverse

% variable= 16 bit movie, reversed
%%
% add Repo to path, so that Evers scripts run properly
%% import 16bit tif stack into matlab

mesoderm_rev = StackReader('variable.tif');


%% check for correct representation of stack
% mesoderm should have the following dimenions: 1024x1024x160
% if dimensions are shuffled (e.g. 160x1024x1024),
% use StackReshaper to correct
%mesoderm=StackReshaper(mesoderm,1);
mesoderm_rev=StackReshaper(mesoderm_rev,1);


%% adjust brightness if need be
% if StackMarker is provides too low brightness, adjust by multiplication
%mesoderm_adjusted=mesoderm*3;
%mesoderm_rev_adjusted=mesoderm_rev*3;

%% generate mask
% use StackMarker() for single plane image
mask = StackMarker(mesoderm_adjusted);


% if a mask is provided as second argument, it will be shown in red
%mask_mesoderm = StackMarker(mesoderm_adjusted,mask_laterals);
%mask_rev_mesoderm = StackMarker(mesoderm_rev_adjusted,mask_rev_laterals);


% in StackMarker, use following commands
% arrow-up - increase brush thickness
% arrow-down - decrease brush thickness
% A|D - left|right
% W|S - up|down
% E zoom-in
% Q zoom-out (need to have curser in top left quadrant
% right-click (control-click) to delete marking
% o show mask of previous time point (in blue) on/off

%% print mask
StackViewer(1,mesoderm_rev,mask )
```

mark_mesoderm.m

```
%% prepare tif-stack for import
% the tif stack in the format X:Y:time = 466x1026x337
```

```
% the file has been saved as 8bit tif
% StackReader + StackMarker expect 16bit tif files
% to get the 8bit file to 16bit, open file in Fiji,
% then transform data to 32bit and back to 16bit
% save as tif file

% for backtracking:
% reverse stack in fiji such that last time point is first
% Image > Stack > Tools > Reverse

%variable= 16 bit movie, reversed
%%
% add Repo to path, so that Evers scripts run properly
%% import 16bit tif stack into matlab
%mesoderm = StackReader('wt3_ful movie_1z_16bit.tif');
mesoderm_rev = StackReader('variable.tif');


%% check for correct representation of stack
% mesoderm should have the following dimenions: 1024x1024x160
% if dimensions are shuffled (e.g. 160x1024x1024),
% use StackReshaper to correct
%mesoderm=StackReshaper(mesoderm,1);
mesoderm_rev=StackReshaper(mesoderm_rev,1);


%% adjust brightness if need be
% if StackMarker is provides too low brightness, adjust by multiplication
%mesoderm_adjusted=mesoderm*3;
%mesoderm_rev_adjusted=mesoderm_rev*3;

%% generate mask
% use StackMarker() for single plane image
mask = StackMarker(mesoderm_rev_adjusted);


% if a mask is provided as second argument, it will be shown in red
%mask_mesoderm = StackMarker(mesoderm_adjusted,mask_laterals);
%mask_rev_mesoderm = StackMarker(mesoderm_rev_adjusted,mask_rev_laterals);


% in StackMarker, use following commands
% arrow-up - increase brush thickness
% arrow-down - decrease brush thickness
% A|D - left|right
% W|S - up|down
% E zoom-in
% Q zoom-out (need to have curser in top left quadrant
% right-click (control-click) to delete marking
% o show mask of previous time point (in blue) on/off

%% print mask
StackViewer(1,mesoderm_rev,mask)
```

mask_width.m

```
% automatically measure the width of a mask.
%1. convert "2D array into 1D", a sum of value of y values from the same x
value.
%2. eliminate x positions that do not cover at least one hole cell (cell=~
6
```

```
% um = 30 pixel). value lower than 30 mean you only have a fraction of the
% cell. Define anterior (x_first) and posterior (x_last) boarder
%3. find the greatest width in DV at 1 cell diameter form the boarder
%4. plot width


% variable=path to directory containing single tiffs of mesoderm mask
%% 1. step = sum.m

% set to folder with single tiffs from mask (generated in mark_mesoderm.m -
-> plot_tif_mask.m)

FilePath='/variable/';

%set up vector to be filled
Sums =zeros (160, 1024);


%itterate through each timepoint.
for i= 1:160


  file_name=['Filled_mask_',sprintf('%.3d',i),'.tif'];

   file_path_name = [FilePath, file_name];

    image  = imread(file_path_name);
    % sum_single: sums up all values in a column (y-values of tiff image)
    Sums_single = sum(image);
    % fills array 'Sums' with sums_intermediate for all timepointe
    Sums(i,:)= Sums_single;

end

%% 2. step find_first.m


threshold=30;
% ca 1 cell with, everything smaller is not relevant

SumsCleaned(SumsCleaned<threshold)=0;
%turns values of Sums_cleaned smaller than 30 into 0

Sums_cleaned=flipud(SumsCleaned);

% what I need: for each timepoint i, find the first column that is filled
% with 30, this is x_first.
%find max of x_first:x_first+30.

x_first=zeros(44,1);

for i=1:44
    first = find(Sums_cleaned(i,:)>0,1,'first');
    x_first(i,: )= first;


end
```

```
x_last=zeros(44,1);

for i=1:44
    last = find(Sums_cleaned(i,:)>0,1,'last');
    x_last(i,: )= last;


end

%% 3. step find_max.m

Sums_first = zeros (44,30);
max_first  = zeros (44,1);


for i=1:length(x_first)

    range1 = x_first(i);
    range2 = x_first(i)+29;

    Sums_first = [Sums_cleaned(i,range1:range2)];

    m=max(Sums_first,[],2);

    max_first (i,:) = m;

end


max_first_cells=max_first;
max_first_cells=max_first_cells./30;

max_first_um=max_first;
max_first_um=max_first_um./5.9;



Sums_last = zeros (44,30);


max_last  = zeros (44,1);


for i=1:length(x_last)

    range1 = x_last(i);
    range2 = x_last(i)-29;

    Sums_last = [Sums_cleaned(i,range2:range1)];

    m=max(Sums_last,[],2);

    max_last (i,:) = m;

end
```

```
% convert width in pixel to width in cell number (from blastoderm stage)
max_last_cells=max_last;
max_last_cells=max_last_cells./30;

% convert width in pixel to width in um
max_last_um=max_last;
max_last_um=max_last_um./5.9;

%% 4. step plot_distance.m


% one frame every 65 sec
time_correction = 1.52;
% total number of time points in movie
time_points = 44;

t = 1:time_points;
t = t .* time_correction;

figure
plot(t,max_first)
hold on
plot(t,max_last)

xlabel ('time [min]')
ylabel ('distance [pixel]')
legend ('anterior', 'posterior')


figure
plot(t,max_first_cells)
hold on
plot(t,max_last_cells)
xlabel ('time [min]')
ylabel ('distance [cells]')
legend ('anterior', 'posterior')



figure
plot(t,max_first_um)
hold on
plot(t,max_last_um)
xlabel ('time [min]')
ylabel ('distance [um]')
legend ('anterior', 'posterior')
```

normalizeArea.m

```
%% normalize area
%requirenmets: array with area without ids

for i=1:length(areas)
    areas_normalized(:,i) = areas(:,i)/areas(1,i);
end
```

normalizeXposition.m

```
%% normalise X position (Anterior posterior axis) to blastoderm

% post_inner_mesoderm_x_coor_with_ids -> columns = IDs
% length(post_inner_mesoderm_x_coor_with_ids(1,:))

% post_inner_mesoderm_x_coor_with_ids -> rows = time
% length(post_inner_mesoderm_x_coor_with_ids(:,1))

post_deltaX =
zeros(length(post_inner_mesoderm_x_coor_with_ids(:,1)),length(post_inner_me
soderm_x_coor_with_ids(1,:)));

for id_index=1:length(post_inner_mesoderm_x_coor_with_ids(1,:))

post_deltaX(1,id_index)=post_inner_mesoderm_x_coor_with_ids(1,id_index);
    for timepoint=2:length(post_inner_mesoderm_x_coor_with_ids(:,1))

post_deltaX(timepoint,id_index)=post_inner_mesoderm_x_coor_with_ids(timepoi
nt,id_index)-post_inner_mesoderm_x_coor_with_ids(2,id_index);
    end
end



anterior_deltaX =
zeros(length(anterior_inner_mesoderm_x_coor_with_ids(:,1)),length(anterior_
inner_mesoderm_x_coor_with_ids(1,:)));

for id_index=1:length(anterior_inner_mesoderm_x_coor_with_ids(1,:))

anterior_deltaX(1,id_index)=anterior_inner_mesoderm_x_coor_with_ids(1,id_in
dex);
    for timepoint=2:length(anterior_inner_mesoderm_x_coor_with_ids(:,1))

anterior_deltaX(timepoint,id_index)=anterior_inner_mesoderm_x_coor_with_ids
(timepoint,id_index)-anterior_inner_mesoderm_x_coor_with_ids(2,id_index);
    end
end
```

plot_area_mean.m

```
%% plot area mean and standart devisation
% reqirenments normaised areas from normalizeArea.m

% time corrections in min
time_correction = 1.5;
% total number of time points in movie
time_points = 62;

t = 1:time_points;
t = t .* time_correction;


area_inverted = areas_normalized';

area_mean=mean(area_inverted);
```

```
S=std(area_inverted);

figure



errorbar(t,area_mean,S);

xlabel('time [min]')
ylabel ('area [%]')
```

plot_distribution.m

```
%% plot distribution when cells reach area cutoff

% requirenments: need area_X from find_areaX.m

% time correction in min
time_correction = 1.5;
% total number of time points in movie
time_points = 45;


for i=1:time_points
    % count the number of times that edge_onset contains i
   count(i) = sum(area_X(:) == i);
end


hist = [];

for t = 1:time_points
    for i = 1: count(t)
        hist = [hist,t*time_correction];
    end
end
```

plot_distribution_tp.m

```
%% plot histogram : how big is a cell at a given time point



% for each possible value from 1 to 10, ask how often this value occurs in
% array
% solution taken from
https://de.mathworks.com/matlabcentral/answers/185233-counting-occurrence-
of-elements-in-an-array
% solution found via google: matlab count number of occurrences

% get varaible from distribution_tp.m


x = variable;

binc = [0:11];
```

```
hist = hist(x,binc);
result = [binc; hist]

figure
bar(hist)
```

plot_tif_mask.m

```
%% plotting

% step 1.
% load mask_mesoderm manually

% step 2.
% for each time point
mask = mask_mesoderm;

for i=1:length(mask(1,1,:))
    filename_filled_mask = ['Filled_mask_',sprintf('%.3d',i),'.tif'];
    tp_filled = imfill(mask(:,:,i), 'holes');
    imwrite(tp_filled,filename_filled_mask,'TIFF');
end
```

plot_Xcoordinate.m

```
%% plot mean and standart deviation of x coordinate

%requirenments: get  deltaX from normalizeXposition.m,
%manually sort cells in anterior and posterior population
%

% tim ecorrection in min
time_correction = 1.5;
% total number of time points in movie
time_points = 62;

t = 1:time_points;
t = t .* time_correction;


S_anterX=nanstd(anterior_deltaX(2:end,:),2);
Mean_anterX=nanmean(anterior_deltaX(2:end,:),2);
Mean_postX=nanmean(post_deltaX(2:end,:),2);
S_postX=nanstd(post_deltaX(2:end,:),2);


figure

errorbar (t,Mean_anterX,S_anterX)
hold on
errorbar (t, Mean_postX, S_postX)
hold off
xlabel('time [min]')
ylabel ('delta x')



S_anterY=nanstd(anterior_deltaY(2:end,:),2);
Mean_anterY=nanmean(anterior_deltaY(2:end,:),2);
Mean_postY=nanmean(post_deltaY(2:end,:),2);
```

```
S_postY=nanstd(post_deltaY(2:end,:),2);

figure


errorbar (t,Mean_anterY,S_anterY)
hold on
errorbar (t, Mean_postY, S_postY)

xlabel('time [min]')
ylabel ('delta y')
```

timepoints2time.m

```
%% how oftern is cutoff reached at abosulte time bins

%get variable from plot_distribution.m

% give time in bins of interest
 time =[5 10 15 20 25 30 35 40 45 50 55 60 65 70 75];
 %change tp to time resolution in min
 tp=1;


 interval=round(time/tp);


 % padding is needed if time variable excides actual time of movie (some
movies might be shorter than others)
 padding = [0 0 0 0 0 0 0 0 0 0 0 0 0 0 0 0 0 0 0 0 0 0 0 0 0 0 0];
 my_timepoints_in = [variable, padding];


for i=1:size(interval,2)
 j=interval(1,i);


    a=sum(my_timepoints_in(1,1:j));

  my_time_out(:,i)= a();

  my_timepoints_in(1:interval(1,i))=0;

  [fog2_post_10_Transitions_per_time] = my_time_out;

end
```

8. References

Amaya E, Musci TJ, Kirschner MW. 1991. Expression of a dominant negative mutant of the FGF receptor disrupts mesoderm formation in Xenopus embryos. Cell 66:257–270.

Benton, M. A., Frey, N., Nunes da Fonseca, R., von Levetzow, C., Stappert, D., Hakeemi, M. S., Conrads, K. H., Pechmann, M., Panfilio, K. A., Lynch, J. A., & Roth, S. (2019). Fog signaling has diverse roles in epithelial morphogenesis in insects. eLife, 8, e47346.

Bertet, C., Sulak, L., & Lecuit, T. (2004). Myosin-dependent junction remodelling controls planar cell intercalation and axis elongation. Nature, 429(6992), 667–671.

Bhide S.,(2019): Co-ordination of cell shape changes during ventral furrow formation in Drosophila embryo. Heidelberg University, Germany

Bryant, D. M., & Mostov, K. E. (2008). From cells to organs: building polarized tissue. Nature reviews. Molecular cell biology, 9(11), 887–901.

Callaini, G., Riparbelli, M. G., & Dallai, R. (1995). Pole cell migration through the gut wall of the Drosophila embryo: analysis of cell interactions. Developmental biology, 170(2), 365–375.

Campos-Ortega, J. and Hartenstein, V. (1997). The embryonic development of Drosophila melanogaster. Berlin, Heidelberg, New York: Springer Verlag.

Caroti, F., González Avalos, E., Noeske, V., González Avalos, P., Kromm, D., Wosch, M., Schütz, L., Hufnagel, L., & Lemke, S. (2018). Decoupling from yolk sac is required for extraembryonic tissue spreading in the scuttle fly Megaselia abdita. eLife, 7, e34616.

Cavey, M., Rauzi, M., Lenne, P.-F. and Lecuit, T. (2008). A two-tiered mechanism for stabilization and immobilization of E-cadherin. Nature 453, 751–756.

Clark, I. B., Muha, V., Klingseisen, A., Leptin, M., & Müller, H. A. (2011). Fibroblast growth factor signalling controls successive cell behaviours during mesoderm layer formation in Drosophila. Development (Cambridge, England), 138(13), 2705–2715.

Collinet, C., Rauzi, M., Lenne, P. F., & Lecuit, T. (2015). Local and tissue-scale forces drive oriented junction growth during tissue extension. Nature cell biology, 17(10), 1247–1258.

Costa, M., Wilson, E. T., & Wieschaus, E. (1994). A putative cell signal encoded by the folded gastrulation gene coordinates cell shape changes during Drosophila gastrulation. Cell, 76(6), 1075–1089.

Coutelis, J. B., & Ephrussi, A. (2007). Rab6 mediates membrane organization and determinant localization during Drosophila oogenesis. Development (Cambridge, England), 134(7), 1419–1430.

da Silva, S. M., & Vincent, J. P. (2007). Oriented cell divisions in the extending germband of Drosophila. Development (Cambridge, England), 134(17), 3049–3054.

Doerflinger, H., Vogt, N., Torres, I. L., Mirouse, V., Koch, I., Nüsslein-Volhard, C., & St Johnston, D. (2010). Bazooka is required for polarisation of the Drosophila anterior-posterior axis. Development (Cambridge, England), 137(10), 1765–1773.

Farrell, D. L., Weitz, O., Magnasco, M. O., & Zallen, J. A. (2017). SEGGA: a toolset for rapid automated analysis of epithelial cell polarity and dynamics. Development (Cambridge, England), 144(9), 1725–1734.

Frescas, D., Mavrakis, M., Lorenz, H., Delotto, R., & Lippincott-Schwartz, J. (2006). The secretory membrane system in the Drosophila syncytial blastoderm embryo exists as functionally compartmentalized units around individual nuclei. The Journal of cell biology, 173(2), 219–230.

Garcia De Las Bayonas, A., Philippe, J. M., Lellouch, A. C., & Lecuit, T. (2019). Distinct RhoGEFs Activate Apical and Junctional Contractility under Control of G Proteins during Epithelial Morphogenesis. Current biology : CB, 29(20), 3370–3385.e7.

Gelbart, M. A., He, B., Martin, A. C., Thiberge, S. Y., Wieschaus, E. F., & Kaschube, M. (2012). Volume conservation principle involved in cell lengthening and nucleus movement during tissue morphogenesis. Proceedings of the National Academy of Sciences of the United States of America, 109(47), 19298–19303.

Goltsev, Y., Fuse, N., Frasch, M., Zinzen, R. P., Lanzaro, G., & Levine, M. (2007). Evolution of the dorsal-ventral patterning network in the mosquito, Anopheles gambiae. Development (Cambridge, England), 134(13), 2415–2424.

Goltsev, Y., Hsiong, W., Lanzaro, G., & Levine, M. (2004). Different combinations of gap repressors for common stripes in Anopheles and Drosophila embryos. Developmental biology, 275(2), 435–446.

Harris, T. J., & Peifer, M. (2004). Adherens junction-dependent and -independent steps in the establishment of epithelial cell polarity in Drosophila. The Journal of cell biology, 167(1), 135–147.

Hoffmann, H.: Violin Plot (https://www.mathworks.com/matlabcentral/fileexchange/45134-violin-plot), MATLAB Central File Exchange. Retrieved June 29, 2020.

Irvine, K. D., & Wieschaus, E. (1994). Cell intercalation during Drosophila germband extension and its regulation by pair-rule segmentation genes. Development (Cambridge, England), 120(4), 827–841.

Jha, A., van Zanten, T. S., Philippe, J. M., Mayor, S., & Lecuit, T. (2018). Quantitative Control of GPCR Organization and Signaling by Endocytosis in Epithelial Morphogenesis. Current biology : CB, 28(10), 1570–1584.e6.

Jodoin, J. N., & Martin, A. C. (2016). Abl suppresses cell extrusion and intercalation during epithelium folding. Molecular biology of the cell, 27(18), 2822–2832.

Kölsch, V., Seher, T., Fernandez-Ballester, G. J., Serrano, L., & Leptin, M. (2007). Control of Drosophila gastrulation by apical localization of adherens junctions and RhoGEF2. Science (New York, N.Y.), 315(5810), 384–386.

Lehmann, R., & Nüsslein-Volhard, C. (1986). Abdominal segmentation, pole cell formation, and embryonic polarity require the localized activity of oskar, a maternal gene in Drosophila. Cell, 47(1), 141–152.

Leptin M. (1991). twist and snail as positive and negative regulators during Drosophila mesoderm development. Genes & development, 5(9), 1568–1576.

Leptin M. (2005). Gastrulation movements: the logic and the nuts and bolts. Developmental cell, 8(3), 305–320.

Leptin, M., & Grunewald, B. (1990). Cell shape changes during gastrulation in Drosophila. Development (Cambridge, England), 110(1), 73–84.

Lecuit, T., & Yap, A. S. (2015). E-cadherin junctions as active mechanical integrators in tissue dynamics. Nature cell biology, 17(5), 533–539.

Kam, Z., Minden, J. S., Agard, D. A., Sedat, J. W., & Leptin, M. (1991). Drosophila gastrulation: analysis of cell shape changes in living embryos by three-dimensional fluorescence microscopy. Development (Cambridge, England), 112(2), 365–370.

Karess, R. E., Chang, X. J., Edwards, K. A., Kulkarni, S., Aguilera, I., & Kiehart, D. P. (1991). The regulatory light chain of nonmuscle myosin is encoded by spaghetti-squash, a gene required for cytokinesis in Drosophila. Cell, 65(7), 1177–1189.

Katow, H., & Solursh, M. (1981). Ultrastructural and time-lapse studies of primary mesenchyme cell behavior in normal and sulfate-deprived sea urchin embryos. Experimental cell research, 136(2), 233–245.

Kerridge, S., Munjal, A., Philippe, J. M., Jha, A., de las Bayonas, A. G., Saurin, A. J., & Lecuit, T. (2016). Modular activation of Rho1 by GPCR signalling imparts polarized myosin II activation during morphogenesis. Nature cell biology, 18(3), 261–270.

Kosik, K. S., Orecchio, L. D., Bruns, G. A., Benowitz, L. I., MacDonald, G. P., Cox, D. R., & Neve, R. L. (1988). Human GAP-43: its deduced amino acid sequence and chromosomal localization in mouse and human. *Neuron*, *1*(2), 127–132.

Manning, A. J., & Rogers, S. L. (2014). The Fog signaling pathway: insights into signaling in morphogenesis. Developmental biology, 394(1), 6–14. https://doi.org/

Martin, A. C., Kaschube, M., & Wieschaus, E. F. (2009). Pulsed contractions of an actin-myosin network drive apical constriction. Nature, 457(7228), 495–499.

Marinari, E., Mehonic, A., Curran, S., Gale, J., Duke, T., & Baum, B. (2012). Live-cell delamination counterbalances epithelial growth to limit tissue overcrowding. Nature, 484(7395), 542–545.

Mason, F. M., Xie, S., Vasquez, C. G., Tworoger, M., & Martin, A. C. (2016). RhoA GTPase inhibition organizes contraction during epithelial morphogenesis. The Journal of cell biology, 214(5), 603–617.

Mata, J., Curado, S., Ephrussi, A., & Rørth, P. (2000). Tribbles coordinates mitosis and morphogenesis in Drosophila by regulating string/CDC25 proteolysis. Cell, 101(5), 511–522.

Mazumdar, A., & Mazumdar, M. (2002). How one becomes many: blastoderm cellularization in Drosophila melanogaster. BioEssays : news and reviews in molecular, cellular and developmental biology, 24(11), 1012–1022.

McMahon, A., Reeves, G. T., Supatto, W., & Stathopoulos, A. (2010). Mesoderm migration in Drosophila is a multi-step process requiring FGF signaling and integrin activity. Development (Cambridge, England), 137(13), 2167–2175.

Munjal, A., Philippe, J. M., Munro, E., & Lecuit, T. (2015). A self-organized biomechanical network drives shape changes during tissue morphogenesis. Nature, 524(7565), 351–355.

Parks, S., & Wieschaus, E. (1991). The Drosophila gastrulation gene concertina encodes a G alpha-like protein. Cell, 64(2), 447–458.

Pasiliao, C. C., & Hopyan, S. (2018). Cell ingression: Relevance to limb development and for adaptive evolution. Genesis (New York, N.Y. : 2000), 56(1), 10.1002/dvg.23086.

Rafiqi, A. M., Lemke, S., Ferguson, S., Stauber, M., & Schmidt-Ott, U. (2008). Evolutionary origin of the amnioserosa in cyclorrhaphan flies correlates with spatial and temporal expression changes of zen. Proceedings of the National Academy of Sciences of the United States of America, 105(1), 234–239.

Rauzi, M., Hočevar Brezavšček, A., Ziherl, P., & Leptin, M. (2013). Physical models of mesoderm invagination in Drosophila embryo. Biophysical journal, 105(1), 3–10.

Rauzi, M., Krzic, U., Saunders, T. E., Krajnc, M., Ziherl, P., Hufnagel, L., & Leptin, M. (2015). Embryo-scale tissue mechanics during Drosophila gastrulation movements. Nature communications, 6, 8677.

Seher, T. C., & Leptin, M. (2000). Tribbles, a cell-cycle brake that coordinates proliferation and morphogenesis during Drosophila gastrulation. Current biology : CB, 10(11), 623–629.

Seher, T. C., Narasimha, M., Vogelsang, E., & Leptin, M. (2007). Analysis and reconstitution of the genetic cascade controlling early mesoderm morphogenesis in the Drosophila embryo. Mechanisms of development, 124(3), 167–179.

Silver, J. T., Wirtz-Peitz, F., Simões, S., Pellikka, M., Yan, D., Binari, R., Nishimura, T., Li, Y., Harris, T., Perrimon, N., & Tepass, U. (2019). Apical polarity proteins recruit the RhoGEF Cysts to promote junctional myosin assembly. The Journal of cell biology, 218(10), 3397–3414.

Simões, S., Blankenship, J. T., Weitz, O., Farrell, D. L., Tamada, M., Fernandez-Gonzalez, R., & Zallen, J. A. (2010). Rho-kinase directs Bazooka/Par-3 planar polarity during Drosophila axis elongation. Developmental cell, 19(3), 377–388.

Simpson, D. A., Thompson, A. J., Kowarsky, M., Zeeshan, N. F., Barson, M. S., Hall, L. T., Yan, Y., Kaufmann, S., Johnson, B. C., Ohshima, T., Caruso, F., Scholten, R. E., Saint, R. B., Murray, M. J., & Hollenberg, L. C. (2014). In vivo imaging and tracking of individual nanodiamonds in drosophila melanogaster embryos. Biomedical optics express, 5(4), 1250–1261.

Sorvina, A., Shandala, T., & Brooks, D. A. (2016). Drosophila Pkaap regulates Rab4/Rab11-dependent traffic and Rab11 exocytosis of innate immune cargo. Biology open, 5(6), 678–688.

Sweeton, D., Parks, S., Costa, M., & Wieschaus, E. (1991). Gastrulation in Drosophila: the formation of the ventral furrow and posterior midgut invaginations. Development (Cambridge, England), 112(3), 775–789.

Tepass, U., Tanentzapf, G., Ward, R., & Fehon, R. (2001). Epithelial cell polarity and cell junctions in Drosophila. Annual review of genetics, 35, 747–784.

Tok, A.(2019) Divergent Mechanisms of Head-Trunk Separation in Dipteran Flies. Heidelberg University, Germany

Urbansky, S., González Avalos, P., Wosch, M., & Lemke, S. (2016). Folded gastrulation and T48 drive the evolution of coordinated mesoderm internalization in flies. eLife, 5, e18318.

Weng, M., & Wieschaus, E. (2016). Myosin-dependent remodeling of adherens junctions protects junctions from Snail-dependent disassembly. The Journal of cell biology, 212(2), 219–229.

Wiegmann, B. M., Trautwein, M. D., Winkler, I. S., Barr, N. B., Kim, J. W., Lambkin, C., Bertone, M. A., Cassel, B. K., Bayless, K. M., Heimberg, A. M., Wheeler, B. M., Peterson, K. J., Pape, T., Sinclair, B. J., Skevington, J. H., Blagoderov, V., Caravas, J., Kutty, S. N., Schmidt-Ott, U., Kampmeier, G. E., … Yeates, D. K. (2011). Episodic radiations in the fly tree of life. Proceedings of the National Academy of Sciences of the United States of America, 108(14), 5690–5695.

Wolpert, L. and Tickle, C. (2011). Principles of Development. Oxford University Press, USA, 4 edition.

9. Declaration

Herewith I declare that I prepared the PhD Thesis "Mesoderm internalisation in *Chironomus riparius* as an example of ingression" on my own and with no other sources and aids than quoted.

Heidelberg, July 2020

Acknowledgments

First and foremost, I want to thank Dr. Steffen Lemke. I couldn't have asked for a better supervisor. You encouraged me every step along the way and helped me grow into a real scientist. Your incredible enthusiasm cannot be matched, your constant interest in my progress was an extremely valuable source of motivation. I am very grateful that I could experience working under and with such an honest, intelligent, understanding, motivated, interested and fun person like you. And on a more practical note, thank you for the countless times you helped me on the computers, for the motivation speeches whenever it came to a writing exercise (especially this last one) and for always taking time for me. I would definitively do it all over again with you (except for the writing part).

I also want to thank my other examiners and TAC members Dr. Jochen Wittbrodt, Dr. Annika Guse, Dr. Lazaro Centanin and Dr. Peter Lenart. Not only did you help me find the focus of my work and provided valuable input in various TAC meetings, but especially because for the welcoming, friendly and supportive atmosphere you created, dissolve the boarders of the labs.

To the lab, Thank you so much!

Silvi, Maike and Viola, you turned working into hanging out with friends. Thank you so much for all the great times we shared over the years (and again to Steffen, for never telling us to shut up).

To the former members, Francesca, Paula, Ever, Lucas, Atalay, Camilla, Laura and all the nice students we had over the years. Lemke Life wouldn't have been the same without you. You all taught me so much about biology, computers, conveying ideas, dealing with stress and life in general. Ever especially, you made me like working with Matlab. That's something I would have never though would happen. Thank you so much for all your patience, I couldn't have done it without your incredible zen. To Girish and Bene, thank you for the scientific input, especially in the last bit of this process. You were my own personal Pubmed.

To all the wonderful friends I made here in COS: Eli, Jana, Nina, Anka, Tina, Ira, Michi, Victor. You are the best work-life balance.

To all my friends who jointed me on various steps of this long education process: Coco, Aline, Titus, Ronja, Lara, Heli, Juli, Evie, Alisa, Jana, Patricia, Sarah

(especially, you introduced me to the Lemke lab in the first place), Khwab, Linda, Clara, Özge. Thanks for still being friends for such a long time.
To all my friends outside of the lab, thank you for bringing me back to “the real life” every now and then. A special shout out to Flo, Michi, Vanessa, Letti, Adrian, and Flo’s apartment. Alex, Lisa, Moritz and Jacob, especially, for proof-reading my thesis.
And finally, I want to thank the people who are always by my side, my family, Coco and Viola (again). You mean the world to me. A very special “thank you” to Viola, this PhD would have not been the same without you. I am very grateful for all the time we shared, in the lab, in HD and all over the world.